NAVAL POSTGRADUATE SCHOOL

MONTEREY, CALIFORNIA

THESIS

OPTIMAL ATTITUDE MANEUVERS FOR THE KEPLER K2 MISSION

by

Matthew R. Argenziano

December 2014

Thesis Advisor: Mark Karpenko
Co-Advisor Isaac M. Ross

Approved for public release; distribution is unlimited

THIS PAGE INTENTIONALLY LEFT BLANK

REPORT DOCUMENTATION PAGE

Form Approved OMB No. 0704–0188

1. AGENCY USE ONLY *(Leave blank)*	**2. REPORT DATE** December 2014	**3. REPORT TYPE AND DATES COVERED** Master's Thesis

4. TITLE AND SUBTITLE
OPTIMAL ATTITUDE MANEUVERS FOR THE KEPLER K2 MISSION

5. FUNDING NUMBERS

6. AUTHOR(S) Matthew R. Argenziano

7. PERFORMING ORGANIZATION NAME(S) AND ADDRESS(ES)
Naval Postgraduate School
Monterey, CA 93943–5000

8. PERFORMING ORGANIZATION REPORT NUMBER

9. SPONSORING /MONITORING AGENCY NAME(S) AND ADDRESS(ES)
N/A

10. SPONSORING/MONITORING AGENCY REPORT NUMBER

11. SUPPLEMENTARY NOTES The views expressed in this thesis are those of the author and do not reflect the official policy or position of the Department of Defense or the U.S. Government. IRB Protocol number ____N/A____.

12a. DISTRIBUTION / AVAILABILITY STATEMENT
Approved for public release; distribution is unlimited

12b. DISTRIBUTION CODE
A

13. ABSTRACT (maximum 200 words)

The Kepler satellite was designed to detect stars with planets capable of supporting life. After completing its primary mission, two of the satellite's four reaction wheels failed, severely degrading the spacecraft attitude control system. In order to continue providing useful data to the scientific community, NASA has arranged a new mission for the Kepler satellite known as the K2 mission. The K2 mission currently uses a hybrid control approach for rotating the satellite that relies on thrusters for augmenting the authority of the remaining wheels. This thesis explores the application of optimal control for minimizing fuel consumption in support of the K2 mission. Such an approach is useful not only for momentum management during pointing but also for large angle slews needed to support non-science operation. Reducing fuel consumption will further extend the life of the K2 mission. Optimal control was shown in this thesis to reduce fuel consumption by as much as 28 percent during momentum management and 30 percent for large angle maneuvers. The results of this thesis are also applicable to other missions where it is desired to operate an underactuated spacecraft in the most fuel-efficient manner possible.

14. SUBJECT TERMS Kepler, K2, Optimal Control, Momentum Dumping, Momentum Management, Pontryagin's Principle

15. NUMBER OF PAGES
107

16. PRICE CODE

17. SECURITY CLASSIFICATION OF REPORT	**18. SECURITY CLASSIFICATION OF THIS PAGE**	**19. SECURITY CLASSIFICATION OF ABSTRACT**	**20. LIMITATION OF ABSTRACT**
Unclassified	Unclassified	Unclassified	UU

THIS PAGE INTENTIONALLY LEFT BLANK

Approved for public release; distribution is unlimited

OPTIMAL ATTITUDE MANEUVERS FOR THE KEPLER K2 MISSION

Matthew R. Argenziano
Lieutenant Commander, United States Navy
B.S., University of North Dakota, 2001

Submitted in partial fulfillment of the
requirements for the degree of

MASTER OF SCIENCE IN ASTRONAUTICAL ENGINEERING

from the

NAVAL POSTGRADUATE SCHOOL
December 2014

Author: Matthew R. Argenziano

Approved by: Dr. Mark Karpenko
Thesis Advisor

Dr. Isaac M. Ross
Co-Advisor,

Dr. Garth Hobson
Chair, Department of Mechanical and Aerospace Engineering

THIS PAGE INTENTIONALLY LEFT BLANK

ABSTRACT

The Kepler satellite was designed to detect stars with planets capable of supporting life. After completing its primary mission, two of the satellite's four reaction wheels failed, severely degrading the spacecraft attitude control system. In order to continue providing useful data to the scientific community, NASA has arranged a new mission for the Kepler satellite known as the K2 mission. The K2 mission currently uses a hybrid control approach for rotating the satellite that relies on thrusters for augmenting the authority of the remaining wheels. This thesis explores the application of optimal control for minimizing fuel consumption in support of the K2 mission. Such an approach is useful not only for momentum management during pointing but also for large angle slews needed to support non-science operation. Reducing fuel consumption will further extend the life of the K2 mission. Optimal control was shown in this thesis to reduce fuel consumption by as much as 28 percent during momentum management and 30 percent for large angle maneuvers. The results of this thesis are also applicable to other missions where it is desired to operate an underactuated spacecraft in the most fuel-efficient manner possible.

THIS PAGE INTENTIONALLY LEFT BLANK

TABLE OF CONTENTS

I. INTRODUCTION....1
A. THE KEPLER MISSION....1
B. THE KEPLER BUS....2
C. KEPLER MISSION OPERATIONS....5
D. REACTION WHEEL FAILURE....7
E. K2 MISSION....7
F. K2 SCIENCE CAMPAIGNS....9
G. PRIORITIZED MISSION OBJECTIVES....11
H. OPPORTUNITIES FOR IMPROVEMENT....12
I. THESIS OBJECTIVE AND SCOPE....12

II. KEPLER ATTITUDE CONTROL MODEL....15
A. RIGID BODY EQUATIONS OF MOTION....15
B. REACTION WHEEL DYNAMICS....16
C. THRUSTER EQUATIONS....17
D. SOLAR TORQUE....18
E. ATTITUDE CONTROL EQUATIONS....18
F. THRUSTER ALLOCATION....19
G. CONVENTIONAL CONTROL SYSTEM SIMULATION....24
H. K2 HYBRID CONTROL CONCEPT....26

III. MOMENTUM MANAGEMENT USING THRUSTERS....31
A. COMPARISON OF TWO METHODS TO DUMP MOMENTUM....31
1. Method 1: Open-Loop Thruster Commanding....32
2. Method 2: Closed-Loop Thruster Commanding....36

IV. OPTIONS FOR K2 MOMENTUM MANAGEMENT....41
A. EXAMPLE RESATURATION MANEUVER....41
B. STATIC OPTIMAL THRUSTER ALLOCATION....44
C. STATIC OPTIMAL ALLOCATION WITH HYBRID CONTROL....48
D. OPTIMAL CONTROL SOLUTION....52
E. VALIDATION AND VERIFICATION (V&V)....58
F. RESULTS SUMMARY....63

V. WHEELS ONLY LARGE ANGLE SLEW....65
A. APPLICATION OF OPTIMAL CONTROL TO A LARGE ANGLE MANEUVER....67
B. WHEELS ONLY SLEW RESULTS....70
C. VERIFICATION AND VALIDATION....73
D. RESULTS SUMMARY....75

VI. CONCLUSIONS AND FURTHER WORK....77
A. RESEARCH SUMMARY....77
B. FURTHER WORK....77

APPENDIX. APPLICATION OF PONTRYAGIN'S PRINCIPLE....79

A. DERIVATION OF THE NECESSARY CONDITIONS 81
LIST OF REFERENCES.....87
INITIAL DISTRIBUTION LIST.....89

LIST OF FIGURES

Figure 1 Kepler in its Orbit, after [6] 2
Figure 2 Cross-Sectional View of the Photometer and inset of the Focal Plane, from [1] 3
Figure 3 Kepler ADCS Block Diagram, from [6] 4
Figure 4 Kepler Flight System, from [6, 7] 5
Figure 5 Telemetry for an Earth Point to Science Point Maneuver : Euler Angles (data obtained from NASA) 6
Figure 6 Telemetry Data for an Earth Point to Science Point Maneuver: Reaction Wheel Speeds (data obtained from NASA) 6
Figure 7 K2 Science Orientation, after [9] 8
Figure 8 K2 Mission Campaigns, from [10] 9
Figure 9 Campaign Breakout, from [10] 10
Figure 10 K2 Observation Locations for Each Campaign, from [10] 11
Figure 11 Sample of Pulse Width Modulation 23
Figure 12 Plant Block Diagram 24
Figure 13 Maneuver from Earth Point to Science Point with 4 RWAs Using Conventional Attitude Control: Euler Angles 25
Figure 14 Failed Maneuver from Earth Point to Science Point with 2 RWAs Using Conventional Attitude Control: Euler Angles 26
Figure 15 Hybrid Control Block Diagram 30
Figure 16 Momentum Management Model 1; Open-Loop Thruster Commanding 32
Figure 17 Momentum Management Model 2:Closed-Loop Thruster Commanding 32
Figure 18 Thruster Pulse Allocation for Open-Loop Thruster Commanding (thruster forces given in Newtons) 34
Figure 19 RWA Speeds Under Open-Loop Thruster Commanding 35
Figure 20 Cumulative Thruster Pulse Time for Open-Loop Thruster Commanding 36
Figure 21 RWA Speeds for Closed-Loop Thruster Commanding 37
Figure 22 Thruster Pulse Allocation for Closed-Loop Thruster Commanding (thruster force given in Newtons) 38
Figure 23 Cumulative Thruster Pulse Time for Closed-Loop Thruster Commanding 39
Figure 24 Thruster Pulse Allocation Telemetry Data for Sample K2 Resat Operation (thruster force given in Newtons) 42
Figure 25 Euler Angle Telemetry Data for K2 Reaction Wheel Resat (data obtained from NASA) 43
Figure 26 RWA Telemetry Data for K2 Reaction Wheel Resat (data obtained from NASA) 43
Figure 27 Cumulative Thruster Pulse Time for K2 Mission Reaction Wheel Resat (data obtained from NASA) 44
Figure 28 Euler Angles for Static Reaction Wheel Resat 46
Figure 29 RWA Speed for Static Reaction Wheel Resat 46
Figure 30 Thruster Pulses for Static Reaction Wheel Resat (thruster force given in Newtons) 47

Figure 31 Zoomed in Thruster Pulses for Static Reaction Wheel Resat (thruster force given in Newtons) 48
Figure 32 Euler Angles for Static Reaction Wheel Resat with Hybrid Allocation 49
Figure 33 RWA Speed for Static Reaction Wheel Resat with Hybrid Allocation 50
Figure 34 Thruster Pulses for Static Reaction Wheel Resat with Hybrid Allocation (thruster force given in Newtons) 50
Figure 35 Zoomed in Thruster Pulses for Static Reaction Wheel Resat with Hybrid Allocation (thruster force given in Newtons) 51
Figure 36 Euler Angles (in Arcsec) for Optimal Momentum Resat 54
Figure 37 RWA Speed for Optimal Momentum Resat 55
Figure 38 Reaction Wheel Control Trajectories for Optimal Momentum Resat 55
Figure 39 Thruster Control Trajectories for Optimal Momentum Resat 56
Figure 40 Maneuver Time vs. Cumulative Thruster Pulse Time for Optimal Momentum Resat 57
Figure 41 Propagated Euler Angles 58
Figure 42 Propagated Quaternions 59
Figure 43 Propagated Spacecraft Angular Velocity 60
Figure 44 Propagated Reaction Wheel Momentum 60
Figure 45 Time History of the Hamiltonian 61
Figure 46 Control Signal and Switching Function for Thruster 3 (u7) 62
Figure 47 Control Signal and Switching Function for Reaction Wheel 1 (u_1) 63
Figure 48 Spacecraft Approximate Initial Orientation (Science Point) 65
Figure 49 Spacecraft Approximate Final Orientation (Earth Point) 66
Figure 50 RWA Telemetry for K2 Large Angle Maneuver 66
Figure 51 Attitude Telemetry for K2 Large Angle Maneuver 67
Figure 52 Optimal Control Maneuver in Quaternions 70
Figure 53 Reaction Wheel Control Trajectory 71
Figure 54 Angle between Solar Vector and the Y-Axis 72
Figure 55 Angle between Solar Vector and the Boresight 72
Figure 56 Propagated Quaternions for Large Angle Maneuver 73
Figure 57 Propagated Angular Velocity for Large Angle Maneuver 74
Figure 58 Propagated Reaction Wheel Momentum for Large Angle Maneuver 74
Figure 59 Time History of the Hamiltonian for Large Angle Maneuver 75

LIST OF TABLES

Table 1 Campaign Area of Observation, from [11] 10
Table 2 Thrust Time Allocation for Each Maneuver, from [12] 12
Table 3 Initial and Final Reaction Wheel Speeds for Momentum Dumping Simulation 31
Table 4 Comparison of Two Different Momentum Management Approaches 39
Table 5 Reaction Wheel States for a Resat Operation (K2 telemetry) 41
Table 6 Optimal Thruster Pulse Distribution for Resat Operation 45
Table 7 Optimal Thruster Pulse Distribution for Resat Operation with Hybrid Allocation 51
Table 8 Resat Problem Boundary Conditions 53
Table 9 Results of Optimal Control K2 Reaction Wheel Resaturation 57
Table 10 Summary of K2 Momentum Resat Results 64
Table 11 Initial and Final Conditions for a K2 Rest-to-Rest Slew from Science Point to Earth Point 67
Table 12 Large Angle Maneuver Boundary Conditions 69
Table 13 Summary of Fuel Consumption for a Large Angle Maneuver 76

THIS PAGE INTENTIONALLY LEFT BLANK

LIST OF ACRONYMS AND ABBREVIATIONS

ETHO	Earth-trailing heliocentric orbit
CCD	charge-coupled device
FOV	field of view
Mbps	megabits per second
ADCS	attitude determination and control system
RWA	reaction wheel assembly
IMU	inertial measurement unit
HGA	high gain antenna
PMO	primary mission objective
PWM	pulse width modulator
Arcsec	arcseconds
V&V	validation and verification

THIS PAGE INTENTIONALLY LEFT BLANK

ACKNOWLEDGMENTS

As with any endeavor that is worth pursuing, this one has required much of my time and resources to complete. First and foremost, I would like to thank God, for Whom all my efforts of every day are offered up. He created this great universe and inspires us to explore. Second, I wish to thank those who have helped me directly on this project. Thanks to my thesis advisors, Dr. Mark Karpenko and Dr. Isaac M. Ross, both of whom have given me guidance through their expertise and exemplary professionalism along the way. Third, I wish to thank Marcie Smith at NASA Ames research center, who was able to provide me with the data necessary to conduct this research. Thanks also to the NPS faculty and research assistants, who provided me with the knowledge to complete this endeavor. Finally, I wish to thank my wife, Julie, and my children, John Paul, Ethan, Naomi, and Caleb, for their patience and support while I worked on my research.

THIS PAGE INTENTIONALLY LEFT BLANK

I. INTRODUCTION

A. THE KEPLER MISSION

The Kepler mission was launched by NASA on 6 March 2009 to observe targets in space between the constellations of Cygnus and Lyra. This field of view was chosen, in part, because the declination was greater than 55° from the ecliptic plane, which met the 55° sun avoidance angle for the photometer [1]. The goal of the Kepler mission was to determine the frequency of Earth sized planets in the habitable zone of stars similar to our sun using the transit photometry method [2]. The Kepler satellite is in an Earth-trailing heliocentric orbit (ETHO), with an orbital period of 372.5 days, as shown in Figure 1. In the original mission, the satellite conducted a "roll" each quarter to keep the solar panels pointing at the sun to maximize power generation. The planned primary mission of Kepler was 3.5 years.

The Kepler mission has been a large success. As of 23 October 2014, the satellite has identified 4,718 planet candidates, 1,763 confirmed planets, and 454 multi planet systems [3]. In April 2014, Kepler discovered the first Earth–sized planet in the habitable zone, known as Kepler-186f [4]. The data from the Kepler mission has also led to secondary fields of the study. One such field is the study of the interior of stars, now known as asteroseismology. This is made possible through Kepler's ability to observe, with high quality, stars for long periods of time [5].

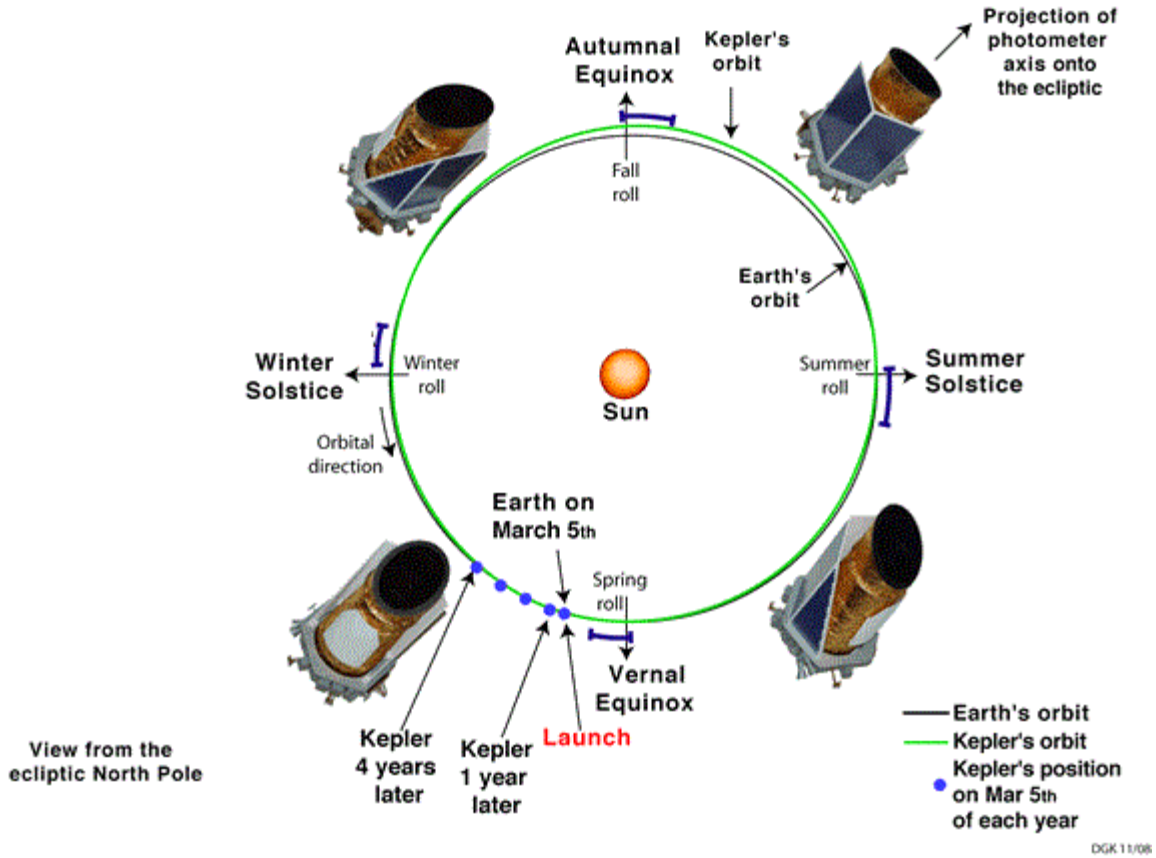

Figure 1 Kepler in its Orbit, after [6]

B. THE KEPLER BUS

The Kepler spacecraft was manufactured by Ball Aerospace & Technologies Corporation and was commissioned 67 days after launch. Kepler commenced science operations on 13 May 2009. The heart of the spacecraft is the photometer, which has a 95 megapixel focal plane composed of 42 science CCDs and four fine guidance sensor CCDs (see Figure 2, inset). Figure 2 also shows the photometer, which has a 0.95 m aperture that is fed from a 1.4 meter primary mirror at the base of a metering structure giving the telescope a 115 degree^2 field of view (FOV) [1, 7].

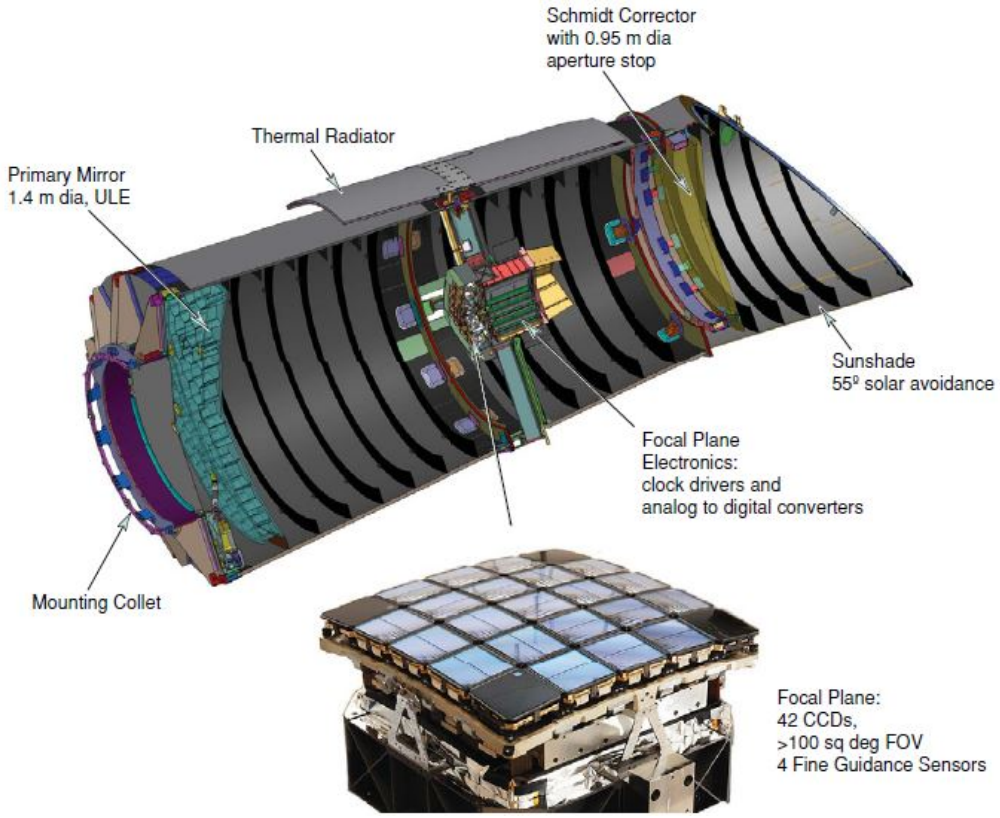

Figure 2 Cross-Sectional View of the Photometer and inset of the Focal Plane, from [1]

The spacecraft structure hosts all the equipment required to support the operations of the photometer. These systems include the command and data handling subsystem, the power subsystem, the attitude control subsystem and the telecommunication subsystem. The telecommunications system uses an X-band up and X/Ka-band down transceiver to achieve a maximum downlink rate of 4.33 Mbps. Transmissions are sent and received though a 0.85 meter high gain antenna. The satellite has a body fixed solar array designed to produce enough power for nominal operations when angled away from the sun by as much as 30° [7].

The attitude determination and control subsystem (ADCS) is used for pointing and slewing the satellite. The attitude determination portion consists of 2 star trackers and 2 IMU's. The attitude control portion consists of 4 reaction wheel assemblies (RWAs) with 200 mNm of torque and 16.6 Nms of momentum storage capacity. The RWAs are used for satellite slewing, momentum storage and pointing. A set of eight 1.0 N thrusters

are used for momentum management, which is required due to the accumulation of momentum from solar radiation pressure, the dominant environmental disturbance on the spacecraft. The thrusters use a hydrazine monopropellant fuel [6]. Figure 3 shows a block diagram of the attitude control system, while Figure 4 shows a complete layout of the satellite and its subsystems.

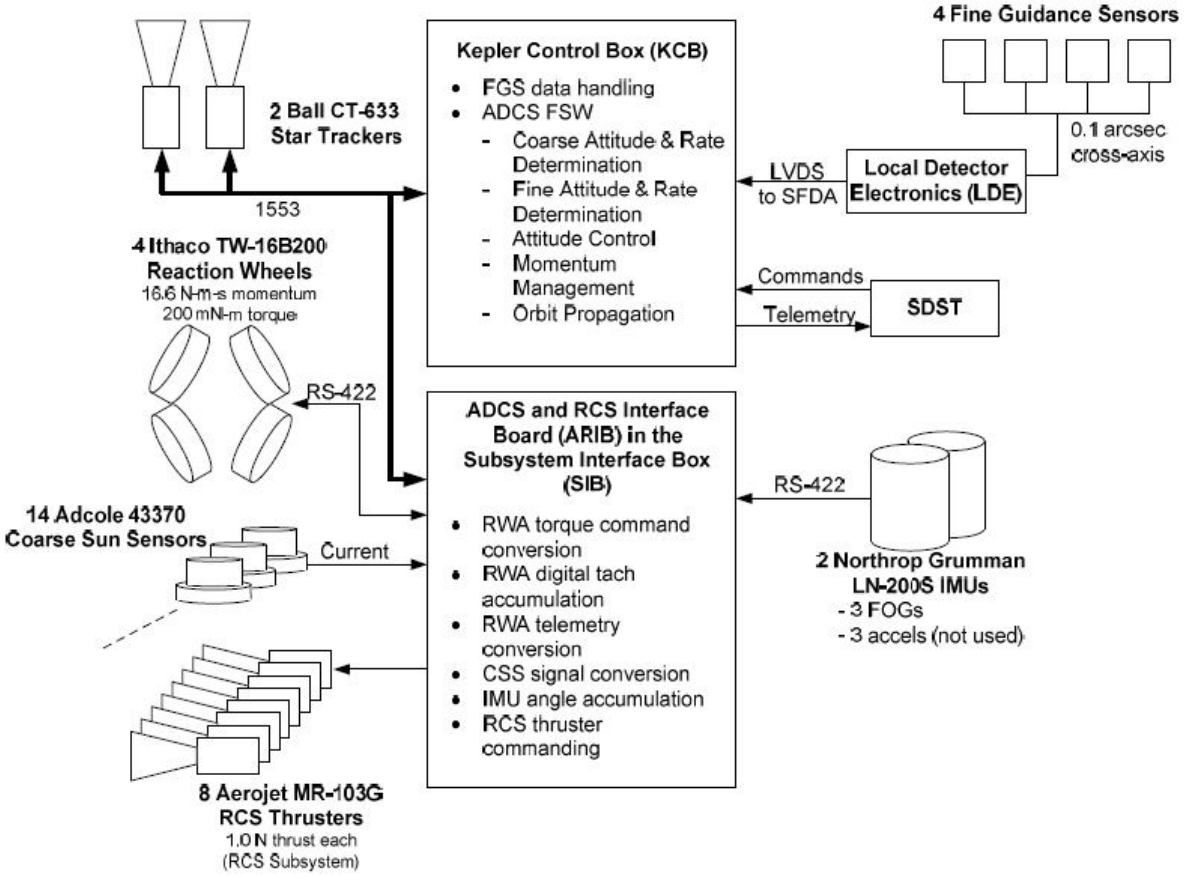

Figure 3 Kepler ADCS Block Diagram, from [6]

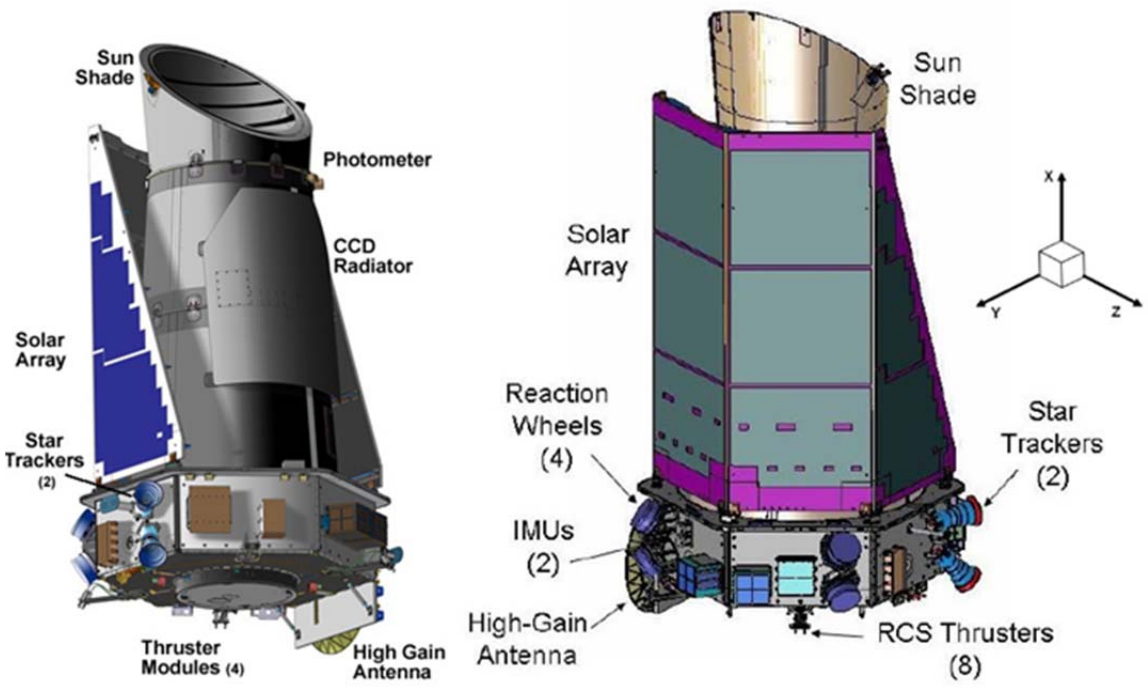

Figure 4 Kepler Flight System, from [6, 7]

C. KEPLER MISSION OPERATIONS

As part of Kepler mission operations, different activities occur on weekly, monthly and quarterly cadences. Weekly operations include mission planning, routine housekeeping, command uploads and health and safety monitoring, along with momentum management. Desaturating the RWAs occurs twice-weekly during 8 hour X-band contacts [7, 8]. Monthly operations include stored engineering and science data download, and monthly data processing. Science data downloading is done by pointing the high gain antenna towards Earth to downlink stored engineering and science data using the high rate Ka-band system. Quarterly operations include target management, data processing and the quarterly 90° reorientation roll about the photometer boresite to reorient the solar panels toward the sun and the CCD radiator at deep space [7]. Telemetry for a maneuver of the spacecraft from an earth point data dump attitude to a science collection attitude is shown in Figure 5. It can be seen that the satellite rolls approximately 16°, pitches approximately -30°, and yaws approximately -30°. In order to complete the maneuver, the satellite must use all four reaction wheels, as shown in Figure 6.

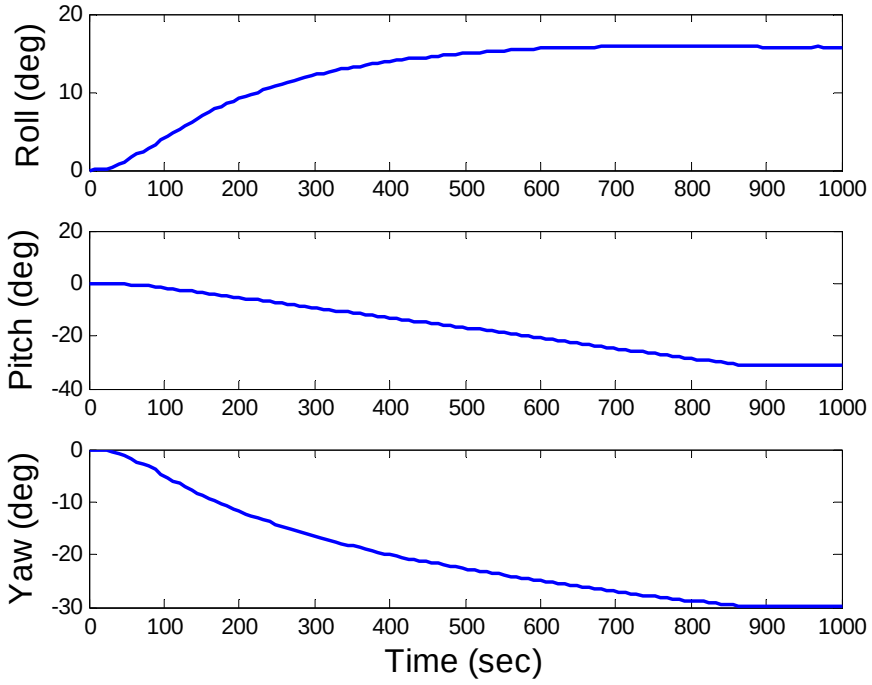

Figure 5 Telemetry for an Earth Point to Science Point Maneuver : Euler Angles (data obtained from NASA)

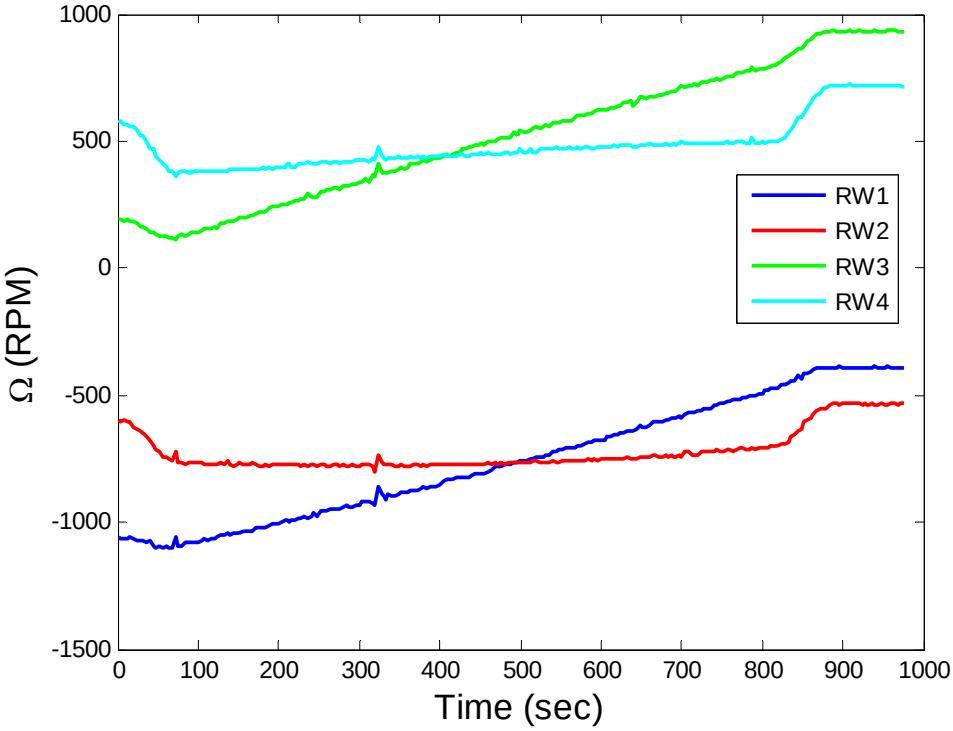

Figure 6 Telemetry Data for an Earth Point to Science Point Maneuver: Reaction Wheel Speeds (data obtained from NASA)

D. REACTION WHEEL FAILURE

Kepler completed its 2.5 year primary mission in September of 2012. However, before doing so, Kepler suffered the failure of the first of its four reaction wheels on 13 July 2012. Due to the four for three redundancy of reaction wheels in the attitude control system, the satellite was able to continue with its mission. A second wheel failed on 11 May, 2013, leaving the spacecraft with only two operational wheels, and thus unable to perform 3-axis control using wheels alone [9].

E. K2 MISSION

The K2 mission is the follow on mission that has repurposed Kepler in a way that can take advantage of the satellite's still operational high precision photometry hardware using a hybrid control system based on a combination of thrusters and the remaining operational reaction wheels. Since the failure of the second reaction wheel, Kepler has been unable to maintain accurate pointing at the constellation of Cygnus. The primary reason for the inability to point was the orientation of the satellite at science attitude. In the original science orientation, solar pressure from the Sun imparts a large disturbance torque on the satellite. Without a minimum of three reaction wheels, Kepler cannot properly absorb the torque imparted by the solar pressure on all three axes. This causes rotation of the satellite, preventing long term pointing at the same portion of space.

The K2 mission concept is driven by the spacecraft's ability to maintain pointing in two of three axes with the remaining two reaction wheels. Spacecraft pointing along the uncontrolled axis is maintained by using a combination of thrusters. Since the concept uses thrusters and the remaining RWAs, it is called a hybrid control concept [9]. Solar pressure remains the dominant disturbance torque in the new science attitude and its effects are controlled by wheels about the y and z-axes and by thrusters about the *x*-axis. In order to obtain the best pointing accuracy, the x-axis disturbance force is minimized by pointing in the heliocentric orbital plane where the motion of the spacecraft with respect to the sun follows the spacecraft line of symmetry in the x-y plane. This symmetry provides a balanced solar pressure and minimizes the x-axis disturbance [10]. The orientation for the satellite in science mode for the K2 mission can be seen in Figure 7.

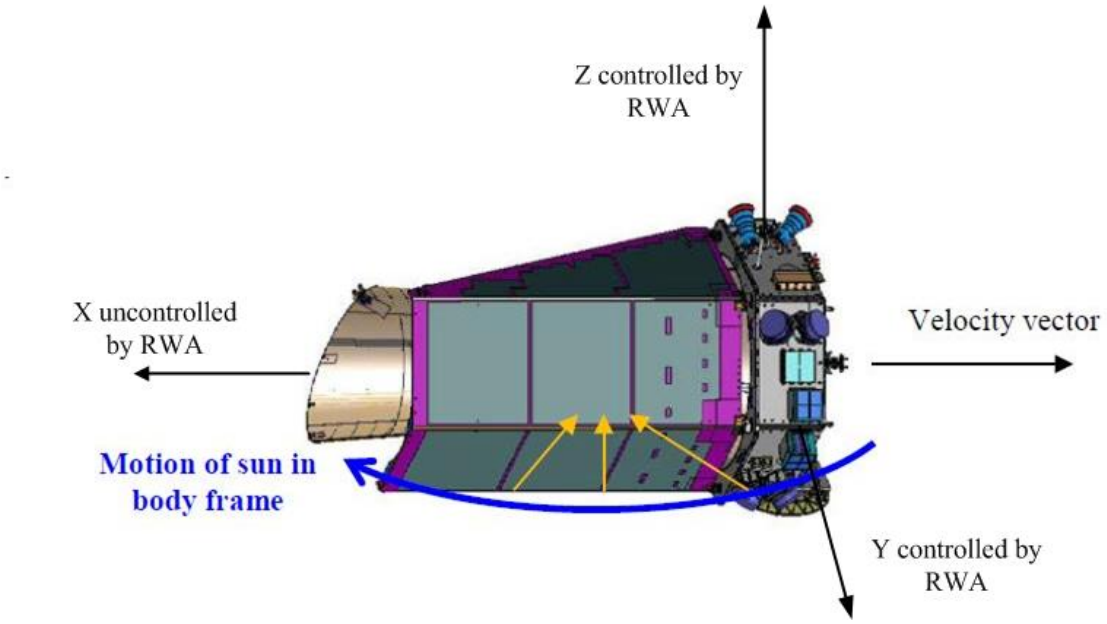

Figure 7 K2 Science Orientation, after [9]

In this new orientation, K2 will observe a series of independent target fields in the orbital plane over a series of 83 day campaigns. An overview of the mission concept can be seen in Figure 8. While the new orientation is favorable for continued science, communications with the satellite are limited during data collection due to unfavorable low gain antennae view angles. Because of this, the spacecraft must maneuver to point the high gain antenna (HGA) towards Earth in order to downlink accumulated science data.

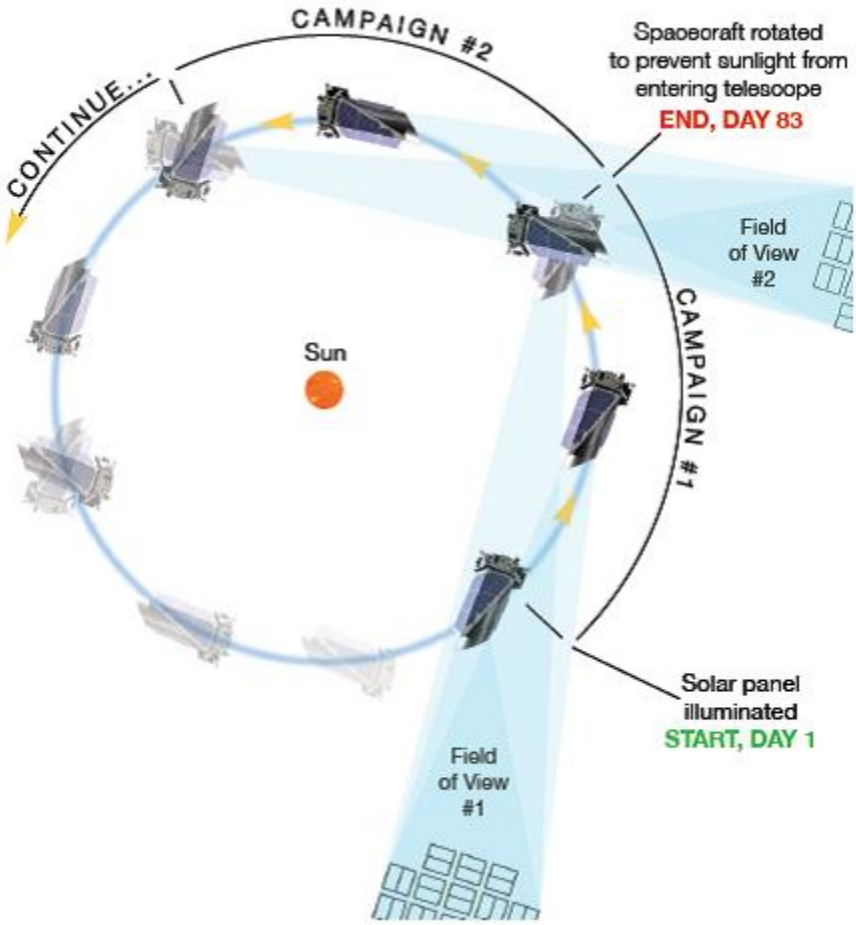

Figure 8 K2 Mission Campaigns, from [10]

F. K2 SCIENCE CAMPAIGNS

Referring to Figure 9 which shows a breakout of the schedule for a proposed campaign, a K2 science campaign starts when the target field comes into view. Before science begins, a checkout period will be implemented to upload target tables and the attitude control system will be configured for the campaign. Once completed, the spacecraft will be reoriented to the science attitude in the ecliptic plane to collect pointing and alignment data that is downlinked to the ground. The pointing and alignment data is analyzed by the ground segment and adjustments to the configurations are made as needed prior to commencing science observations for the campaign. Data from the science observations will be stored onboard until the end of the campaign and downlinked using the HGA before the next campaign begins [10].

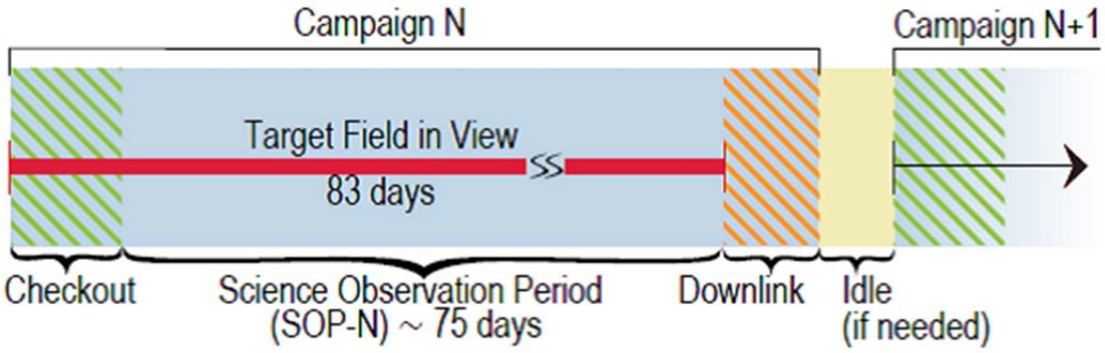

Figure 9 Campaign Breakout, from [10]

In this new arrangement, K2 is expected to observe 10,000–20,000 targets per campaign, with the science community requesting specific targets. Possible targets include exoplanets, asteroseismology, extra galactic, binary stars, stellar activity, and open clusters. In addition, it is expected that K2 and another deep space telescope like Spitzer or Chandra will make coordinated observations of starspots and flares in a few young clusters of stars [11]. To date, twelve clusters have been proposed for the ten campaigns that have been scheduled and these are listed in Table 1. The locations of the campaign fields planned through FY16 are shown in Figure 10.

Cluster	Age (Myr)	Distance (pc)	Proposed Campaign
Taurus (Gould's Belt)	2	140	4
Upper Sco	10	130	2
M21	12	1200	9
M18	32	1300	9
M25	92	620	9
M35	100	800	0
M45 (Pleiades)	125	135	4
NGC 1647	144	540	10
NGC 6716	150	547	7
Hyades	630	46	4
M44 (Praesepe)	630	160	5
M67	3600	908	5

Table 1 Campaign Area of Observation, from [11]

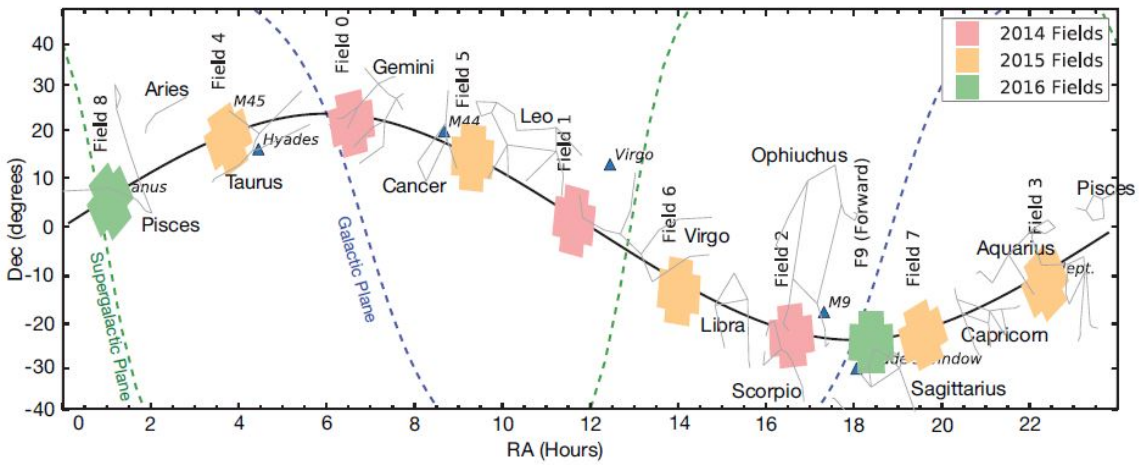

Figure 10 K2 Observation Locations for Each Campaign, from [10]

G. PRIORITIZED MISSION OBJECTIVES

To maximize the usage of the Kepler asset, Prioritized Mission Objectives (PMO) for K2 are as follows [11]:

- Minimize fuel usage with a view of science return per kilogram of fuel
- Maximize the number of targets available per campaign
- Gather and return photometric observations on peer-reviewed targets
- Provide a target catalog, calibrated focal plane pixels, time-series target photometry and spacecraft attitude history to a publicly accessible mission archive
- Support science exploitation by:
  - Providing community support via documentation, open-source software, and a mission help desk
  - Providing a funded Guest Observer program
  - Performing systematic noise reduction in the target photometry and archiving lists of transit events and diagnostics for validating them as planet candidates or false positives

The first PMO is to minimize fuel usage. As of December 2013, the Kepler satellite had only 5.6 kg of fuel left aboard. Due to the reduced capacity of the RWAs, fuel must now be expended for maneuvering and pointing the spacecraft. Thus, improving the fuel efficiency of the vehicle is a high priority area.

H. OPPORTUNITIES FOR IMPROVEMENT

The current fuel budget for K2 is shown in Table 2. As is shown, the K2 mission can currently support only 12 campaigns. Due to the fact that Kepler operates using legacy control concepts, there may be opportunites to reduce the fuel consumption of the satellite, prolonging the K2 mission beyond 12 campaigns. Obvious candidates are to reduce the amount of fuel expended during momentum management activities, or conduct fuel efficient two-RWA maneuvers. Both of these possible fuel saving techniques can be explored using optimal control.

	Event	# of Events	Thruster-seconds per Event	Thruster-seconds Total	
				w/o Break	w/ Break
Science Campaign	Maneuver to Ecliptic	1	26.8	27	27
	Wheel Resaturation	41	12.7	515	515
	Post-Resaturation Tweaks	41	1.3	52	52
	Drift Tweaks	81	0.8	62	62
	Maneuver to Earth-point	1	23.0	23	23
	Earth-point Dwell/Data Downlink (hours)	36	2.8	102	102
	Safemode Contingency Allowance	0.34	126.1	126	126
	Mid-Campaign Break	1	137.0		137
	Science Campaign Total			**907**	**1044**
	Available Fuel			11345	11345
	Number of Campaigns			**12.5**	**10.9**

Table 2 Thrust Time Allocation for Each Maneuver, from [12]

I. THESIS OBJECTIVE AND SCOPE

The objective of this thesis is to explore how optimal control concepts can be used to take advantage of the nonlinearities of spacecraft rotational dynamics to reduce fuel consumption during momentum management and attitude slewing. Current methods of controlling an underactuated satellite will be compared to the optimal control approach in order to determine the potential for increasing the spacecraft life. The remainder of this thesis is organized as follows: Chapter II gives an outline of the equations that drive the problem and explains the mathematics behind the conventional control approach and the current hybrid control approach. Chapter III describes two different methods of managing spacecraft momentum and compares the benefits of each. Chapter IV explores numerous

options for momentum management within the context of the K2 mission, and Chapter V shows the feasibility of performing a large angle maneuver using only two reaction wheels with respect to the application of the K2 mission. Chapter VI concludes the thesis and summarizes ideas for future work.

THIS PAGE INTENTIONALLY LEFT BLANK

II. KEPLER ATTITUDE CONTROL MODEL

A spacecraft is able to point in a given direction and slew to different orientations according to the law of conservation of momentum. At any given time, the total amount of momentum in the spacecraft, either stored in the reaction wheels or in the angular momentum of the body of the spacecraft, must be constant in an inertial frame. Momentum exchange devices, such as reaction wheels, allow momentum to be transferred between the reaction wheels and the body of the spacecraft. If it is desired for the spacecraft to point in one direction, the momentum from the spacecraft body will be exchanged from the motion of the spacecraft, to the motion of the reaction wheels. Conversely, if a spacecraft needs to slew, the momentum in the reaction wheels can be transferred to the body of the spacecraft to cause it to rotate. The reaction wheels are also used to absorb momentum imparted on the spacecraft system from external torques, such as solar torque or the torque imparted by spacecraft thrusters. This chapter develops a mathematical model for the Kepler spacecraft that describes this process. This model forms the basis for the conventional, hybrid, and optimal control techniques described in this and in later chapters.

A. RIGID BODY EQUATIONS OF MOTION

The equation of motion for a reaction wheel spacecraft subject to torques associated with thrusters and external disturbances is:

$$J\dot{\omega} + \omega \times (J\omega + h) = T_{Thruster} + T_{dist} - T_{RW} \tag{2.1}$$

Rearranging the equation to solve for angular acceleration gives:

$$\dot{\omega} = J^{-1}[T_{Thruster} + T_{dist} - T_{RW} - \omega \times (J\omega + h)] \tag{2.2}$$

where ω is the angular velocity vector of the spacecraft, h is the angular momentum of the reaction wheels, J is the spacecraft moment of inertia tensor and $T_{Thruster}$, T_{dist}, and T_{RW}, are the torques due to the thrusters, external disturbances and reaction wheels, respectively. For Kepler the inertia tensor is [13]:

$$J = \begin{bmatrix} 642.3 & 0.84 & 0.20 \\ 0.84 & 1732.9 & -16.47 \\ 0.20 & -16.47 & 1789.8 \end{bmatrix} kg \cdot m^2 \tag{2.3}$$

The quaternion kinematics can be represented as:

$$\dot{q} = \frac{1}{2} \begin{bmatrix} 0 & \omega_3 & -\omega_2 & \omega_1 \\ -\omega_3 & 0 & \omega_1 & \omega_2 \\ \omega_2 & -\omega_1 & 0 & \omega_3 \\ -\omega_1 & -\omega_2 & -\omega_3 & 0 \end{bmatrix} * \begin{bmatrix} q_1 \\ q_2 \\ q_3 \\ q_4 \end{bmatrix} \tag{2.4}$$

B. REACTION WHEEL DYNAMICS

The dynamics of each reaction wheel are:

$$T_{RW} = \frac{dh}{dt} = \frac{d\Omega}{dt} * I_{RW} \tag{2.5}$$

The reaction wheel alignment matrix, relates wheel to the principal body axes of the spacecraft [14]. The alignment matrix for a four reaction wheel configuration is:

$$Z_{RW} = \begin{bmatrix} a & -a & a & -a \\ b & b & b & b \\ c & c & -c & -c \end{bmatrix} \tag{2.6}$$

where a=0.574, b=0.485, and c=0.660 [9].

The momentum vector for the reaction wheels in the wheel frame may be written as:

$$\bar{h} = \begin{bmatrix} h_1 \\ h_2 \\ h_3 \\ h_4 \end{bmatrix} \tag{2.7}$$

Thus, the momentum in the spacecraft body frame is:

$$h = Z_{RW} * \bar{h} \tag{2.8}$$

The torque applied by the reaction wheels is defined as the time rate of change of momentum stored in the reaction wheels. Therefore, the torque applied by the RWAs in the reaction wheel frame is shown in Equation (2.9), where u_1-u_4 are the individual reaction wheel torques.

$$\dot{h} = Z_{RW} T_{RW} = Z_{RW} \begin{bmatrix} u_1 \\ u_2 \\ u_3 \\ u_4 \end{bmatrix} \tag{2.9}$$

C. THRUSTER EQUATIONS

The torque on the spacecraft body resulting from the thruster is:

$$\tau = r \times F \tag{2.10}$$

where r is the distance of each individual thruster from the center of mass of the spacecraft, and F is the force vector each thruster imparts on the spacecraft. Similar to the reaction wheel alignment matrix, the torque component of each thruster can be expressed via a thruster alignment matrix. Since Kepler has 8 thrusters each with an x, y and z component, the alignment matrix is:

$$Z_{Thruster} = \begin{bmatrix} -X1 & X2 & -X2 & X1 & -X1 & X2 & -X2 & X1 \\ Y1 & -Y2 & Y2 & -Y1 & -Y1 & Y2 & -Y2 & Y1 \\ -Z1 & Z2 & Z2 & -Z1 & Z1 & -Z2 & -Z2 & Z1 \end{bmatrix} \tag{2.11}$$

The external torque applied by the thrusters is transformed to the x, y and z axes of the spacecraft body by Equation (2.12), where control u_5-u_{12} are the commanded thruster force values for each individual thruster given in the thruster frame:

$$T_{Thruster} = Z_{Thruster} \begin{bmatrix} u_5 \\ u_6 \\ u_7 \\ u_8 \\ u_9 \\ u_{10} \\ u_{11} \\ u_{12} \end{bmatrix} \tag{2.12}$$

D. SOLAR TORQUE

Solar torque is the dominant external disturbance for the Kepler spacecraft and is imparted on the spacecraft due to the nonsymmetrical shape of the vehicle body. The formula for the individual component of the solar torque vector is calculated as shown [15]:

$$T_s = PAL(1+q) \tag{2.13}$$

For the above equation, T_s is the solar torque on the spacecraft caused by a surface A, where units are in N-m, P is the solar pressure in Earth orbit, where the value is 4.59*10–^{6} N/m^2, A is the area of surface projected to the Sun line normal, with units of m^2, L is the distance from the centroid of the surface to the center of mass of the spacecraft, where units are in m, and q is a unitless reflectance factor between 0 and 1. Each component is calculated and the values around each axis are summed together to create a solar torque vector.

E. ATTITUDE CONTROL EQUATIONS

For the conventional control model, an eigenaxis quaternion error feedback model was used for attitude control [16]. The error quaternions are calculated in Equation (2.14). In this equation, the values with the subscript "c" are the commanded quaternions and the non-lettered subscripted quaternions are the actual position of the spacecraft.

$$\begin{bmatrix} q_{1e} \\ q_{2e} \\ q_{3e} \\ q_{4e} \end{bmatrix} = \begin{bmatrix} q_{4c} & q_{3c} & -q_{2c} & -q_{1c} \\ -q_{3c} & q_{4c} & q_{1c} & -q_{2c} \\ q_{2c} & -q_{1c} & q_{4c} & -q_{3c} \\ q_{1c} & q_{2c} & q_{3c} & q_{4c} \end{bmatrix} \begin{bmatrix} q_1 \\ q_2 \\ q_3 \\ q_4 \end{bmatrix} \tag{2.14}$$

For computing a control torque, the quaternion error matrix is truncated to only include the first three elements of (2.14).

$$q_E = \begin{bmatrix} q_{1e} \\ q_{2e} \\ q_{3e} \end{bmatrix} \tag{2.15}$$

The commanded torque can then be calculated using Equation (2.16), where K_P and K_D are the proportional and derivative gains, respectively. The cross product term is a gyroscopic term that enables the controller to null the gyroscopic torque that occurs during a rotational maneuver [16].

$$T = -K_P J q_E - K_D J\omega + \omega \times J\omega \tag{2.16}$$

For fine pointing, an integrator with gain K_I is typically added:

$$T = -K_P J q_E - K_D J\omega + \omega \times J\omega + K_I \int q_E dt \tag{2.17}$$

A torque command is then calculated that is proportional to the attitude error and damping is added from rate feedback. The integrator portion zeroes the steady state error due to disturbances. The torque command is then sent to either thrusters or reaction wheel assemblies. If the torque command is given in the spacecraft body frame, the allocation of the commanded torque to the RWAs is typically calculated using a pseudo-inverse mapping [14]:

$$Z^+ = Z^T (ZZ^T)^{-1} \tag{2.18}$$

F. THRUSTER ALLOCATION

In order to allocate commanded torque to the thrusters, logic different than the pseudo-inverse must be used. Unlike the reaction wheel allocation, the pseudo-inverse method cannot be used as the calculation may yield a negative result, which is not

possible as an individual thruster can only fire in one direction. There are many methods to allocate thrusters, but the method used here was the approach given in [16].

In this approach, the goal is to minimize fuel expended by balancing the momentum equations using the constraints shown in Equation set (2.19).

$$
\begin{aligned}
&J\Delta\omega = \sum_{j=1}^{n} a_j \Delta t_j \\
&J\Delta\omega = \min \sum_{j=1}^{n} c_j x_j \\
&Ax = b \\
&x \geq 0 \\
&Where: \\
&a_j = \text{torque vector of the } j_{th} \text{ thruster} \\
&c_j = j_{th} \text{ jet flow rate} \\
&x_j = \Delta t_j = \text{ jet on time}
\end{aligned}
\tag{2.19}
$$

Term $J\Delta\omega$ in (2.19) is the change in momentum of the spacecraft and term $\Sigma\, a_j \Delta t_j$ from thruster j-1 to thruster n is the sum of the momentum produced by the thrusters given their locations, a_j, from the center of mass and the amount of time, Δt_j, each thruster is on. To solve (2.19), the first step is to write the equation in the form of Ax=b:

$$
\begin{matrix} A & & x & & b \end{matrix}
\qquad
\left[Torque(3x8)\right]\left[\Delta t(8x1)\right] = \left[desired\_net\_Torque(3x1)\right]
\tag{2.20}
$$

Next, the torque matrix, A, is split up into two matrices consisting of a 3x3 matrix $\hat{A}$, and a 3x8 matrix $\tilde{A}$, as shown in Equation (2.21). $\hat{A}$ represents the alignments of the selected thrusters and $\tilde{A}$ are the unused alignments of the thrusters for the current iteration.

$$
\left[Torque(3x8)\right] = \left[\begin{matrix} \hat{A} & \tilde{A} \end{matrix}\right]
\tag{2.21}
$$

The next step in the algorithm of [16] is to determine if the rank of $\hat{A}$ is equal to 3. If it is, the currently selected thruster set is kept for further analysis. If not, the matrix is discarded and the algorithm proceeds to the next iteration. The third step is to determine the mass flow, which for three identical thrusters is:

$$\hat{c} = \dot{m}\begin{bmatrix}1 & 1 & 1\end{bmatrix} \tag{2.22}$$

Next, the vector of mass flows is multiplied by the inverse of the $\hat{A}$ matrix:

$$\lambda = \hat{c} * \hat{A}^{-1} \tag{2.23}$$

Following the computation of (2.23), a check to verify that the current iteration is indeed a candidate as an optimal solution by using Equation (2.24). If any values in the 'check' vector are greater than one, the results are discarded and the next iteration begins.

$$check = \lambda^T * \tilde{A} \tag{2.24}$$

Next, the Candidate Optimal Group (COG) is calculated in Equation (2.25), where *b* is the desired torque from Equation (2.20).

$$\text{COG}=\text{b} \bullet \lambda \tag{2.25}$$

The thruster on times, $x_i = \Delta t_j$ are then calculated. Since $\hat{x} = \hat{A}^{-1}b$ and $\tilde{x}=0$, $\Delta\hat{t} = \hat{A}^{-1}x$ and $\Delta\tilde{t}=0$. The times $\Delta\hat{t}$ and $\Delta\tilde{t}$ are then mapped back to the corresponding thruster. The process described above is repeated for each combination of thrusters. In the case of Kepler, it is 8 choose 3, or 56 combinations, and all the permutations must be checked. The solution is the one where $\Sigma\hat{x}$ is the smallest. The above method assumes that translation is allowed during the maneuver. Translation occurs when the force due to the thrusters is not equal to zero along the x, y, or z axis. For Kepler, it is assumed that translation of the satellite due to thrusting will not significantly change the satellite's orbit. To illustrate the validity of this assertion, assume that all the fuel was expended by one thruster and all in the same direction. Then the equation for the change in velocity of the spacecraft is given by Equation (2.26). Solving for ΔV, as shown in Equation (2.27), the resulting change in velocity is only 10.98 m/s. Looking at Equation (2.28), the circular velocity of the satellite is calculated to be three orders of magnitude larger than the change in velocity of the satellite. Therefore, it is quite reasonable to assume that any change in velocity due to uneven firing of the thrusters is negligible.

$$\frac{\Delta m}{m} = 1 - e^{-\frac{\Delta V}{I_{sp} g_0}}$$

$$\begin{aligned} &Where: \\ &\Delta m = 5.6\ kg \\ &m = 1045\ kg \\ &I_{sp} = 208.3\ s \\ &g_0 = 9.806\ \frac{m}{s^2} \end{aligned} \tag{2.26}$$

$$\Delta V = 10.98\ \frac{m}{s} \tag{2.27}$$

$$V_{circular} = \sqrt{\frac{\mu_{sun}}{r_{orbit}}} = \sqrt{\frac{32,712,000,000\ \frac{km^3}{s^2}}{146,600,000\ km}} = 29.784\ \frac{km}{s} \tag{2.28}$$

If the translational motion must be null, the same method for finding the thruster allocation can be used but with the following changes:

$$\begin{aligned} &\text{A} \qquad \text{x} \qquad \text{b} \\ &\begin{bmatrix} Torque(3x8) \\ Force(3x8) \end{bmatrix} [\Delta t] = \begin{bmatrix} desired\_net\_Torque \\ desired\_net\_Force \end{bmatrix} \\ &\begin{bmatrix} Torque(3x8) \\ Force(3x8) \end{bmatrix} = \begin{bmatrix} \hat{A} & \tilde{A} \end{bmatrix} \\ &\text{If rank}(\hat{A}) = 6 \text{ then keep} \\ &\hat{c} = \dot{m}[1 \quad 1 \quad 1 \quad 1 \quad 1 \quad 1] \\ &\lambda = \hat{c} * \hat{A}^{-1} \\ &check = \lambda^T * \tilde{A} \text{ if any values are >1 not an optimal solution} \\ &\text{COG=b} \bullet \lambda \\ &\hat{x} = \hat{A}^{-1} b \text{ and } \tilde{x} = 0 \text{ therefore } x = \begin{bmatrix} \hat{x} \\ \tilde{x} \end{bmatrix} \\ &\text{Repeat process for each combination of } \begin{bmatrix} \hat{A} & \tilde{A} \end{bmatrix} \\ &\text{Solution is one with max COG (min sum of x)} \end{aligned} \tag{2.29}$$

The pulse times, Δt_j, from the thruster allocation algorithm are then fed into a pulse width modulator (PWM). A pulse width modulator converts a commanded torque

that has a value smaller or larger than the torque provided by a thruster in the on position by operating the thruster in a full on position for an amount of time that provides the same desired change in momentum to the system. The PWM was developed using the method in Wie [16] and ideas from [17]. The basic principle for the implementation of a PWM uses Equation (2.30).

$$T_{thruster}\Delta t_{on} = T_{required}\Delta t_{PWM} \tag{2.30}$$

An example of how a PWM works is shown in Figure 11. In this example, the maximum torque provided by a thruster set that can fire in both directions around the particular axis is ± 2 Nm. The commanded torque may, however, may be smaller or larger than this value. To realize (2.30), the PWM pulses the thrusters in a manner that attempts to match the area under the PWM curve with the area under the commanded torque curve within the limits of the thruster capabilities.

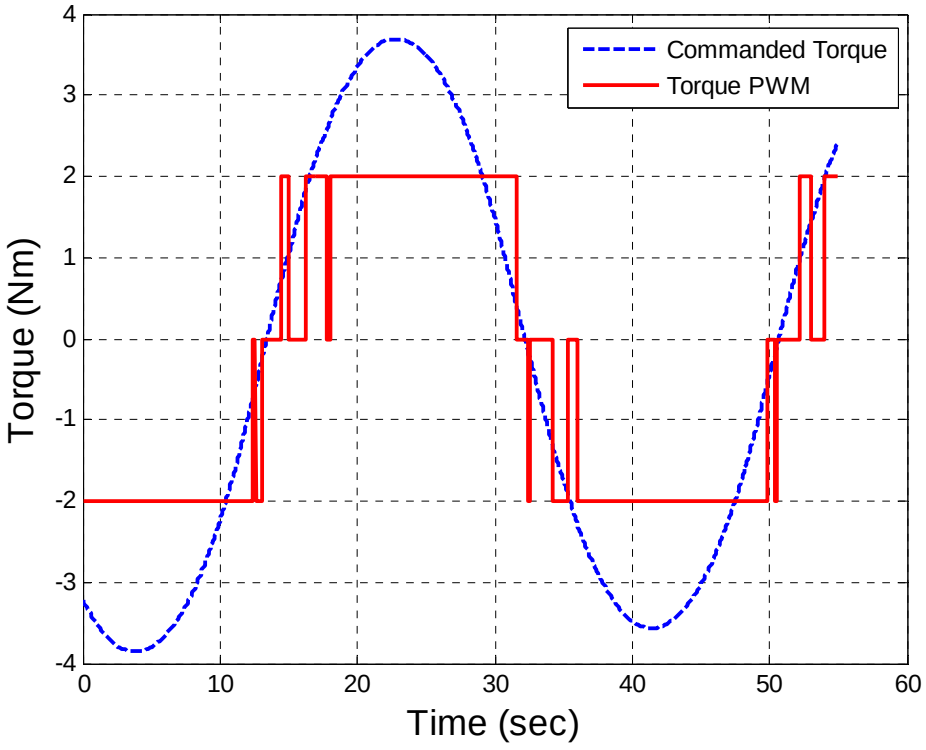

Figure 11 Sample of Pulse Width Modulation

G. CONVENTIONAL CONTROL SYSTEM SIMULATION

The modeled Kepler attitude control system is shown in Figure 12. The plant block represents Equations (2.2) and (2.4). The eigenaxis quaternion feedback block represents Equations (2.14), (2.15), and (2.16). The thruster logic block represents Equations (2.12), (2.19) to (2.25), and (2.30). The reaction wheel logic block represents Equation (2.5) to (2.9), and (2.18). The external torque block represents the solar torque as given by Equation (2.13).

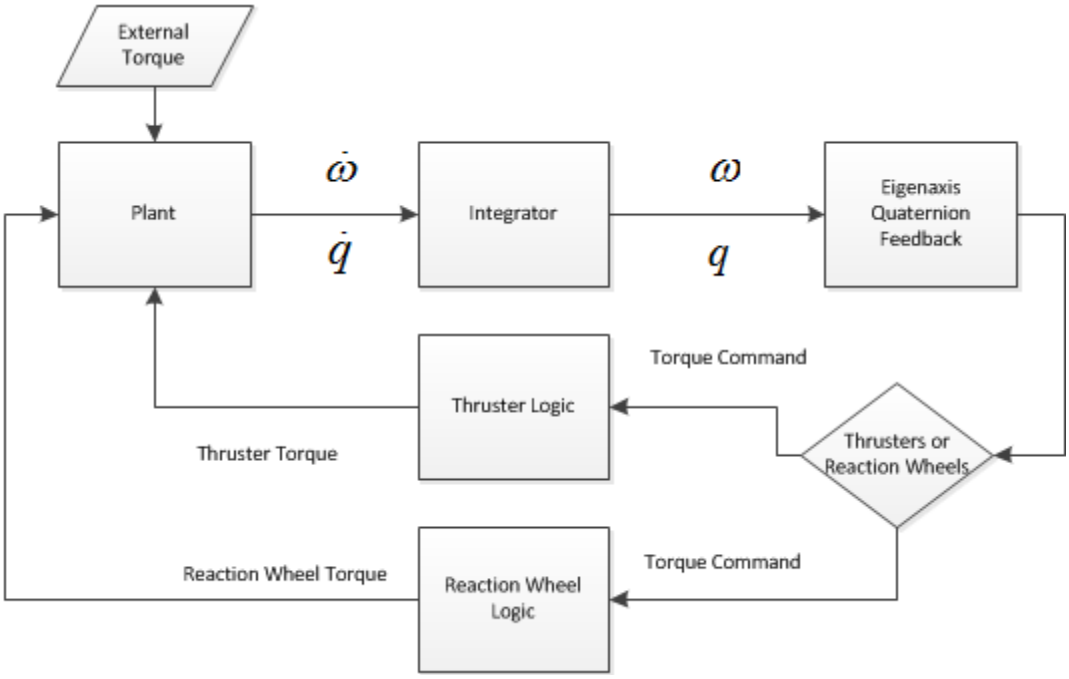

Figure 12 Plant Block Diagram

As per Figure 12, using Matlab/Simulink, a baseline model of the Kepler spacecraft was developed. The Kepler maneuver shown in Figure 5 was then performed using the model, assuming all four reaction wheels were available for the maneuver. Figure 13 shows the simulated maneuver which indicates that the model developed behaves similarly to the Kepler telemetry.

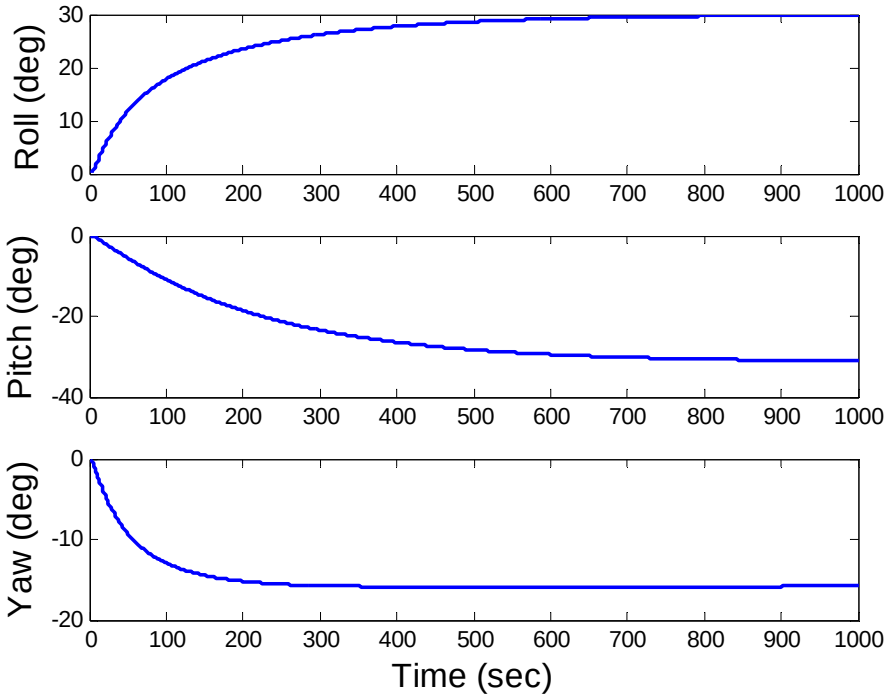

Figure 13 Maneuver from Earth Point to Science Point with 4 RWAs Using Conventional Attitude Control: Euler Angles

The same maneuver was simulated again, using the same conventional control system. However, in this case, RWA2 and RWA4 were disabled to simulate the current failed status of the Kepler spacecraft. Figure 14 shows that with a conventional attitude control system, the spacecraft cannot complete the maneuver even over a longer time horizon. This is because conventional control algorithms fail to work properly for an underactuated satellite. Other methods of attitude control need to be developed.

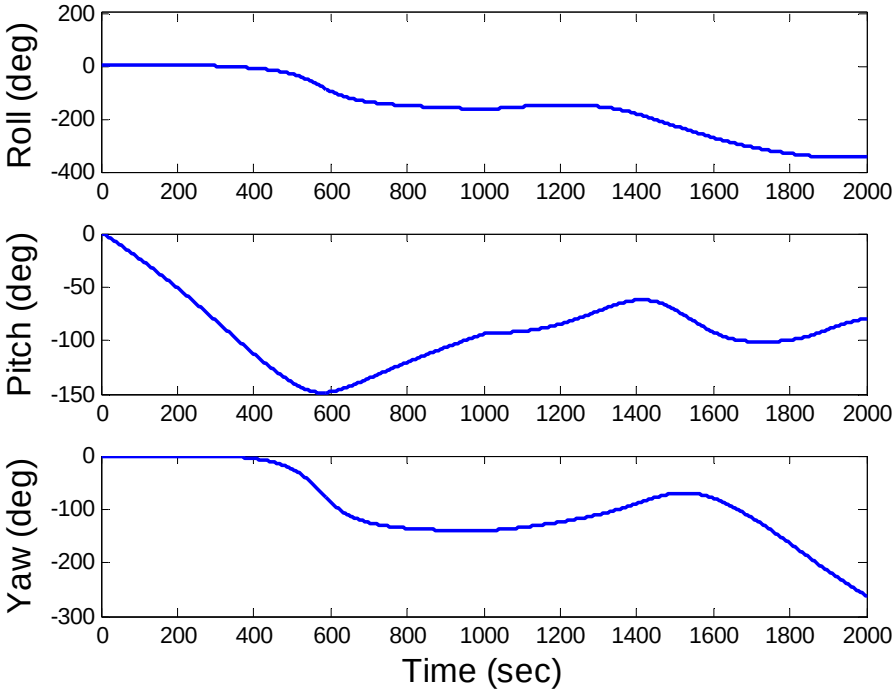

Figure 14 Failed Maneuver from Earth Point to Science Point with 2 RWAs Using Conventional Attitude Control: Euler Angles

H. K2 HYBRID CONTROL CONCEPT

Hybrid control has been investigated for the use in satellites that are underactuated if only the reaction wheels or the thrusters are used [9]. Hybrid control combines the use of two or more actuation systems to provide the three axes stabilization required to operate a satellite. The current solution for the Kepler K2 mission is to use a hybrid control in the following way. First, momentum is loaded evenly onto two wheels to gyroscopically stabilize the third axis. Next, the satellite is oriented in a way that minimizes disturbance torques about the other two axes [9]. Finally, the operational reaction wheels, RWA1 and RWA3, on Kepler are used for momentum stabilization of the spacecraft around two of the spacecraft axes. In order to stabilize around the selected axes, an allocation matrix must be developed to appropriately allocate reaction wheel torques. One approach for determining an allocation matrix can be developed as follows [18].

First, assume the spacecraft moment of inertia tensor is simplified as shown in Equation (2.31)

$$J = \begin{bmatrix} J_x & 0 & 0 \\ 0 & J_y & 0 \\ 0 & 0 & J_z \end{bmatrix} \tag{2.31}$$

Next, assume that the momentum of the operational wheels will be the same but biased in opposite directions as shown in Equation (2.32). This will introduce a gyroscopic force that stiffens the spacecraft against disturbance toques and allows the spacecraft to absorb torques around those axes. Note that since the bias momentum will be reduced as the solar torque is absorbed, it is necessary to periodically re-bias the wheels. This operation must be done using thrusters and thus presents an opportunity for optimizing fuel usage. This will be investigated in later chapters.

$$\bar{h} = \begin{bmatrix} h \\ -h \end{bmatrix} \tag{2.32}$$

The notation for the reaction wheel alignment matrix is as follows for the Kepler satellite with the two operational reaction wheels.

$$Z_{RW} = \begin{bmatrix} a & a \\ b & b \\ c & -c \end{bmatrix} \tag{2.33}$$

From the above equations, the momentum is:

$$h = Z_{RW} * \bar{h} \tag{2.34}$$

Similarly, the torque provided by the reaction wheels is shown in Equation (2.35).

$$T_{RW} = Z_{RW} * \begin{bmatrix} u_1 \\ u_2 \end{bmatrix} \tag{2.35}$$

The external torque acting on Kepler is the solar torque.

$$T_{ext} = \begin{bmatrix} \tau_{sx} \\ \tau_{sy} \\ \tau_{sz} \end{bmatrix} \tag{2.36}$$

The equation for angular rate is found, as before, by rearranging Euler's equation as shown in Equation (2.37).

$$\dot{\omega} = J^{-1}[\mathrm{T}_{\mathrm{ext}} - \mathrm{T}_{\mathrm{RW}} - \omega \times (J\omega + h)] \tag{2.37}$$

Euler's equations are now expanded into the three axis components. Note here that it is not necessary for Equation (2.31) to be diagonal; however, the assumption simplifies the presentation of the results.

$$\begin{aligned}
\dot{\omega}_x &= \frac{1}{J_x}[(J_y - J_z)\omega_y\omega_z - 2ch\omega_y - a(u_1 + u_2) + \tau_{sx}] \\
\dot{\omega}_y &= \frac{1}{J_y}[(J_z - J_x)\omega_x\omega_z + 2ch\omega_x - b(u_1 + u_2) + \tau_{sy}] \\
\dot{\omega}_z &= \frac{1}{J_z}[(J_x - J_y)\omega_x\omega_y + c(u_2 - u_1) + \tau_{sz}]
\end{aligned} \tag{2.38}$$

Next assume that the y and z axes are to be stabilized to get:

$$\begin{aligned}
\omega_y &= \omega_z = 0 \\
\dot{\omega}_y &= \dot{\omega}_z = 0
\end{aligned} \tag{2.39}$$

Rearranging Equation (2.38) with the assumptions in Equation (2.39) gives:

$$\begin{aligned}
a(u_1 + u_2) &= \tau_{sx} \\
b(u_1 + u_2) &= 2ch\omega_x + \tau_{sy} \\
c(u_1 - u_2) &= \tau_{sz}
\end{aligned} \tag{2.40}$$

Next, derive the equations for the y and z axes as these are the two axes that are to be stabilized using the reaction wheels.

$$\begin{aligned}
b(u_1 + u_2) &= 2ch\omega_x + \tau_{sy} \\
c(u_1 - u_2) &= \tau_{sz}
\end{aligned} \tag{2.41}$$

Putting (2.41) in matrix form the equation yields:

$$\begin{matrix} A & x & = & b \end{matrix}$$

$$\begin{bmatrix} b & b \\ c & -c \end{bmatrix}\begin{bmatrix} u_1 \\ u_2 \end{bmatrix} = \begin{bmatrix} 2ch\omega_x + \tau_{sy} \\ \tau_{sz} \end{bmatrix} \tag{2.42}$$

Rearranging to solve for x it is necessary to find the inverse of A which is shown in Equation (2.43).

$$A^{-1} = \frac{1}{2}\begin{bmatrix} \frac{1}{b} & \frac{1}{c} \\ \frac{1}{b} & -\frac{1}{c} \end{bmatrix} \tag{2.43}$$

The reaction wheel torque commands for the stabilized two wheel spacecraft are therefore:

$$\begin{bmatrix} u_1 \\ u_2 \end{bmatrix} = \frac{1}{2}\begin{bmatrix} \frac{1}{b} & \frac{1}{c} \\ \frac{1}{b} & -\frac{1}{c} \end{bmatrix}\begin{bmatrix} 2ch\omega_x + \tau_{sy} \\ \tau_{sz} \end{bmatrix} \tag{2.44}$$

From (2.44), it can be seen that there are only two control torques to counter the three solar torques. (The effect of the x-axis torque appears implicitly via the non-zero rate, ω_x.) This means it will not be possible to control all three axes with reaction wheels. Control of the x-axis will require the use of thrusters to maintain that axis stationary. Continuous control, however, is undesirable because the spacecraft would quickly expend its fuel reserve as the thrusters would be nearly always on. Instead, periodic thrusts can be used to reset the accumulated drift around the roll axis.

When the inverted a matrix is mapped back into a format compatible with a four reaction wheel system, the allocation matrix can then be written as Equation (2.45):

$$Z^* = \begin{bmatrix} 0 & \frac{1}{2b} & \frac{1}{2c} \\ 0 & 0 & 0 \\ 0 & \frac{1}{2b} & \frac{1}{-2c} \\ 0 & 0 & 0 \end{bmatrix} \tag{2.45}$$

The torque command sent to the reaction wheels is then written as Equation (2.46) where T_c is the commanded torque from the eigenaxis quaternion feedback control system.

$$u_{RW} = Z^* T_c \tag{2.46}$$

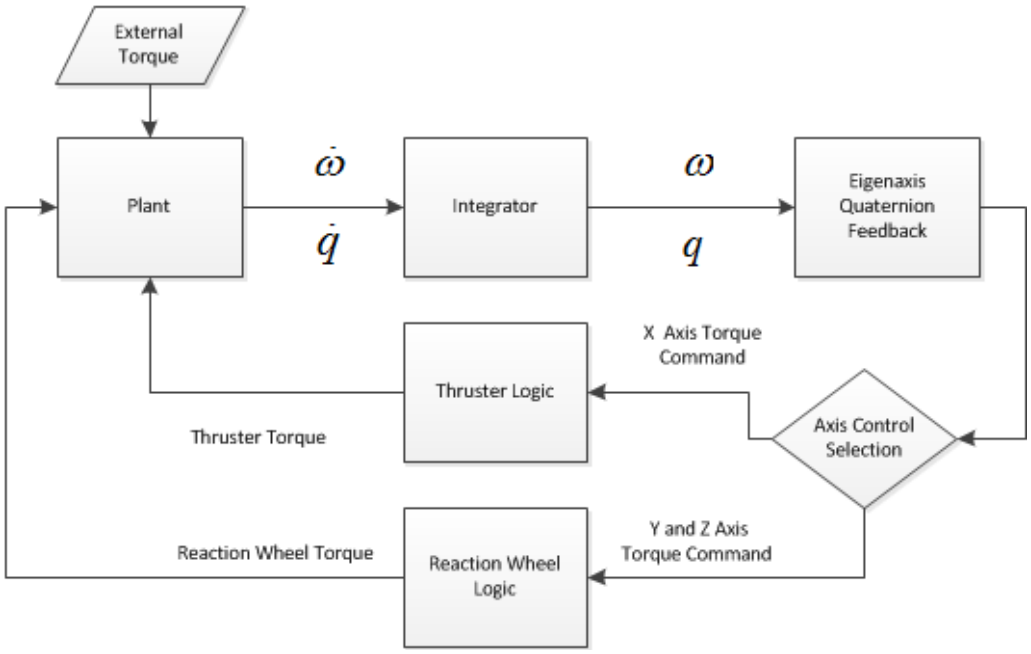

Figure 15 Hybrid Control Block Diagram

A complete block diagram of the hybrid control system is shown in Figure 15. As seen in Figure 15, the x-axis is controlled using thrusters, which expends fuel and shortens mission life. Also, due to assumption that the spacecraft is not moving or accelerating, this model only holds for a spacecraft pointing where there is no rotational motion. The hybrid control cannot be used for large angle maneuvers to reorient the spacecraft. The next chapters will address the latter issue using optimal control methods. As shown in this chapter, conventional methods of controlling a satellite work well when the satellite has at least three reaction wheels, however, if a satellite becomes underactuated, other methods of attitude control, such as hybrid or optimal control, are needed.

III. MOMENTUM MANAGEMENT USING THRUSTERS

Any spacecraft operating in the space environment will experience the effects of all the external torque placed on it. In order to counteract this torque, momentum exchange devices, such as reaction wheels are used. Over time the reaction wheels build up/lose momentum in response to the external torque input and in turn need to be returned to their initial state. This momentum management is done by imparting an additional control torque on the spacecraft. For spacecraft in a magnetic field, like those near the earth, magnetic torque rods can be used. For spacecraft outside of the earth's magnetic field, such as Kepler, thrusters must be used. This chapter explores two different approaches for momentum management using thrusters to establish a baseline model for later comparison with optimal control techniques.

A. COMPARISON OF TWO METHODS TO DUMP MOMENTUM

Two cases for dumping momentum will be examined. The first case is to use thrusters in the open-loop to insert/remove momentum into the system. In this case, closed-loop control of the reaction wheels is used to keep the spacecraft stable. Figure 16 illustrates this type of control system. The second approach is to change reaction wheel speeds from their initial values to a new desired value, e.g., using a ramp command. A loop closed around the thrusters respond to stabilize the spacecraft attitude. This type of control system is illustrated in Figure 17. To explore the relative merits of each approach, an example of momentum management operation is simulated. The desired changes in the reaction wheel speeds are shown in Table 3.

	RW1	RW 2	RW 3	RW 4
Initial RPM	-4573	-2500	1000	2000
Desired Final RPM	-1383	-417	486	379

Table 3 Initial and Final Reaction Wheel Speeds for Momentum Dumping Simulation

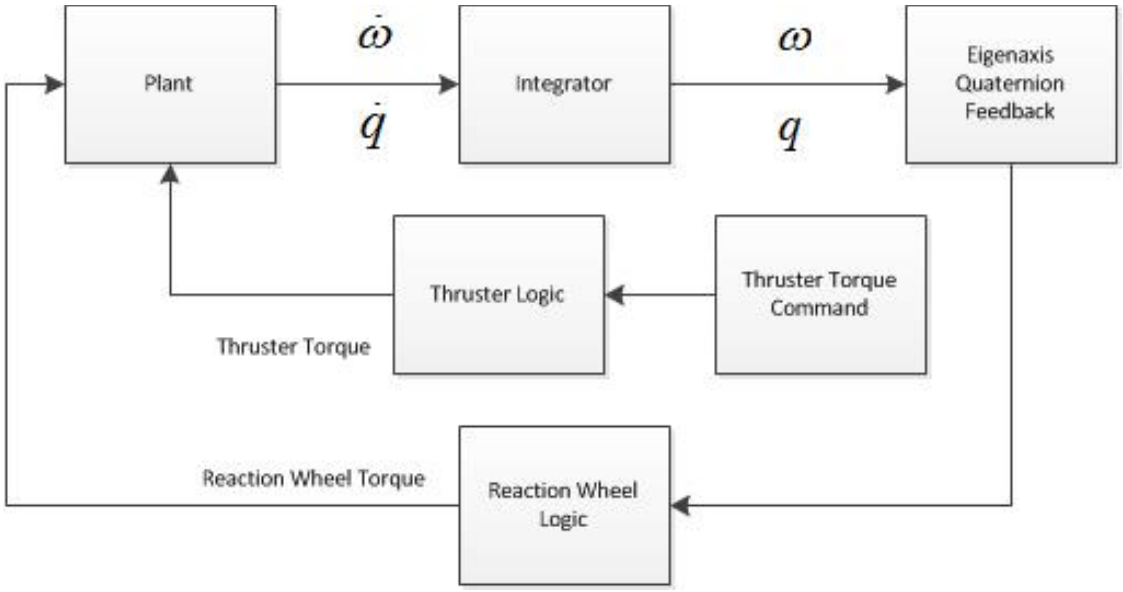

Figure 16 Momentum Management Model 1; Open-Loop Thruster Commanding

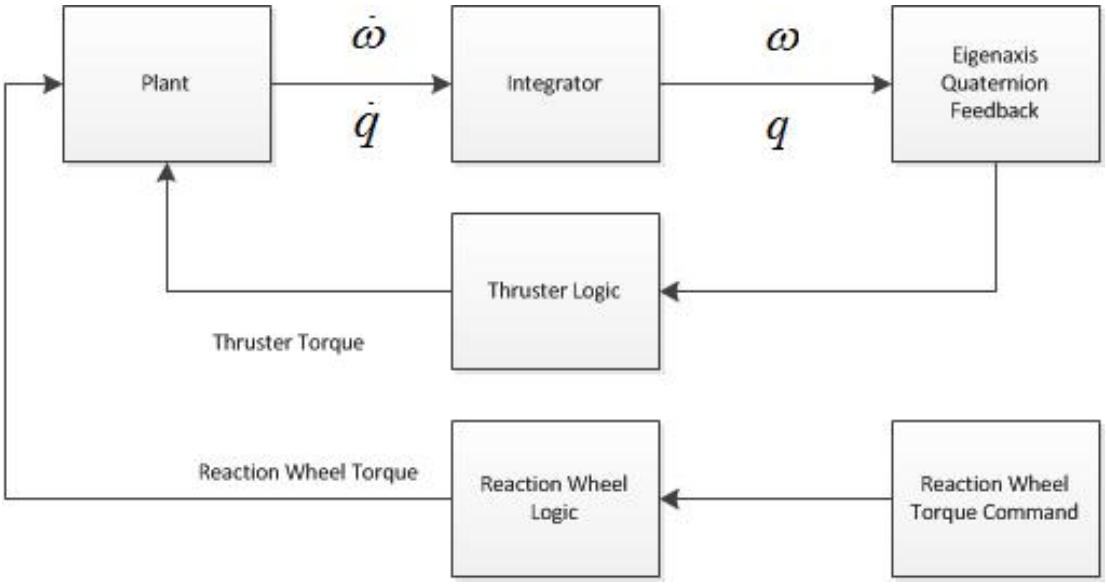

Figure 17 Momentum Management Model 2:Closed-Loop Thruster Commanding

1. Method 1: Open-Loop Thruster Commanding

In the first case, the amount of momentum that must be removed from the reaction wheel array is calculated in advance and the thruster combination required to remove the momentum from the system is determined using a static method that balances the torque applied by the reaction wheels changing speed to the torque applied by the

thrusters. This is done by balancing the momentum inserted by the thrusters to that of the reaction wheels as shown in Equation (3.1).

$$h_{thruster} - h_{RW} = 0 \tag{3.1}$$

Using the thruster allocation method in [16] explained in Chapter II by applying Equations (2.19) through (2.25), the optimal combination of thrusters and the time to fire each thruster is calculated to minimize fuel consumption. In order to change the reaction wheel speeds according to Table 3, thrusters 2, 6 and 8 were determined as the ideal combination of thrusters. Thruster pulse times of 15.17 seconds, 8.21 seconds and 16.9 seconds, respectively, are needed to remove the accumulated momentum from the reaction wheel system. To implement the momentum dump, the thrust times were divided into 10 equal pulses administered over 278 seconds. The time between each thruster pulse was used to allow the reaction wheels to react. The time selected also allowed the RWAs to remain within their torque limits and therefore respond to the torque commands provided to them. The thrusters were then kept from firing (open-loop) for the remainder of the 1000 second simulation. Figure 18 shows the selected thruster pulse allocation.

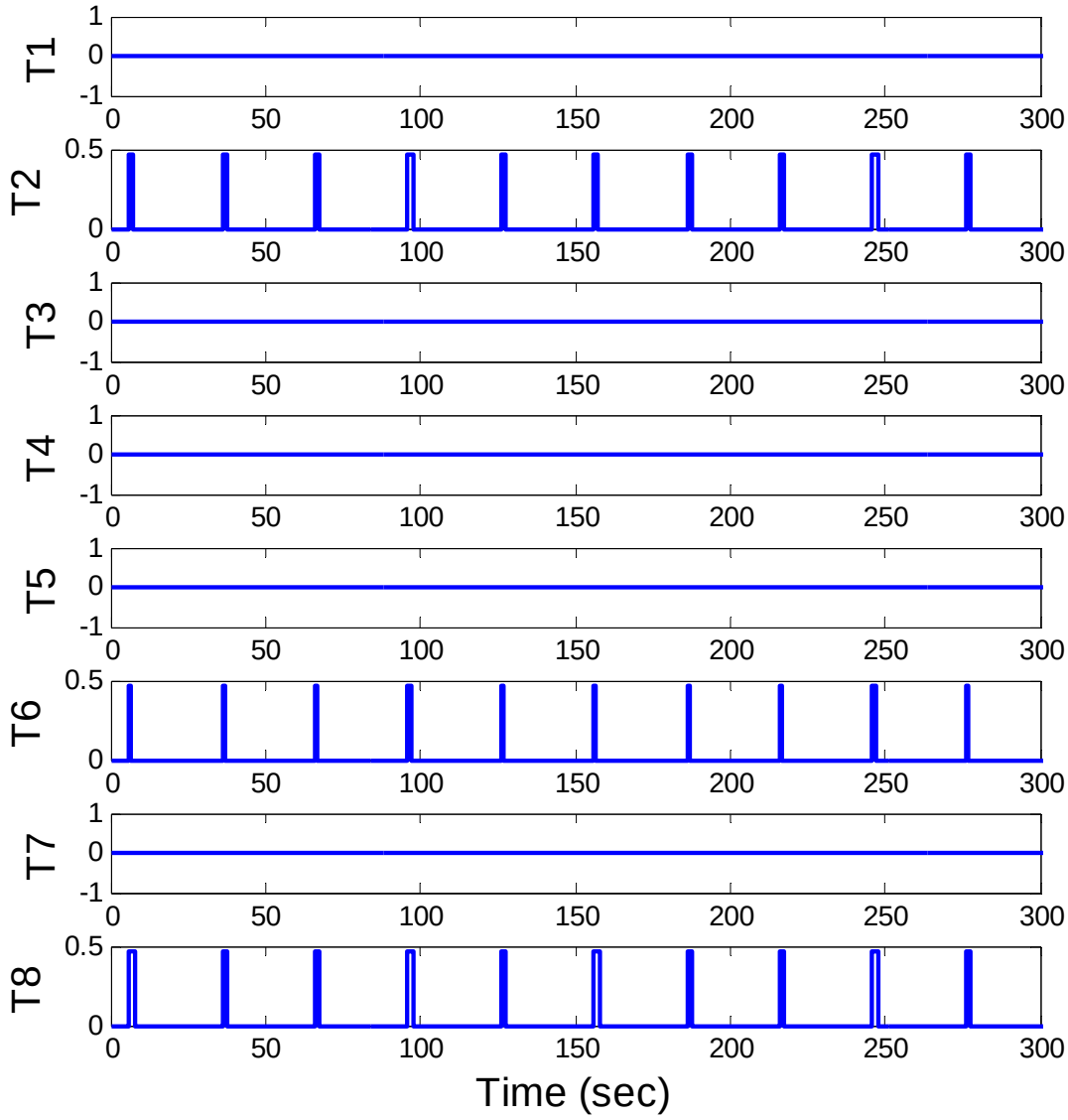

Figure 18 Thruster Pulse Allocation for Open-Loop Thruster Commanding (thruster forces given in Newtons)

The closed-loop attitude control loop around the reaction wheels then responds to the momentum inserted into the system by the thruster pulses in an attempt to keep the spacecraft pointing in the same nominal direction. Figure 19 shows response of the reaction wheel array to the open-loop thruster inputs.

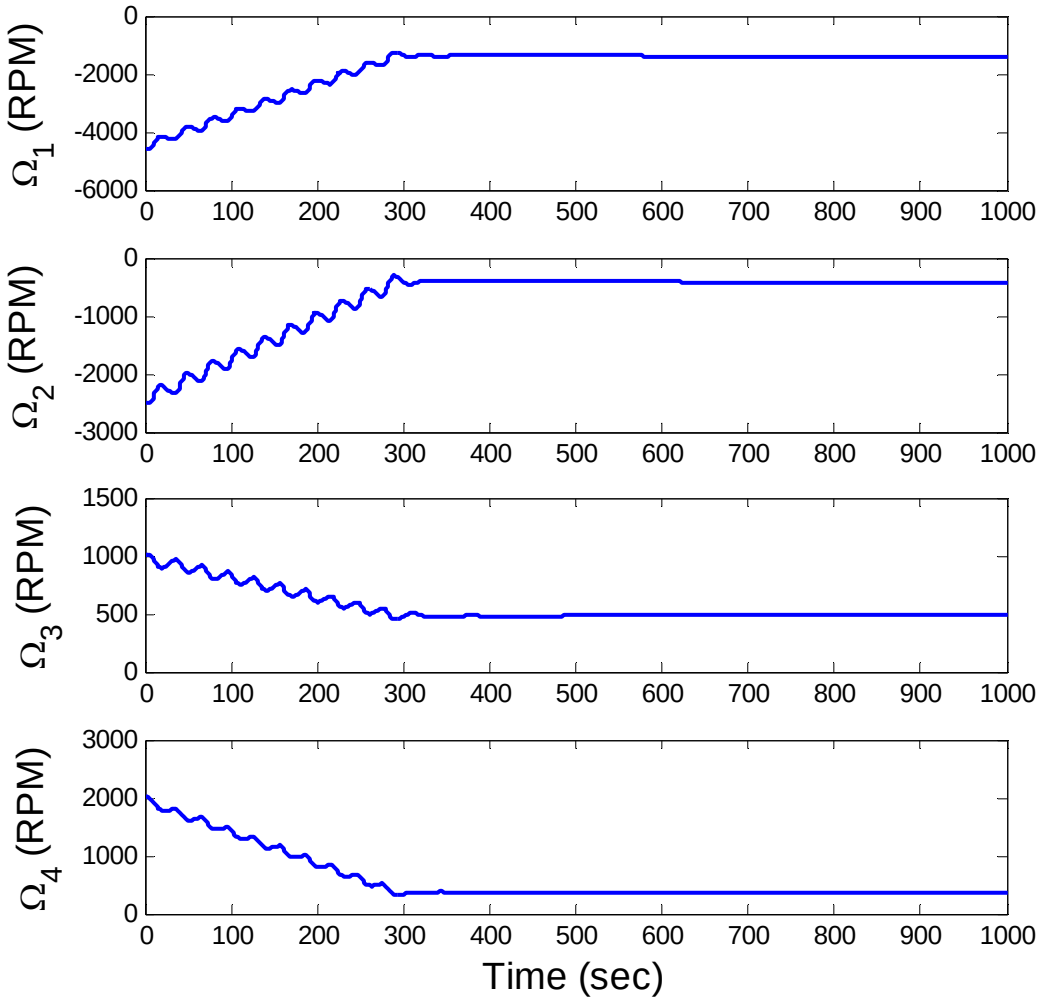

Figure 19 RWA Speeds Under Open-Loop Thruster Commanding

The cumulative effect of pulsing the thrusters correctly reduced the momentum stored in the individual reaction wheels and this, in turn, reduced their rotational velocity to the desired values. The sum total of the individual pulse times was 40.08 seconds. The accumulation of thruster pulse time is shown in Figure 20.

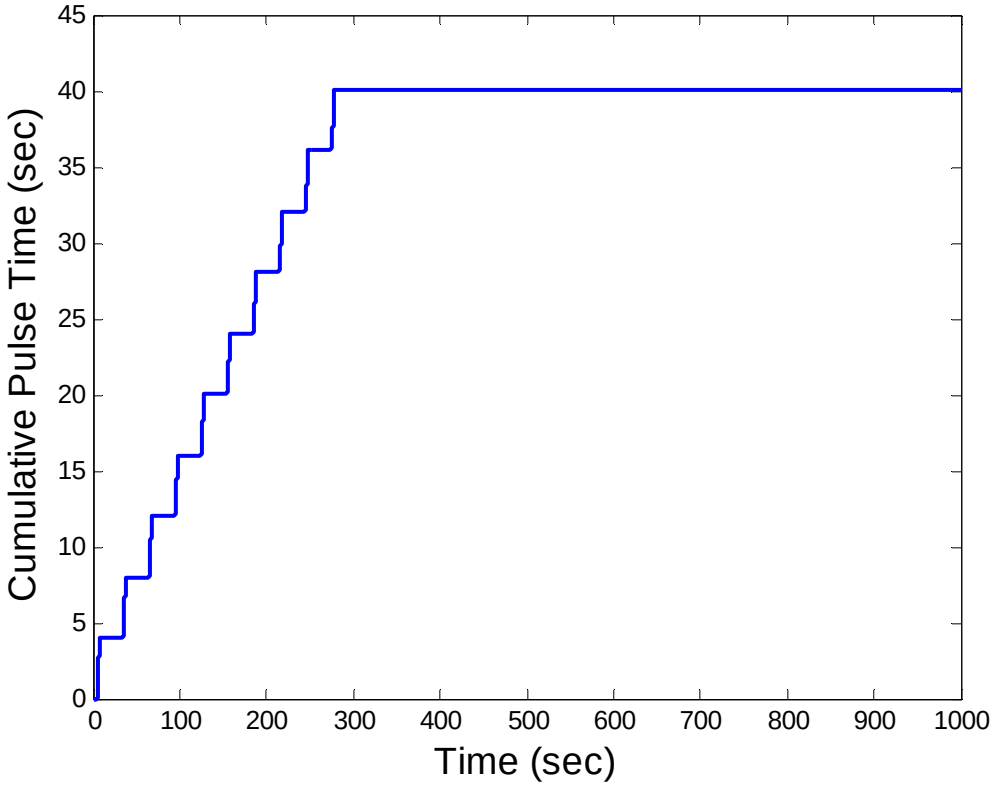

Figure 20 Cumulative Thruster Pulse Time for Open-Loop Thruster Commanding

2. Method 2: Closed-Loop Thruster Commanding

The closed-loop thruster response approach assumes that a ramp command will be applied to the reaction wheels to adjust the stored momenta to the desired values. In response to the reaction wheels, the spacecraft will begin to rotate due to the decrease in stored momentum. In order to counter this motion, the thrusters are fired to absorb momentum from the system and maintain the spacecraft pointing in the same direction. Figure 21 shows the ramp control of the reaction wheel array.

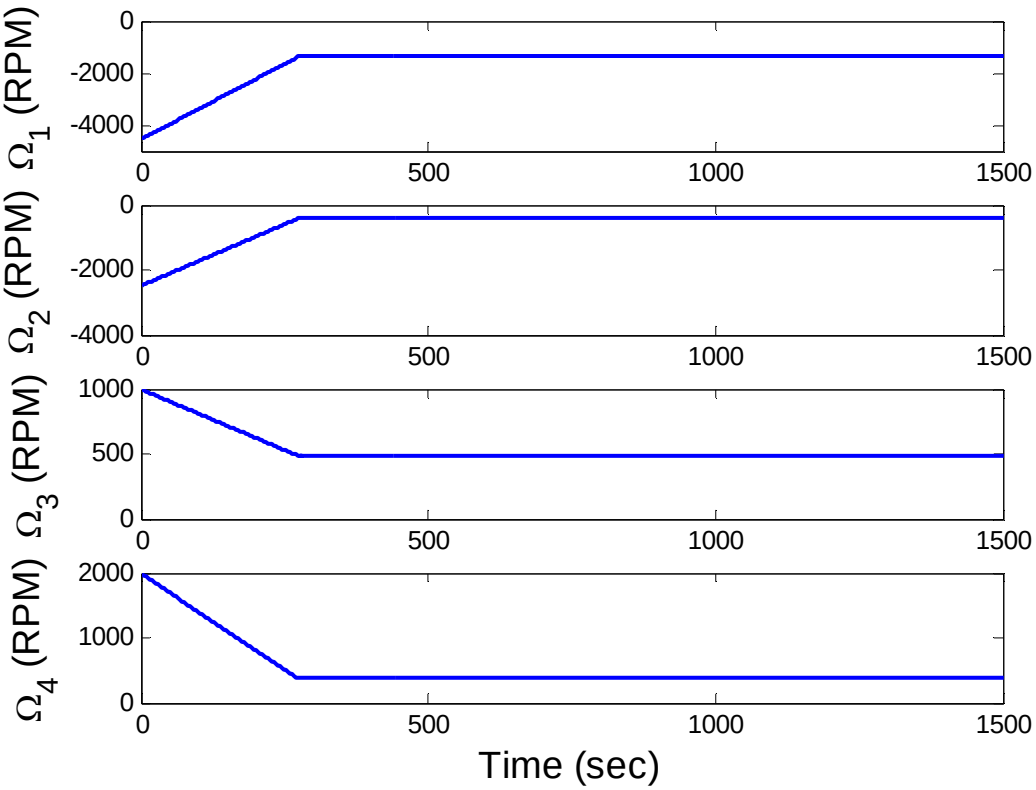

Figure 21 RWA Speeds for Closed-Loop Thruster Commanding

The thruster allocation algorithm as described in Chapter II was used to close the attitude control loop and allocated thrusters 2, 6 and 8, as before. As seen in Figure 22, however, the pulse allocation is now comprised of a larger number of smaller length pulses as compared to the open-loop approach, due to the use of the PWM. In addition, the total pulse time increased to 46.06 seconds, therefore expending more fuel to accomplish the same task as compared to the first approach. Figure 23 shows the cumulative thruster pulse time.

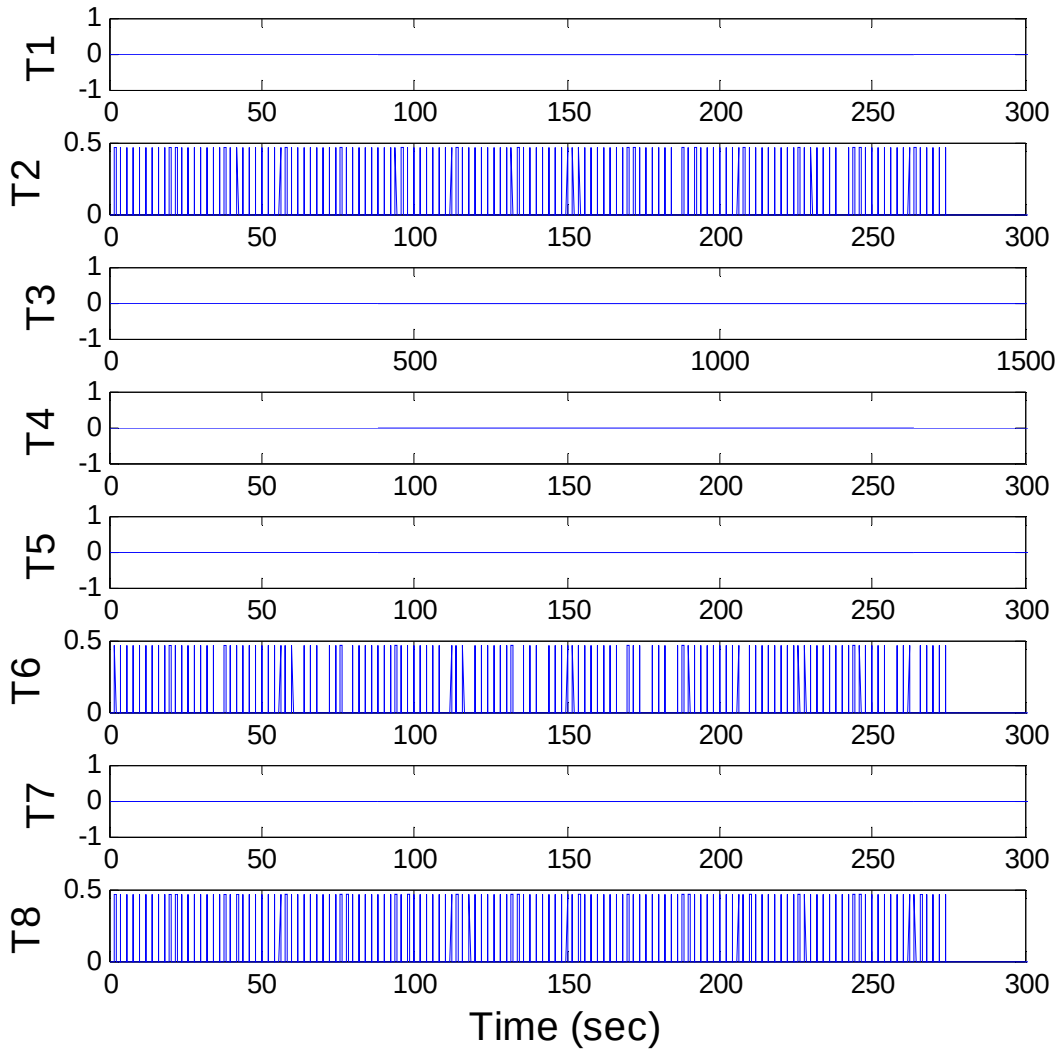

Figure 22 Thruster Pulse Allocation for Closed-Loop Thruster Commanding (thruster force given in Newtons)

Both methods for momentum dumping that were examined were able to meet the objective of reducing the reaction wheel angular velocities to their desired values. However, allowing the reaction wheels to respond to pre-determined open-loop thruster commands reduced fuel usage and also allowed the number of thruster actuations to be selected by the spacecraft operator. Because each thruster is rated for a finite number of actuations, using the open-loop approach allows for an increased life of the individual thruster. Table 4 summarizes the simulation results.

Telemetry from the K2 mission seems to indicate that the approach used for momentum management on Kepler is to operate the thrusters in the open-loop by firing the thrusters for a predetermined period of time and allowing the reaction wheels to respond to the inserted momentum. Therefore, this approach will be used in the remainder of this thesis as part of the baseline control system.

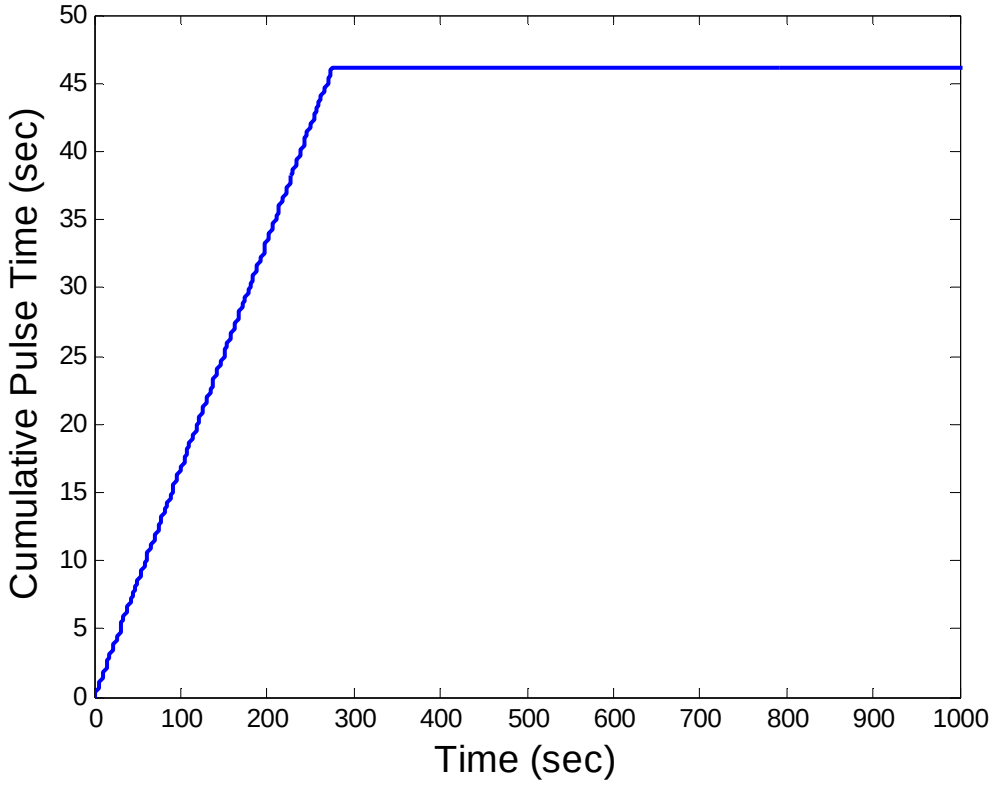

Figure 23 Cumulative Thruster Pulse Time for Closed-Loop Thruster Commanding

Approach	Thrust Time (Seconds)	Thruster Pulse Count
RW Response	40.08	30
Thruster Response	46.06	395

Table 4 Comparison of Two Different Momentum Management Approaches

THIS PAGE INTENTIONALLY LEFT BLANK

IV. OPTIONS FOR K2 MOMENTUM MANAGEMENT

This chapter explores options for K2 momentum management aimed at realizing fuel savings that can be potentially used to extend the mission. The Kepler satellite in its current configuration for the K2 mission uses a momentum bias control. The bias increases the gyroscopic stiffness of the satellite making it more resistant to the effects of disturbance torque, which in turn enhances its ability to point accurately. As solar torque is imparted on the spacecraft, the reaction wheels spin down to absorb the momentum induced by the solar torque. As the wheels spin down, the spacecraft becomes more susceptible to the solar torque due to the reduced gyroscopic stiffness. Eventually, the drift rate would become too large for useful science. Thus, to counter the effects of solar torque, the reaction wheels must be periodically resaturated by inserting momentum into the spacecraft via thrusters.

A. EXAMPLE RESATURATION MANEUVER

A summary of the initial and final states for the reaction wheels for an example K2 resaturation operation is shown in Table 5.

	RW 1 RPM	RW1 h (Nms)	RW 3 RPM	RW 3 h (Nms)
Initial State	3140	10.13	-3265	-10.53
Final State	4605	14.85	-4763	-15.36

Table 5 Reaction Wheel States for a Resat Operation (K2 telemetry)

The telemetry showed that the resaturation operation was performed over a 3600 second interval with the first thruster firing occurring at 600 seconds (see Figure 24). The majority of the thruster pulses occur within 25 seconds of the initiation of the maneuver with small pulses occurring later to fine point the satellite. The Euler angles during the resaturation are shown in Figure 25. From the figure it can be seen that the spacecraft incurs an initial orientation error along the roll, pitch and yaw axes, respectively and

eventually reduces the error towards zero. Beginning with the first thruster pulses at 600 seconds, the reaction wheels respond in order to maintain the y and z-axis pointing. The thrusters are used for wheel resaturation and to maintain the satellite pointing along the x-axis. In the resat operation, thrusters 2, 3, 4, 5, 6, and 8 are used for a total of 11.4 seconds of pulse time. The reaction wheel speed over the course of the resaturation can be seen in Figure 26. The cumulative thruster pulse time is shown in Figure 27.

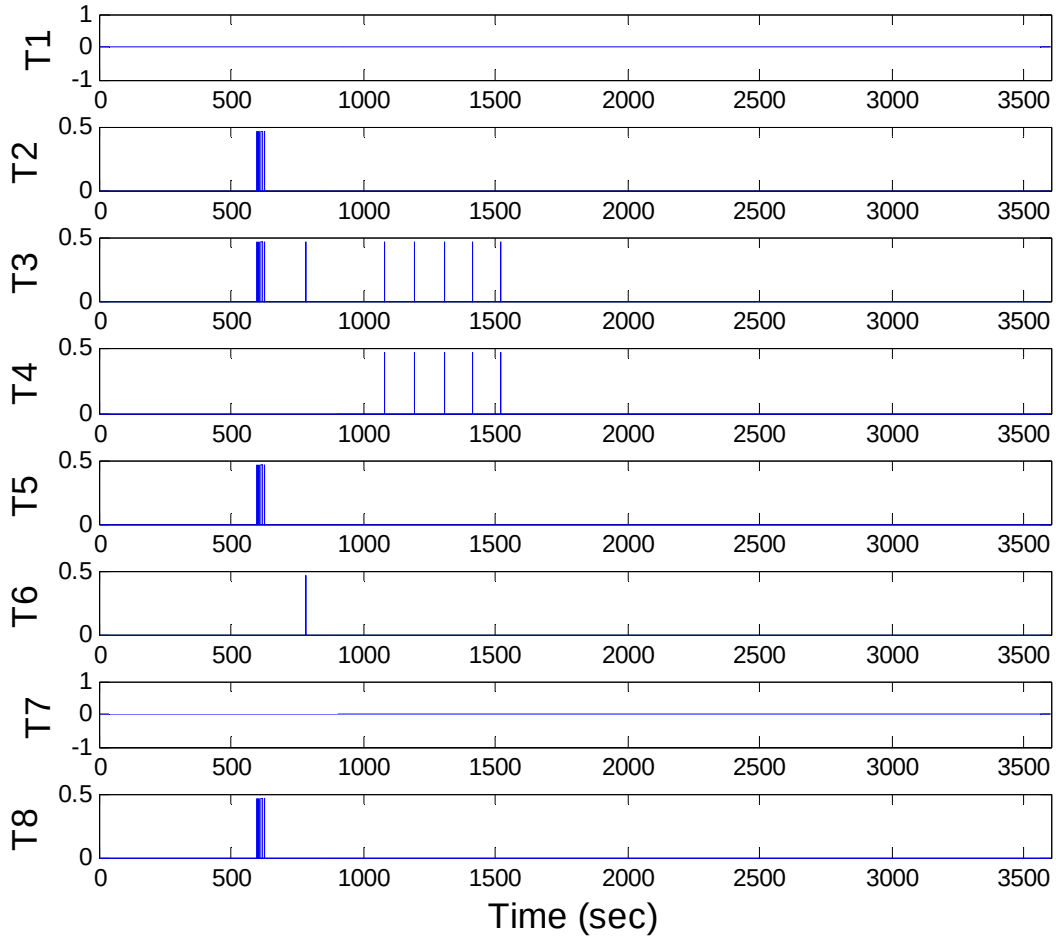

Figure 24 Thruster Pulse Allocation Telemetry Data for Sample K2 Resat Operation (thruster force given in Newtons)

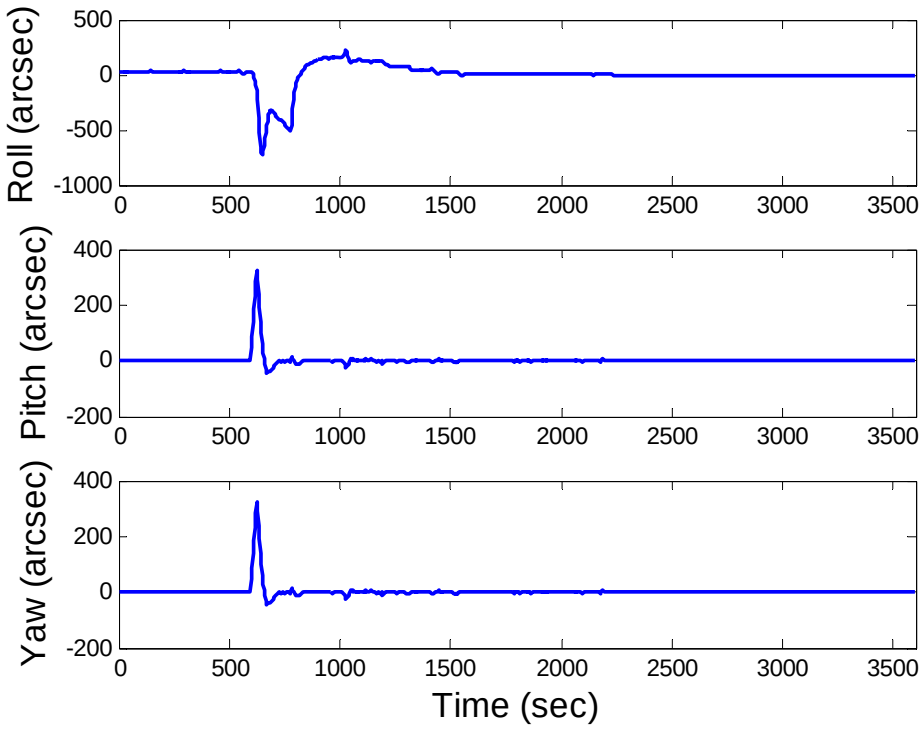

Figure 25 Euler Angle Telemetry Data for K2 Reaction Wheel Resat (data obtained from NASA)

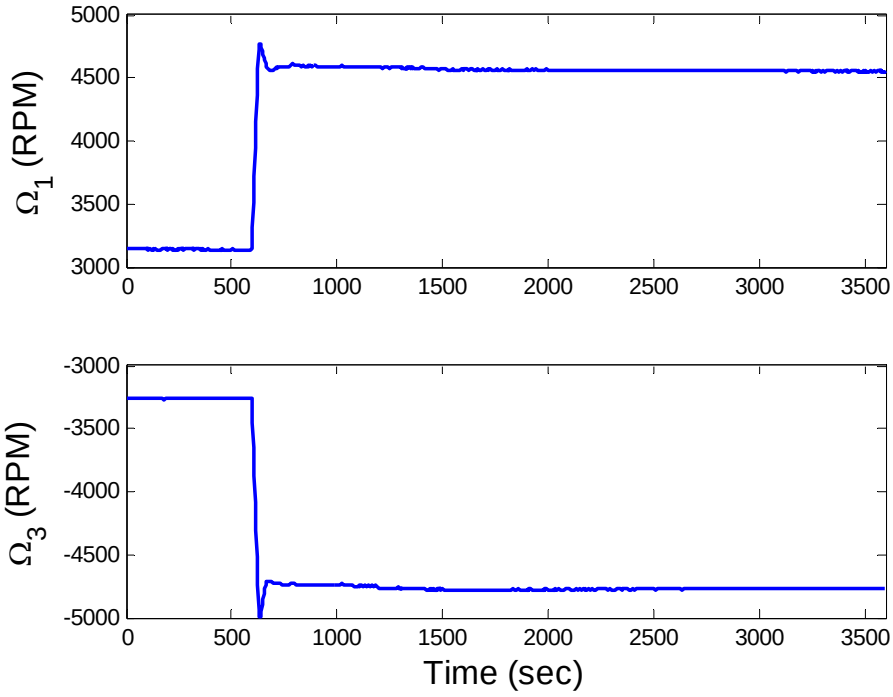

Figure 26 RWA Telemetry Data for K2 Reaction Wheel Resat (data obtained from NASA)

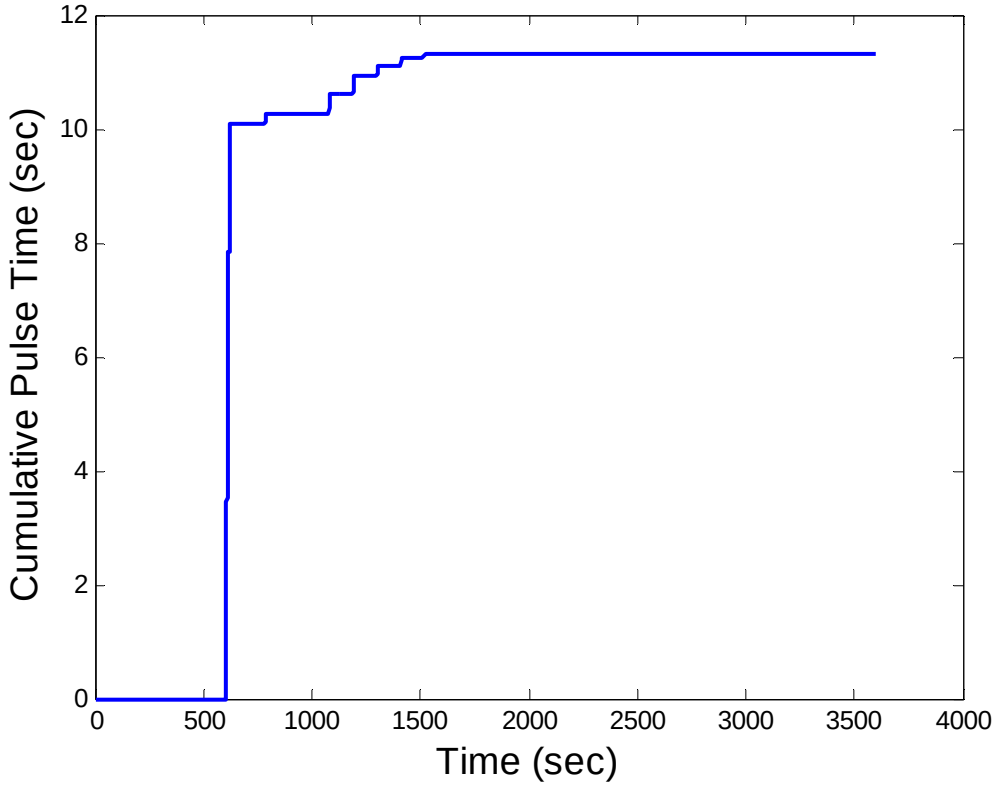

Figure 27 Cumulative Thruster Pulse Time for K2 Mission Reaction Wheel Resat (data obtained from NASA)

B. STATIC OPTIMAL THRUSTER ALLOCATION

In this section, an alternate method is explored to determine if there is room for improvement to the current approach for resaturating Kepler's reaction wheels. As shown in Chapter III, an initial calculation was performed assuming the satellite would remain static during the resaturation operation. In this case, the goal was to match the torques provided by the thrusters to the torques needed to spin up the reaction wheels. The thruster allocation was again solved using the method in [16] by applying Equations (2.19) through (2.25) to meet the requirements in Equation (4.1) while minimizing the amount of fuel expended.

$$h_{thruster} - h_{RW} = 0 \tag{4.1}$$

It was assumed as per the discussion in Chapter II, that translation of the satellite was not a concern. The distribution of pulse time across the thrusters and the total thruster

on times is displayed in Table 6. The solution used thrusters 2, 3 and 5 for a total of 8.84 seconds of pulse time.

Thruster Number	Pulse Time (Seconds)
1	0
2	4.08
3	4.42
4	0
5	0.34
6	0
7	0
8	0
Total	8.84

Table 6 Optimal Thruster Pulse Distribution for Resat Operation

The total pulse time for each thruster was then spread out over 40 seconds to allow the reaction wheels to respond under the two wheel control allocation described in Chapter II. The results of the maneuver were then compared to the K2 telemetry. The Euler angles for the maneuver along with the K2 telemetry are shown in Figure 28. The pitch and yaw axes (y and z-axes) track with the K2 maneuver very closely, however the roll axis (x-axis) shows a steady-state error of about 400 arcseconds since the reaction wheel control system does not close the loop around the roll error. The reaction wheel resaturation trajectories also tracked closely with the K2 telemetry. The reaction wheel speeds over the course of the resaturation can be seen in Figure 29. The allocated open-loop pulses are shown in Figure 30. A zoomed in view of the thruster pulses is shown in Figure 31. Based on the error along the roll axis, the results give indication that not only the amount of thrust applied is important, but the timing of the thrust application is also critical.

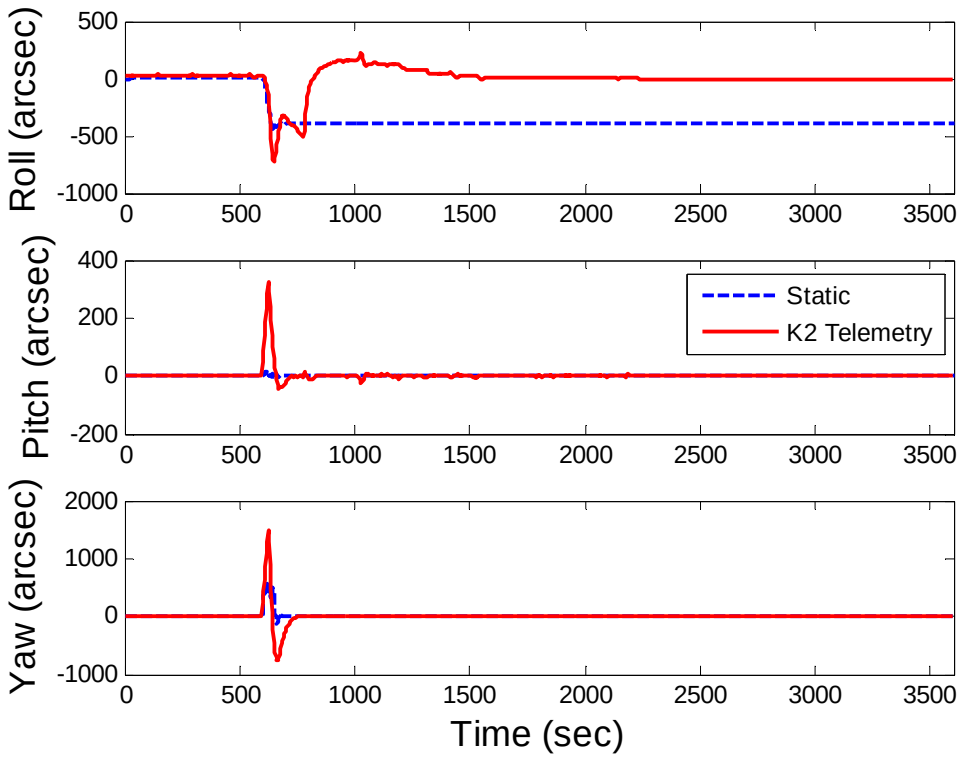

Figure 28 Euler Angles for Static Reaction Wheel Resat

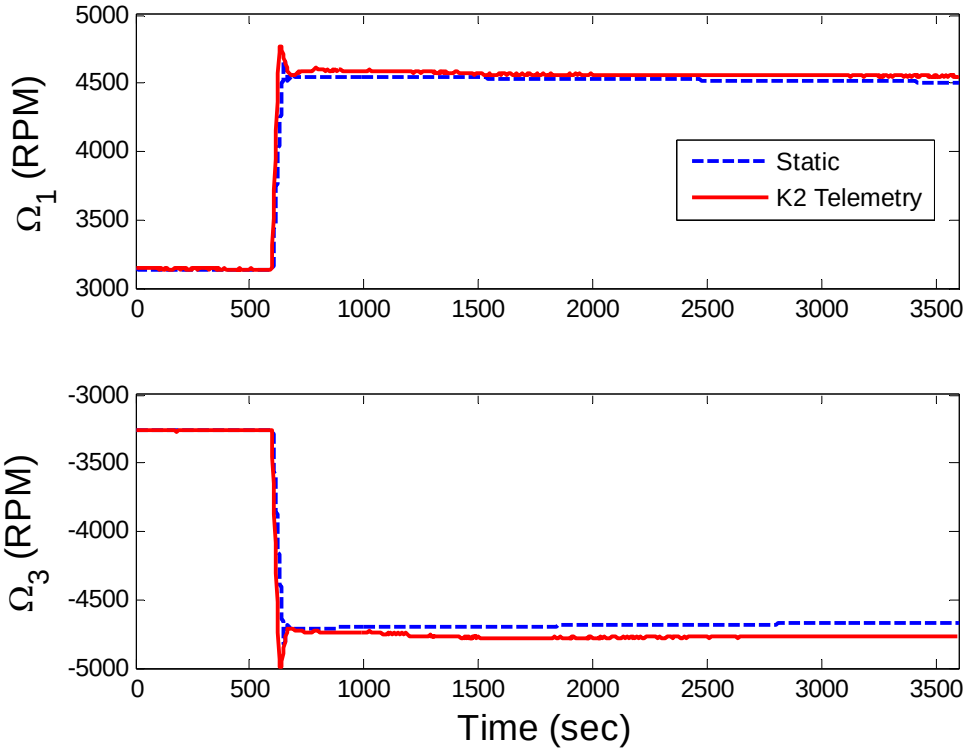

Figure 29 RWA Speed for Static Reaction Wheel Resat

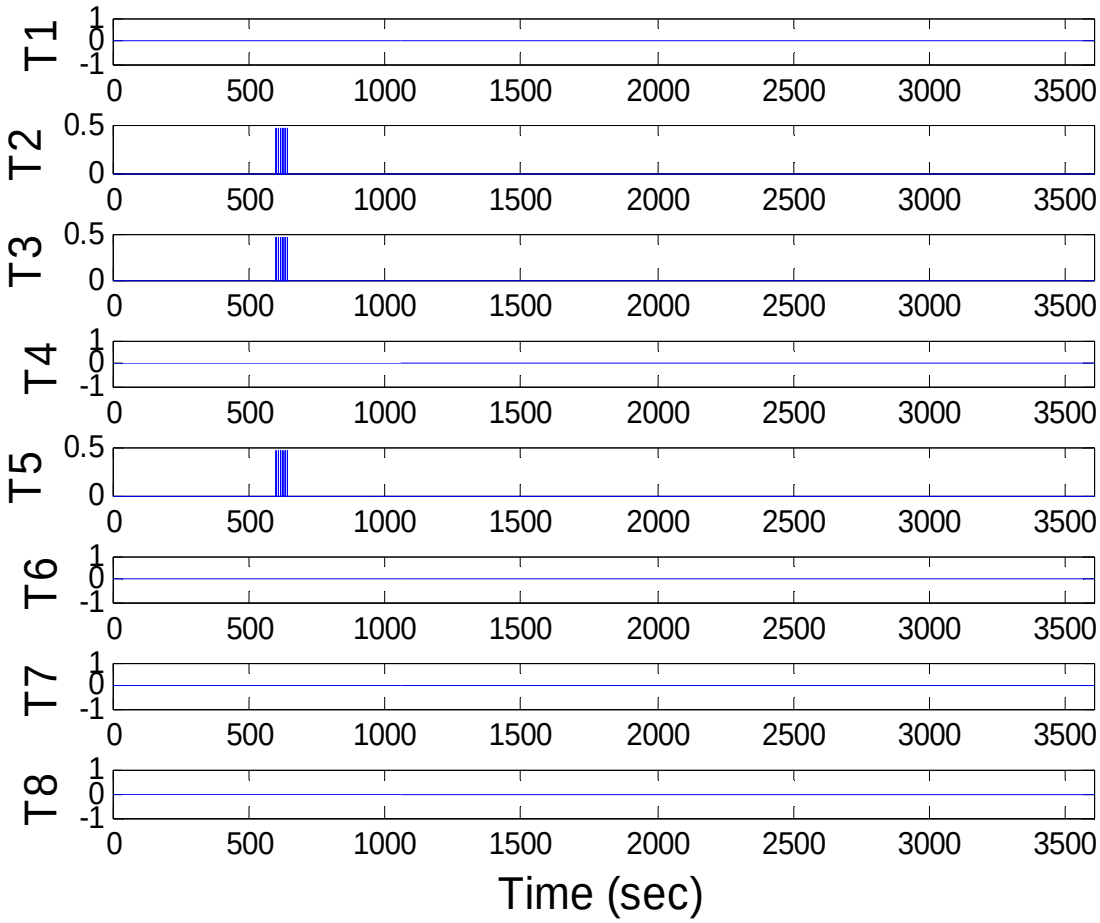

Figure 30 Thruster Pulses for Static Reaction Wheel Resat
(thruster force given in Newtons)

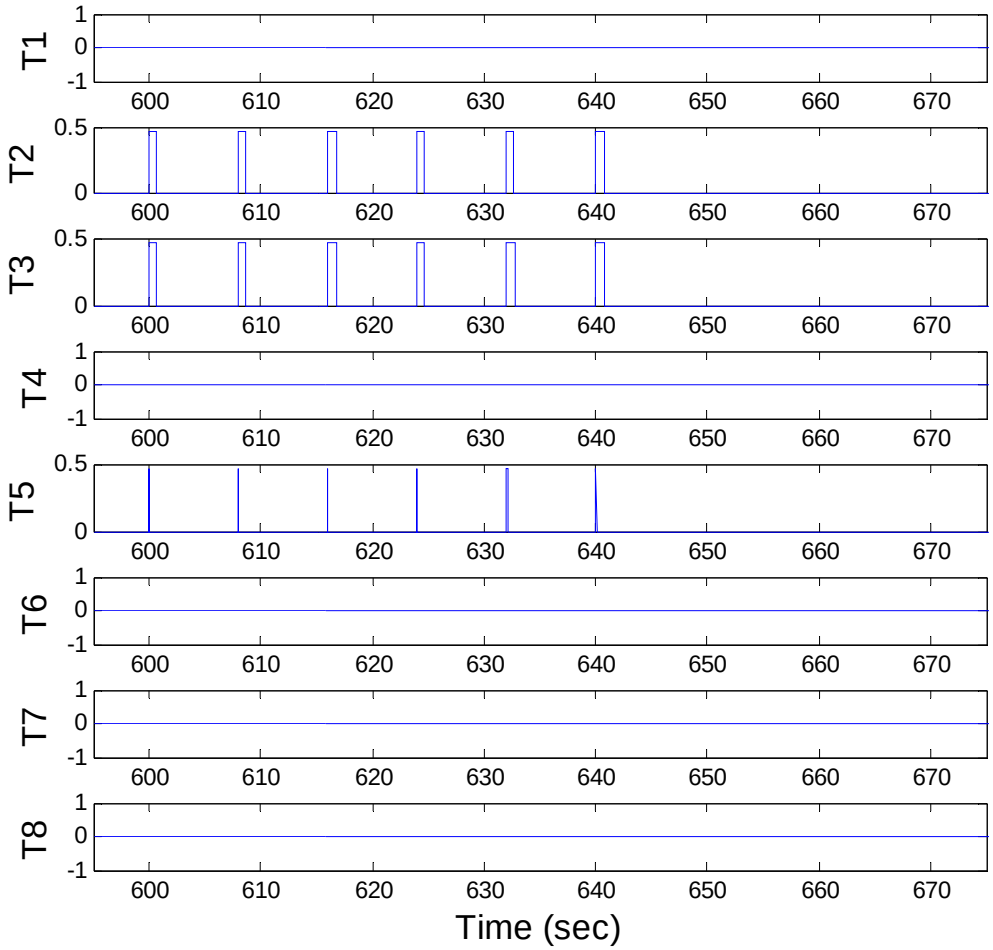

Figure 31 Zoomed in Thruster Pulses for Static Reaction Wheel Resat (thruster force given in Newtons)

C. STATIC OPTIMAL ALLOCATION WITH HYBRID CONTROL

A second case was run using the same open-loop thruster pulses calculated in Section B. When the pulse train was completed, the hybrid feedback loop described in Chapter II was activated to correct any attitude errors that were still present. This arrangement allowed the thrusters to control the x-axis and the reaction wheels to control the y and z-axes, as shown in Figure 15. The Euler angles for the resat operation are shown in the block diagram in Figure 32. Using the hybrid control, the Euler angles are observed to track more closely with the telemetry data results along all axes. In particular, the hybrid controller allows the roll axis error to be nulled out.

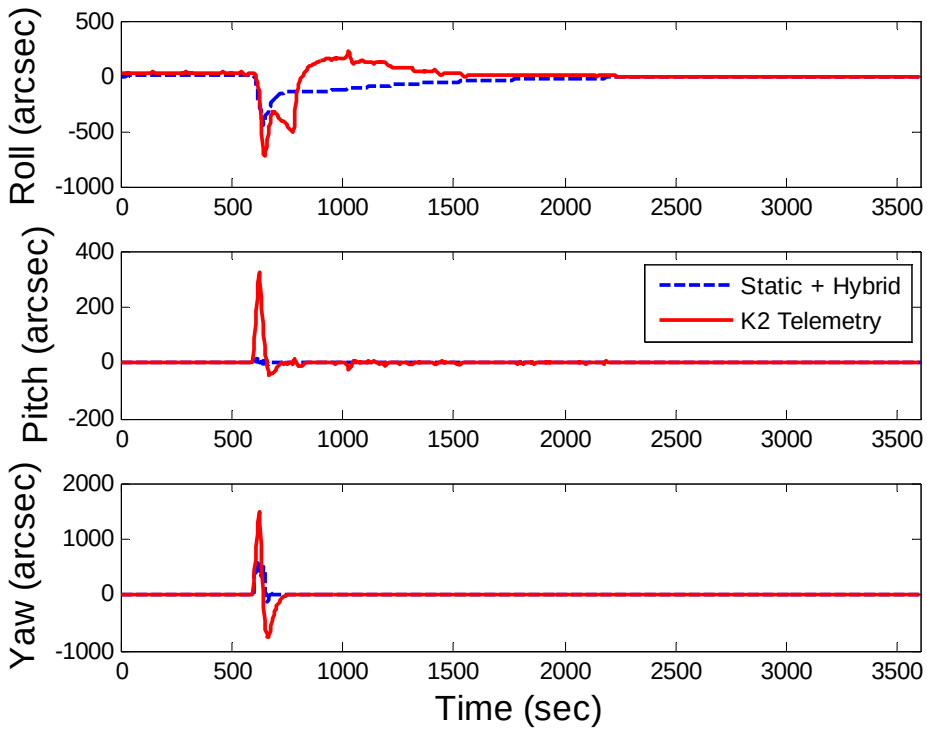

Figure 32 Euler Angles for Static Reaction Wheel Resat with Hybrid Allocation

The reaction wheel response is shown in Figure 33. The results once again compare very well with the telemetry data. The thrusters used during the maneuver were 2, 3, 5 and 6, as shown in Figure 34. The initial maneuver was again performed using thrusters 2, 3 and 5 and the correction maneuver was done using thrusters 2 and 6 as selected by the closed-loop hybrid thrust allocation algorithm. The additional pulses used for roll axis corrections reduced the fuel savings as compared to the static only solution, but the savings was still significant in comparison with K2 telemetry (see Table 7). Thruster pulses are shown in Figure 34. A zoomed in view of the thruster pulses is shown in Figure 35.

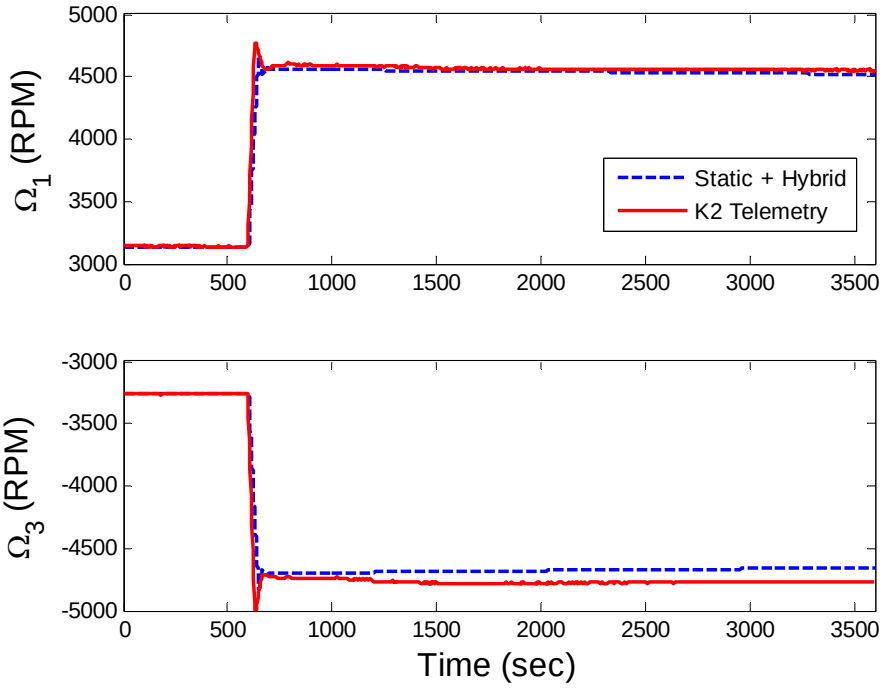

Figure 33 RWA Speed for Static Reaction Wheel Resat with Hybrid Allocation

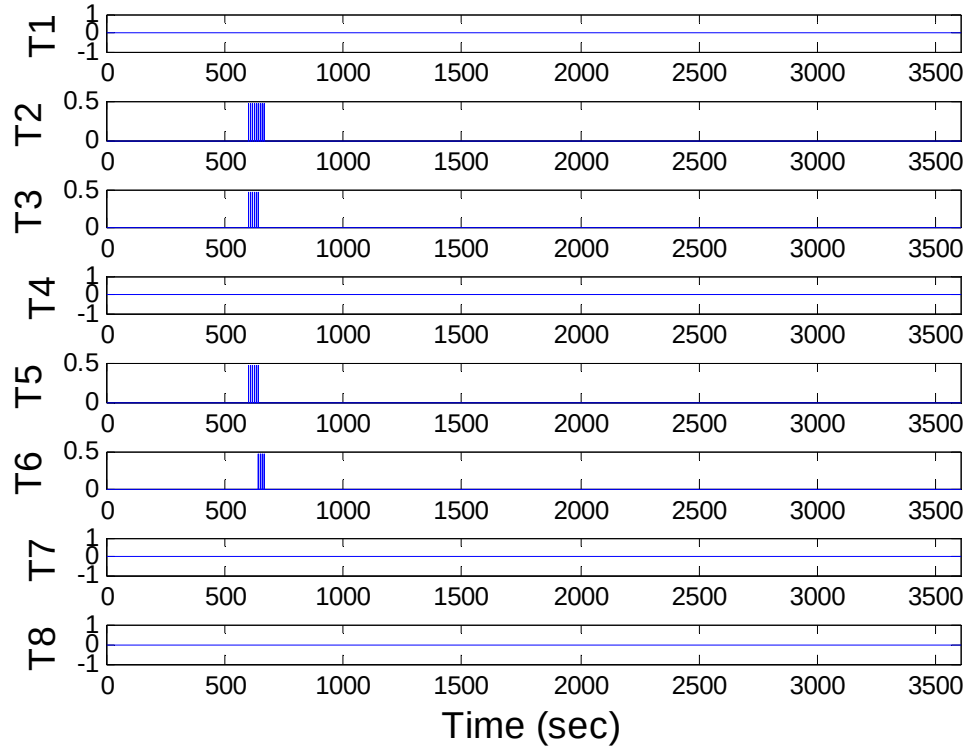

Figure 34 Thruster Pulses for Static Reaction Wheel Resat with Hybrid Allocation (thruster force given in Newtons)

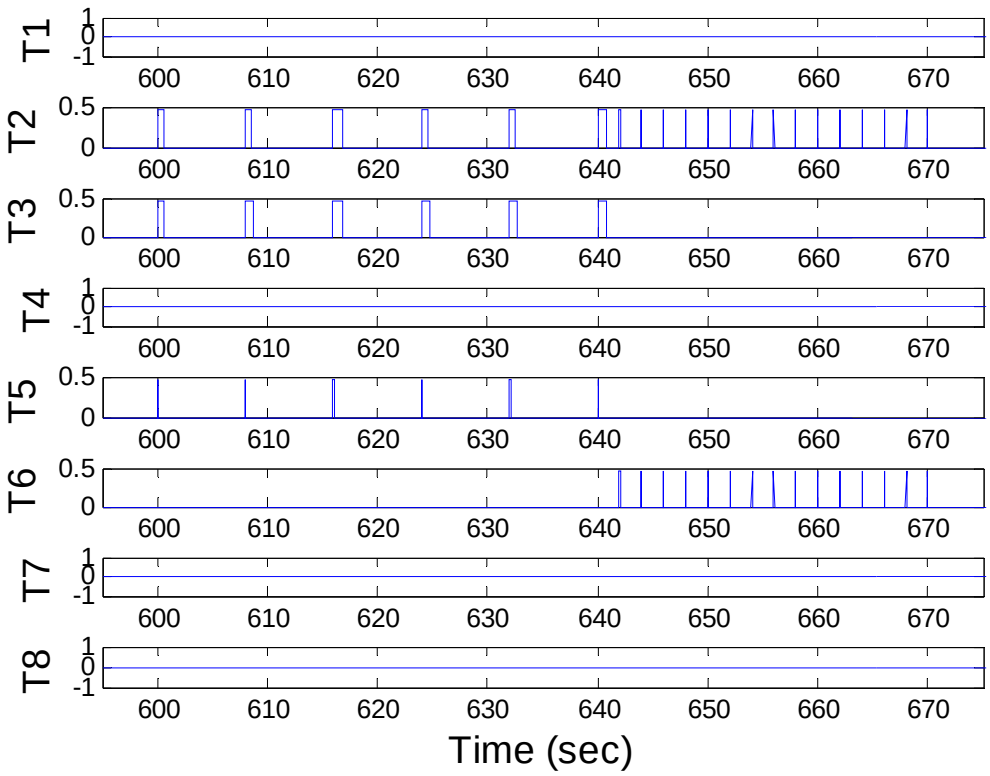

Figure 35 Zoomed in Thruster Pulses for Static Reaction Wheel Resat with Hybrid Allocation (thruster force given in Newtons)

Thruster Number	Pulse Time (Seconds)
1	0
2	4.40
3	4.42
4	0
5	0.34
6	0.32
7	0
8	0
Total	9.48

Table 7 Optimal Thruster Pulse Distribution for Resat Operation with Hybrid Allocation

D. OPTIMAL CONTROL SOLUTION

Optimal control is now applied to the resaturation problem. The problem is defined in Equations (4.2) and was solved using DIDO, an implementation of pseudospectral optimal control theory [19]. The boundary conditions for the problem are shown in Table 8. The goal was to find the most fuel efficient way of spinning up the reaction wheels. For the problem it was assumed that the thrusters could provide any value of thrust within the limits of the thrusters and that a PWM would be used to allocate the thrust as necessary to create a thrust profile needed to re-create the optimal control solution. It was also assumed that the accumulated momentum due to solar torque was negligible over the course of the resaturation operation and was therefore assumed to be zero. Because the goal is to minimize thruster seconds, which correlates directly to fuel consumption, the problem had to be bounded in time. Results varied based on the length of the time horizon. It was found that the minimum time to resaturate the reaction wheels for the given initial and final conditions (see Table 8) was about 26 seconds. The driving factor for this time was the limits on the reaction wheel torques.

$$x = [q_1, q_2, q_3, q_4, \omega_1, \omega_2, \omega_3, h_1, h_2, h_3, h_4]^T \in \mathbb{R}^{11}; u \in \mathbb{R}^{12}$$

Minimize:

$$J[x(\bullet), u(\bullet)] = \int_{t_0}^{t_f} \sum_{i=5}^{12} u_i dt$$

Subject To:

$$\dot{q} = \frac{1}{2} \begin{bmatrix} 0 & \omega_3 & -\omega_2 & \omega_1 \\ -\omega_3 & 0 & \omega_1 & \omega_2 \\ \omega_2 & -\omega_1 & 0 & \omega_3 \\ -\omega_1 & -\omega_2 & -\omega_3 & 0 \end{bmatrix} * \begin{bmatrix} q_1 \\ q_2 \\ q_3 \\ q_4 \end{bmatrix}$$

$$\dot{\omega} = J^{-1}[\mathrm{T}_{ext} - \mathrm{T}_{RW} - \omega \times (J\omega + h)]$$

where:

$$\dot{h}_1 = u_1$$

$$\dot{h}_2 = u_2 = 0$$

$$\dot{h}_3 = u_3$$

$$\dot{h}_4 = u_4 = 0$$

$$t_0 = 0$$

$$[q(t_0), \omega(t_0), h(t_0)] = [q_0, \omega_0, h_0]$$

$$[q(t_f), \omega(t_f), h(t_f)] = [q_f, \omega_f, h_f] \qquad (4.2)$$

$$-0.2 \le [u_1, u_2, u_3, u_4]^T \le 0.2$$

$$0 \le [u_5, u_6, u_7, u_8, u_9, u_{10}, u_{11}, u_{12}]^T \le 0.46$$

$$-1 \le [q_1, q_2, q_3, \mathrm{q}_4]^T \le 1$$

$$[-16.6, 0, -16.6, 0]^T \le [h_1, h_2, h_3, h_4]^T \le [16.6, 0, 16.6, 0]^T$$

	q1	q2	q3	q4	ω_1 (rad/sec)	ω_2 (rad/sec)	ω_3 (rad/sec)	Ω_1 (RPM)	Ω_3 (RPM)
Initial	0	0	0	1	0	0	0	3132	-3265
Final	0	0	0	1	0	0	0	4605	-4763

Table 8 Resat Problem Boundary Conditions

The Euler Angles for the optimal resaturation are shown in Figure 36. Looking at Figure 36, it can be seen that that the optimal control solution may be taking advantage of coupled motion arising from the cross product portion of Equation (2.2) to ensure zero attitude error at the end of the resat. The optimal control approach used 8.83 thruster

seconds, similar to the static approach of 8.84 seconds. Recall that in order to achieve this pointing accuracy the static approach required an additional 0.64 thruster seconds as contributed by the hybrid control logic. Thus, the optimal control approach is indeed more efficient.

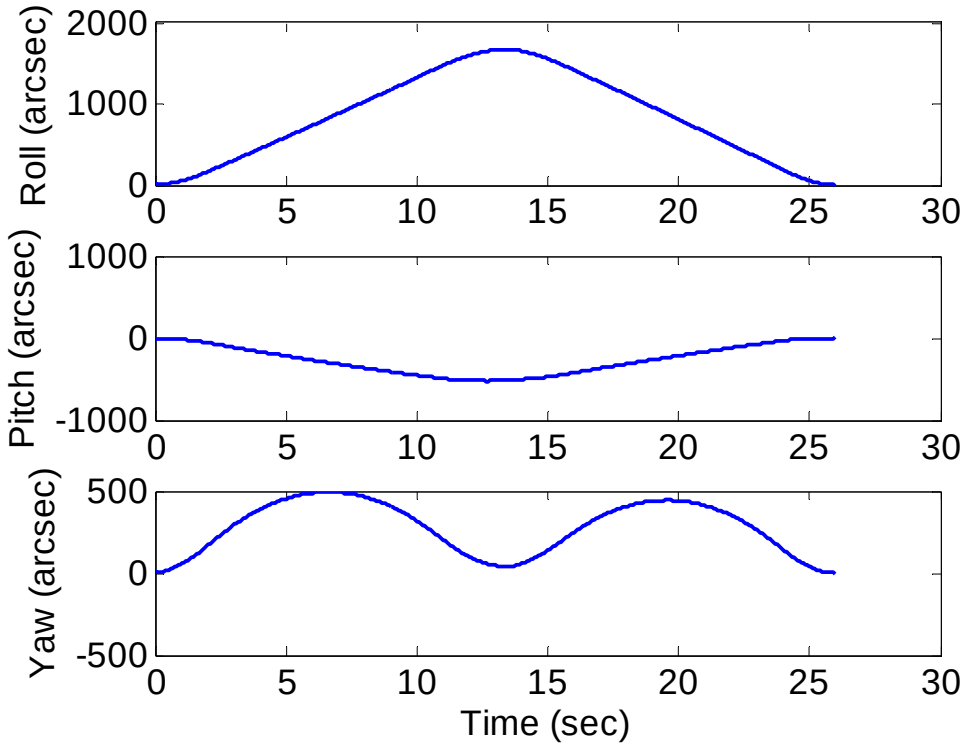

Figure 36 Euler Angles (in Arcsec) for Optimal Momentum Resat

The reaction wheel trajectories are shown in Figure 37. The reaction wheel speed increases nearly linearly during the maneuver, with small variations to account for the coupled motion. Figure 38 shows the reaction wheel torques. As explained above, the reaction wheels have to be at maximum torque in their respective directions in order to reach the desired final desired state for reaction wheel momentum in the shortest amount of time. The reaction wheel controls u_1, u_2, u_3, and u_4 represent the controls for RWA1, RWA2, RWA3, RWA4, respectively. Since only RWA1 and RWA3 are operational, u_2 and u_4 are zero, as expected.

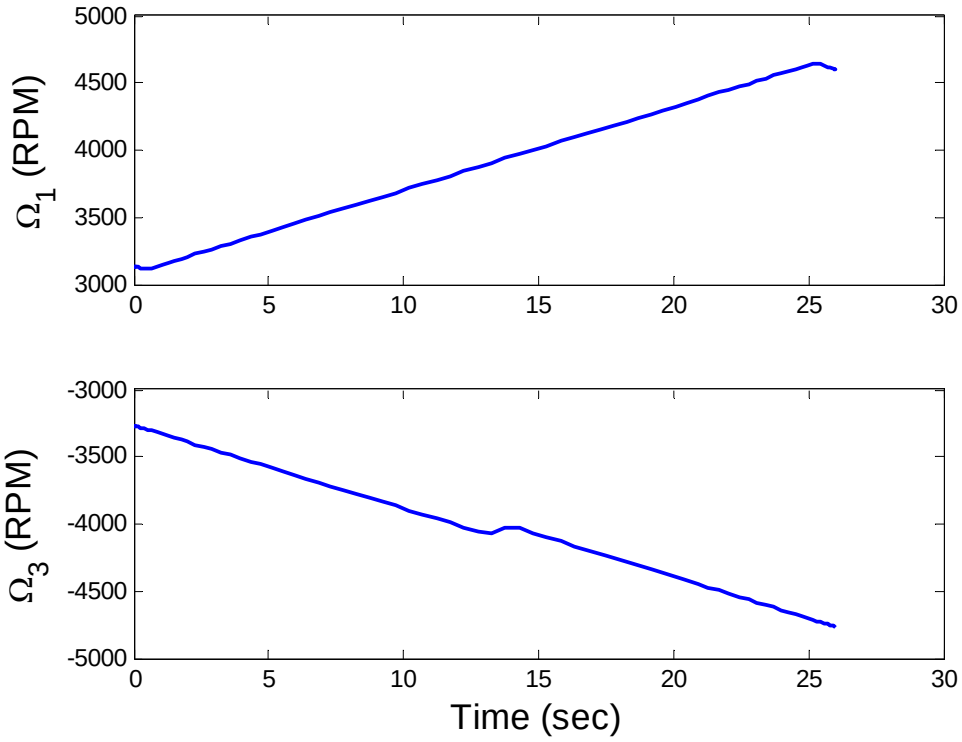

Figure 37 RWA Speed for Optimal Momentum Resat

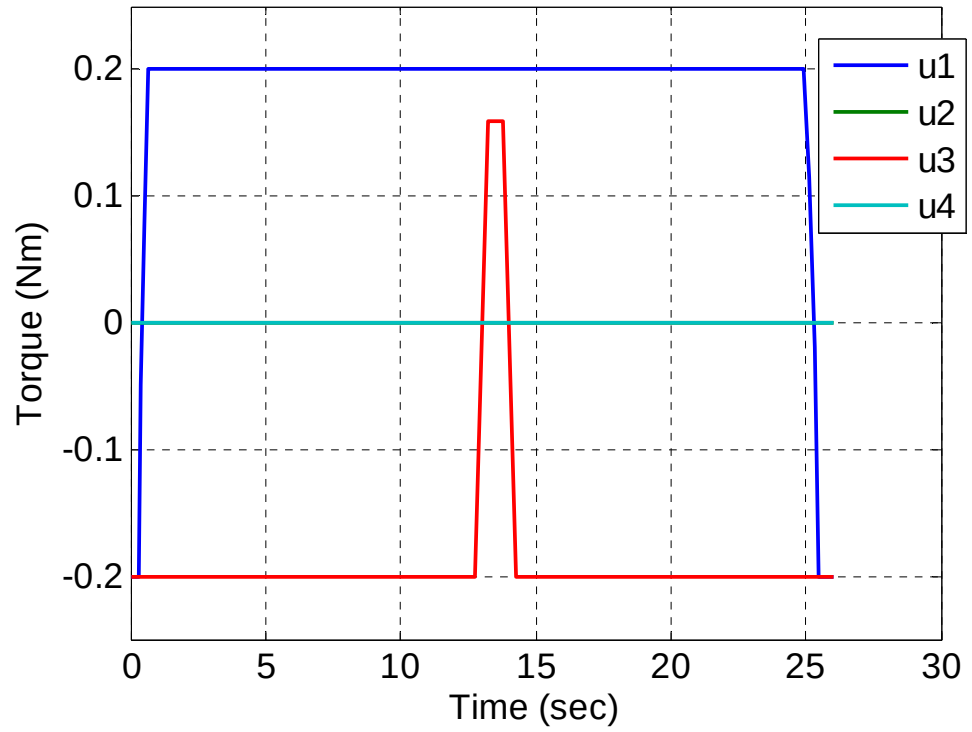

Figure 38 Reaction Wheel Control Trajectories for Optimal Momentum Resat

The thruster control trajectories are shown in Figure 39. Thruster control trajectories u_5 through u_{12} represent thrusters 1 through 8, respectively. It can be seen in the figure that thrusters 2, 3, and 5 are used to conduct the wheel resat. Note that this is the same thruster combination selected by the optimal thruster allocation in Section B. However, the thruster switches are now sequenced in a way that capitalizes on the dynamic coupling that is used to null the accumulation of attitude error.

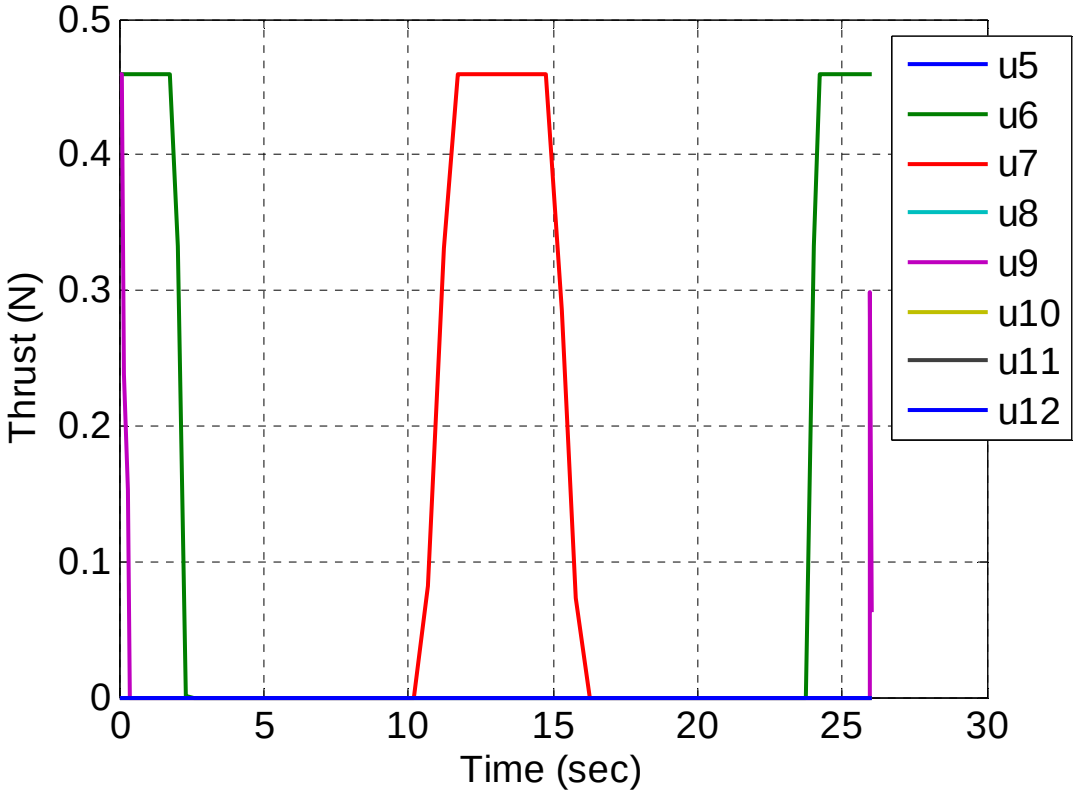

Figure 39 Thruster Control Trajectories for Optimal Momentum Resat

The optimal control problem was solved over a range of time horizons to show the effect of allowing longer resaturation times. As the maneuver time lengthens the satellite incurs more motion around each axis. In turn, however, the amount of fuel used decreases. It was observed that as the maneuver time increases, the rate of change in the amount of fuel saved decreases. This gives indication that the motion of the spacecraft can be used to reduce fuel consumption, but with diminishing return with respect to lengthening the time horizon. Table 9 shows the results of increasing time on the

maneuver and fuel consumption. Figure 40 shows a plot of the fuel consumption with respect to maneuver time. Note that the fuel expended by this method is consistent with the static optimal thrust allocation method.

Resaturation Time (seconds)	Max Roll (deg)	Max Pitch (deg)	Max Yaw (deg)	Thruster Seconds
26	0.46	- 0.15	0.14	8.81
50	3.00	0.44	0.55	8.72
75	4.90	0.85	-0.65	8.67
100	6.64	1.02	-1.02	8.59
150	8.58	3.74	-2.39	8.53
200	18.2	10.7	1.33	8.29
250	23.0	-15.9	-4.88	8.20
300	26.3	-17.9	2.22	8.19

Table 9 Results of Optimal Control K2 Reaction Wheel Resaturation

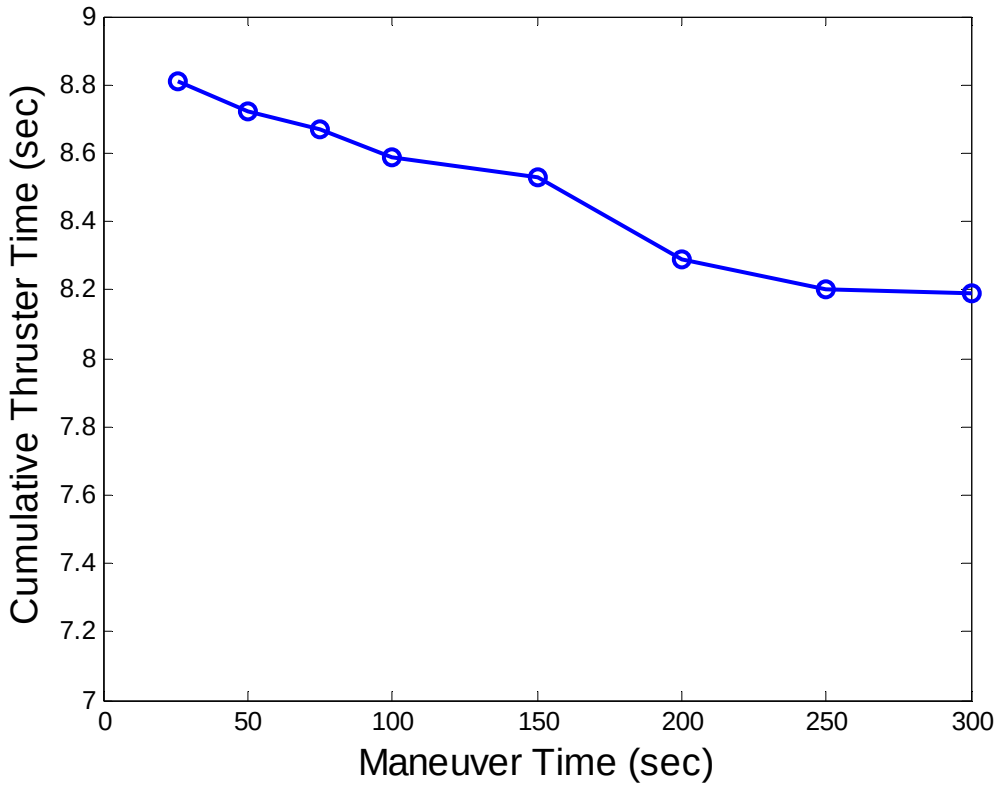

Figure 40 Maneuver Time vs. Cumulative Thruster Pulse Time for Optimal Momentum Resat

E. VALIDATION AND VERIFICATION (V&V)

Numerous tests were performed on the DIDO solutions to validate and verify the results. As shown in the Appendix, the application of the necessary conditions for optimality provides very little information that is useful for validating the solution, instead V&V relied primarily on propagating the control trajectories through the same plant model used in the optimal control problem formulation to verify that the plant response would be the same given the solved control trajectories. The V&V process was carried out for all maneuvers solved using optimal control and yielded similar results. So, only results pertaining to the minimum time solution are given here.

Figure 41 shows the propagated Euler angles using the control inputs from the optimal control solution. The optimal and propagated trajectories are nearly identical.

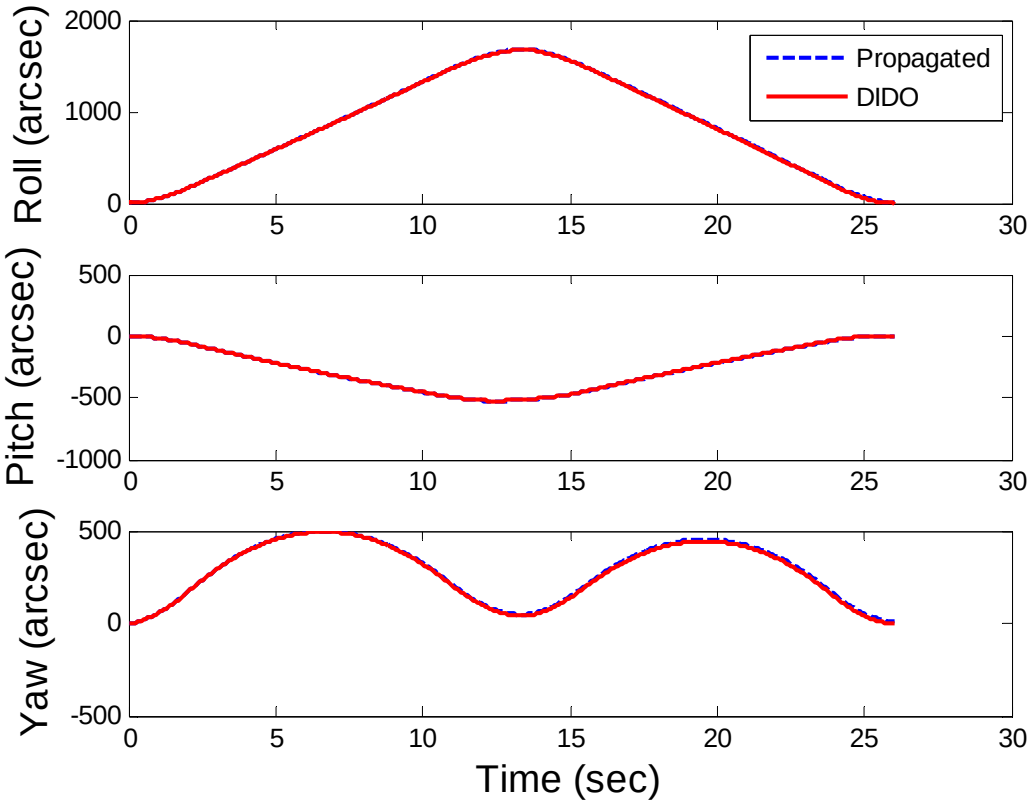

Figure 41 Propagated Euler Angles

The optimal and propagated quaternions are also nearly identical as shown in Figure 42. In addition, the two norm of the quaternions is equal to one, which gives indication that the results are correct. The propagated solutions for the spacecraft angular rate and reaction wheel momentum are also nearly identical to the optimal control solution. The spacecraft angular rate and the reaction wheel momentum are shown in Figure 43 and Figure 44, respectively.

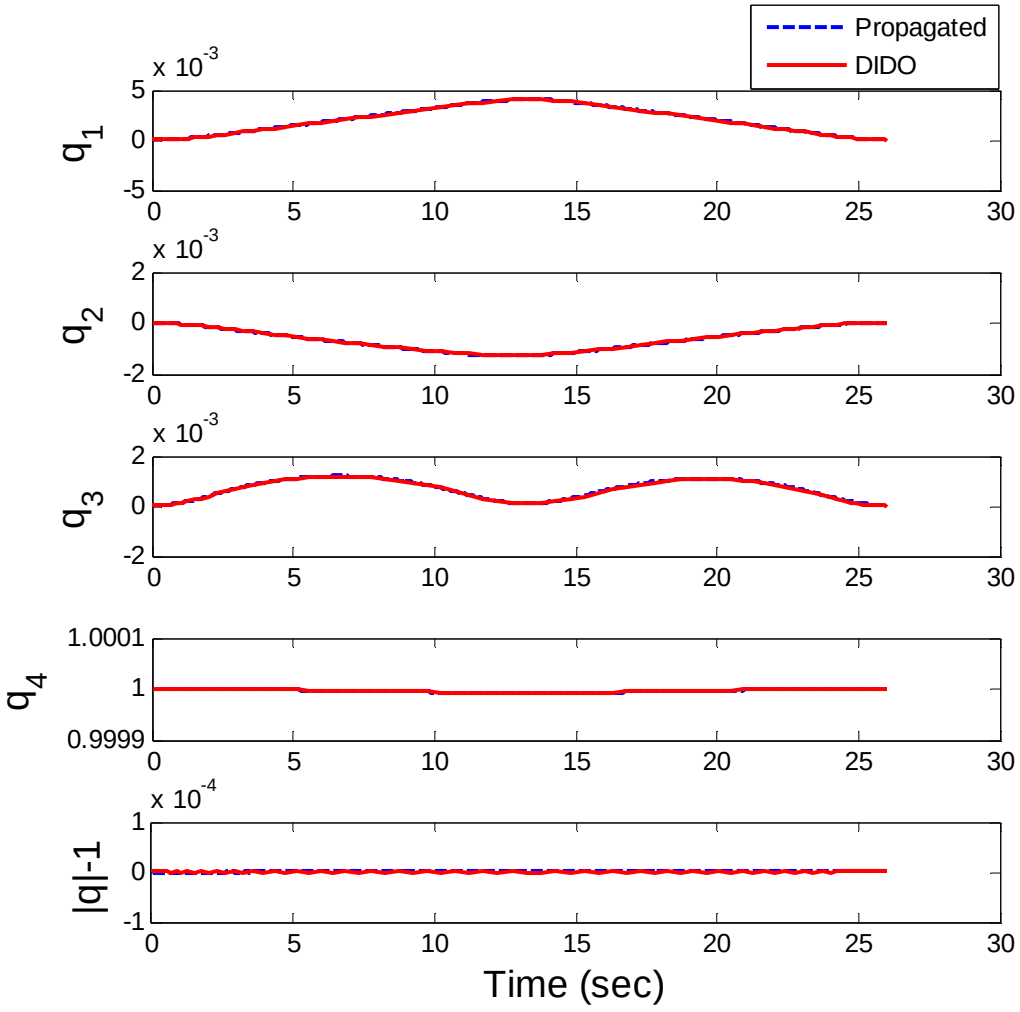

Figure 42 Propagated Quaternions

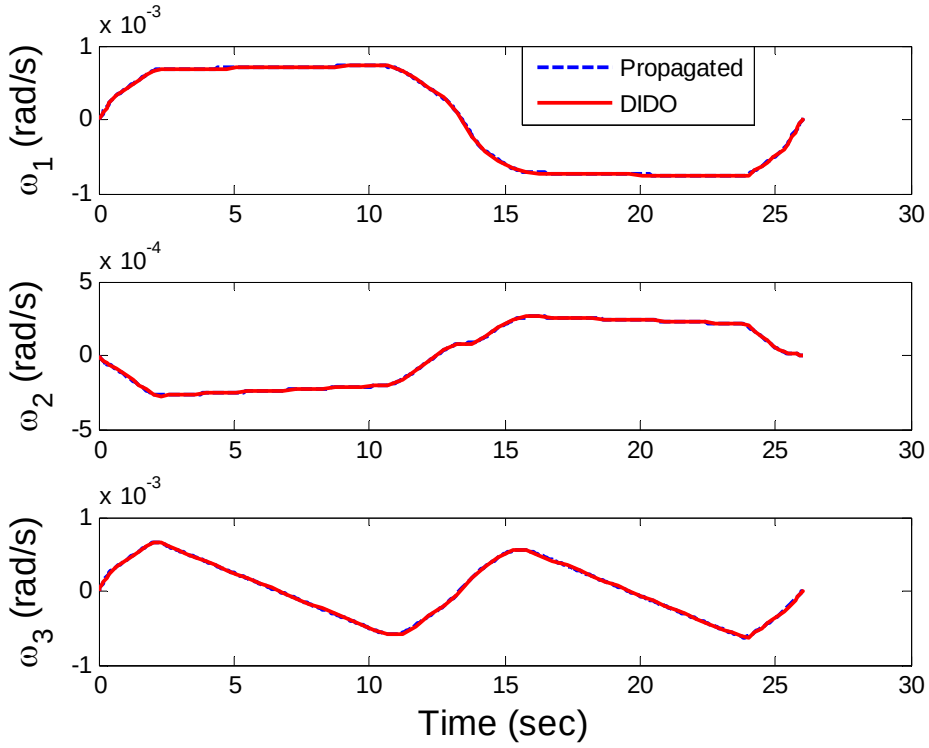

Figure 43 Propagated Spacecraft Angular Velocity

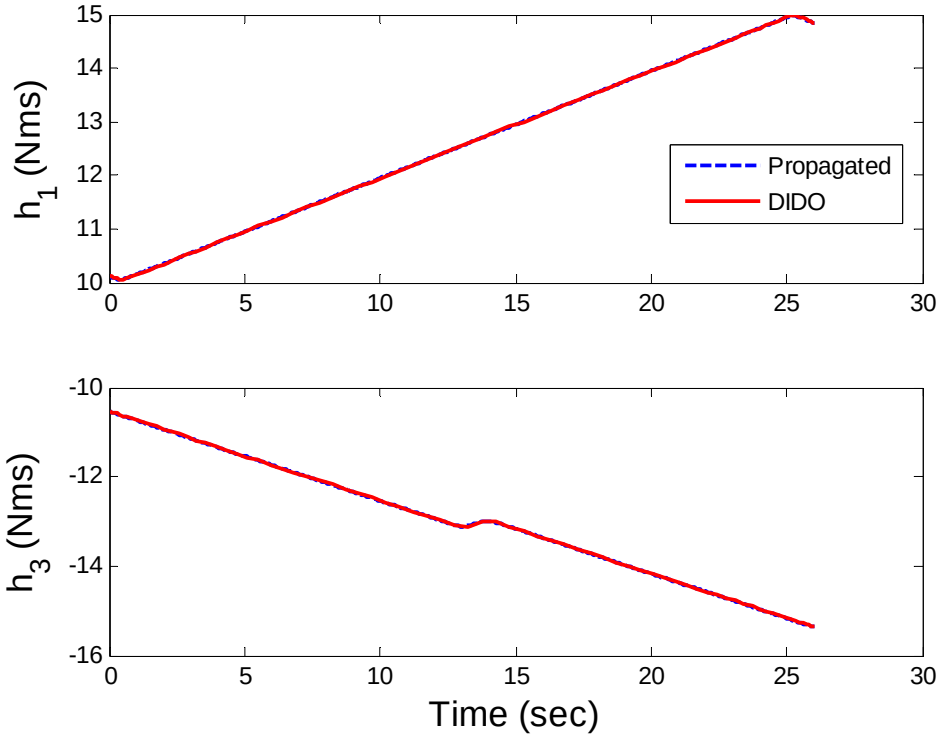

Figure 44 Propagated Reaction Wheel Momentum

The next V&V test performed is to verify the Hamiltonian was a constant value in accordance with the Hamiltonian Value Condition [20]. For a fixed time optimal control problem, the Hamiltonian should be constant. Figure 45 shows the Hamiltonian as a relatively constant value. The peaks are an indication of a large change in the controls input, and are a result of numerics rather than a sign that the solution is invalid

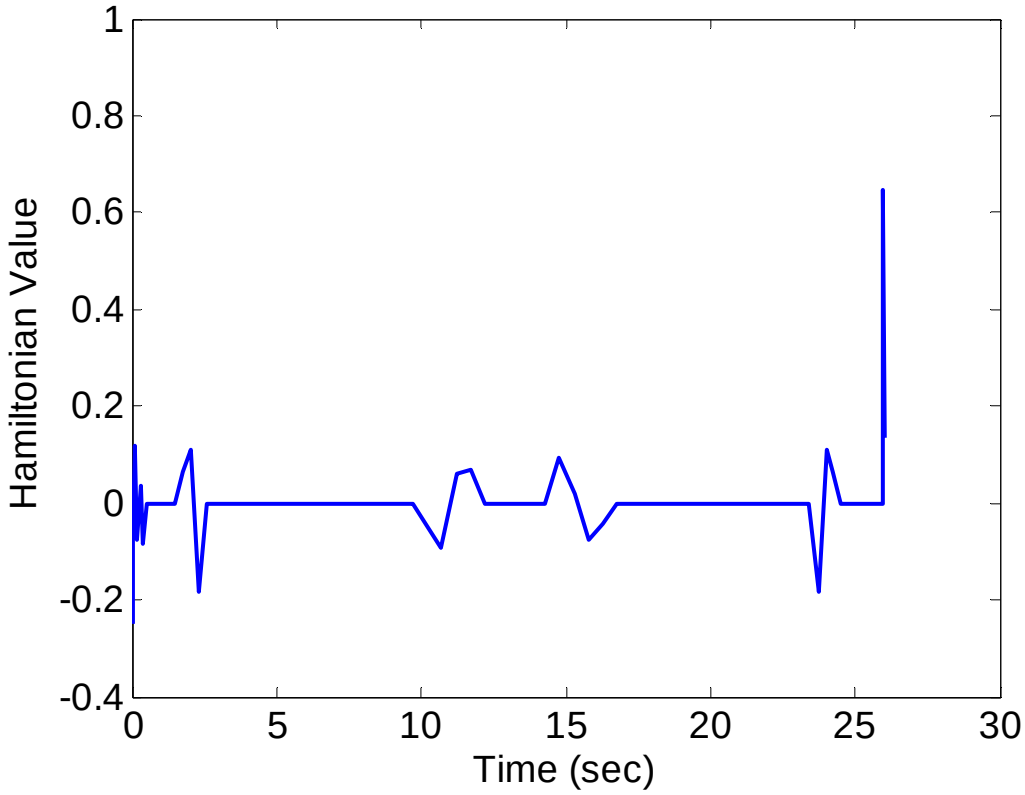

Figure 45 Time History of the Hamiltonian

The final test is to verify that the controls act as they should. As shown in the appendix, the Hamiltonian is linear in the control variables. This indicates that the controls will be defined by their switching functions, meaning the controls will either be at their extremes, or zero. This behavior of the controls phenomenon is observed in Figure 38 and Figure 39.

The switching functions are also plotted against the control trajectories to verify that the control trajectories switched to their opposite extremal value when the switching

function crossed the zero axis. As an example, thruster 3, as controlled by u_7 is compared to its switching function in Figure 46. Note that as the switching function crosses zero the control signal switches from one extreme to the other. The variation between the crossing point of the switching function and the control signal is due to the effects of time discretization. The true control signal would be a vertical line and can be adjusted in post processing. This correct behavior of the optimal controls is consistent across all thrusters.

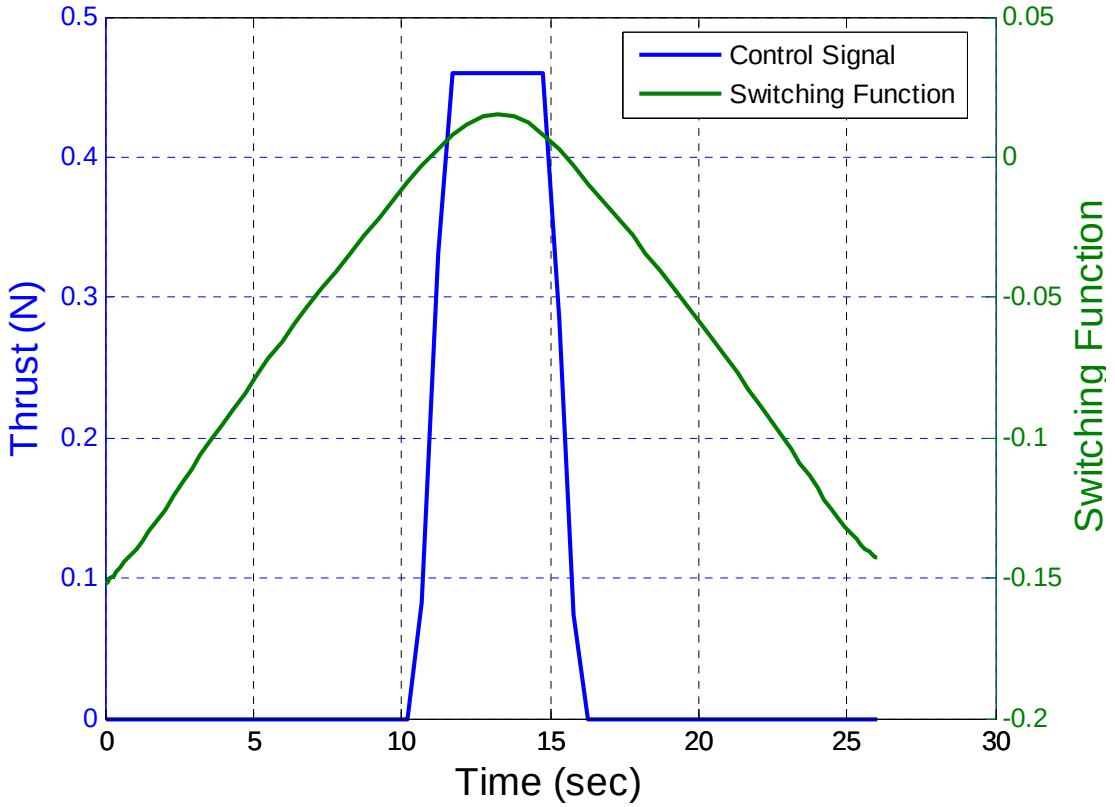

Figure 46 Control Signal and Switching Function for Thruster 3 (u7)

The switching function for the reaction wheels are additionally compared to their control signals. Figure 47 shows the control signal and the switching function for reaction wheel one, as controlled by signal u_1. Once again behavior of the switching function is consistent with the behavior of the control.

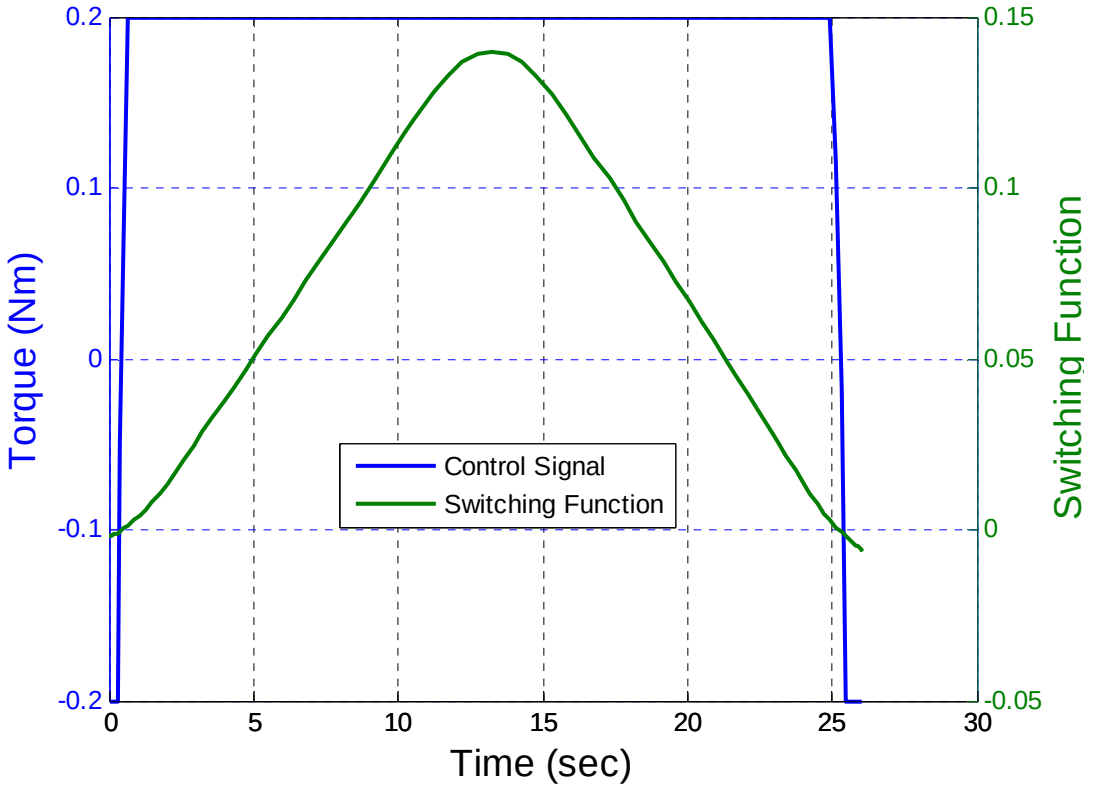

Figure 47 Control Signal and Switching Function for Reaction Wheel 1 (u_1)

F. RESULTS SUMMARY

Each of the approaches for performing a reaction wheel resat described in this chapter was compared to the current method of momentum management implemented on K2. The results of the endpoint roll, pitch and yaw error along with the final reaction wheel speeds were tabulated. The cumulative thruster time and number of pulses were also computed and the percent fuel savings for the maneuver was calculated using Equation (4.3). The results are summarized in Table 10. Table 10 shows, by using a different combination of thrusters as compared to the K2 telemetry, a fuel savings of as much as 28 percent can be realized. The results of the optimal control approach additionally give an indication that fuel savings can be maximized while minimizing the induced pointing error by taking advantage of the nonlinearities in the equations of motion. Furthermore, increasing the time horizon of an optimal control can further reduce fuel consumption, but the additional return diminishes as the allotted time increases.

$$\% \; Fuel \; Savings = \frac{\text{K2 Method} - \text{Method Used}}{\text{K2 Method}} * 100 \qquad (4.3)$$

Method	Roll Error (arcsec)	Pitch Error (arcsec)	Yaw Error (arcsec)	Pulse Time (sec)	# of Pulses	Fuel Savings (%)
K2 Telemetry	-7	0	0	11.4	22	0
Static	-392	0	-2	8.84	18	22.5
Static +Hybrid	-2	0	-2	9.48	48	16.8
Optimal 26 Sec	0	0	0	8.83	N/A	22.5
Optimal 300 Sec	0	0	0	8.19	N/A	28.2

Table 10 Summary of K2 Momentum Resat Results

V. WHEELS ONLY LARGE ANGLE SLEW

Optimal control can also be used to minimize fuel consumption during large angle maneuvers, such as those used to reorient the satellite from science mode, as shown in Figure 48, to Earth point mode. This maneuver is needed to point the high gain antenna at Earth for data transfer, as shown in Figure 49. A maneuver also needs to be performed from Earth point mode back to science mode. This chapter shows the feasibility of using optimal control for such large angle maneuvers. NASA performed a science point to Earth point maneuver in campaign 1 of the K2 mission. Telemetry data was obtained for the slew. During the maneuver, the reaction wheels were spun down to zero, as shown in Figure 50. Thrusters were fired for a total of 18.4 thruster seconds to remove the reaction wheel momentum and also to reorient the satellite to Earth point attitude. The initial and final states of the spacecraft are shown in Table 11. Telemetry for the attitude in quaternions is shown in Figure 51.

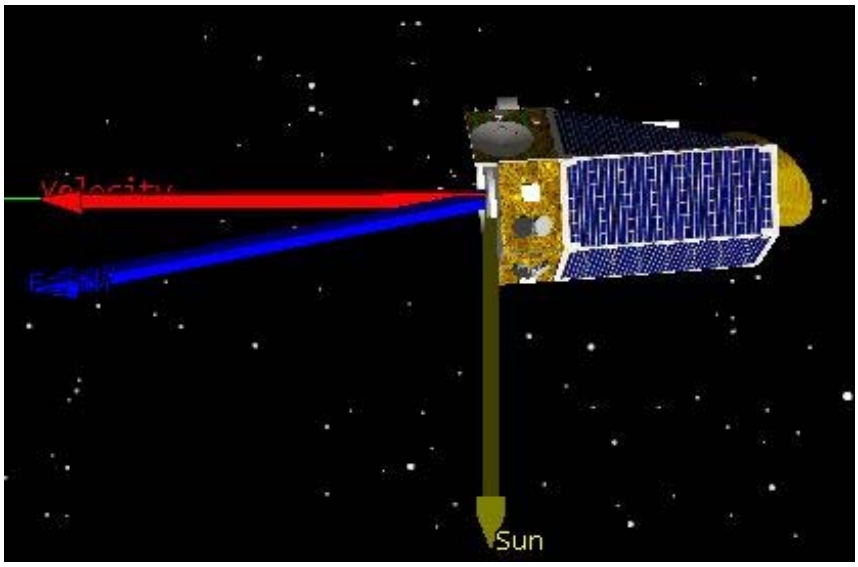

Figure 48 Spacecraft Approximate Initial Orientation (Science Point)

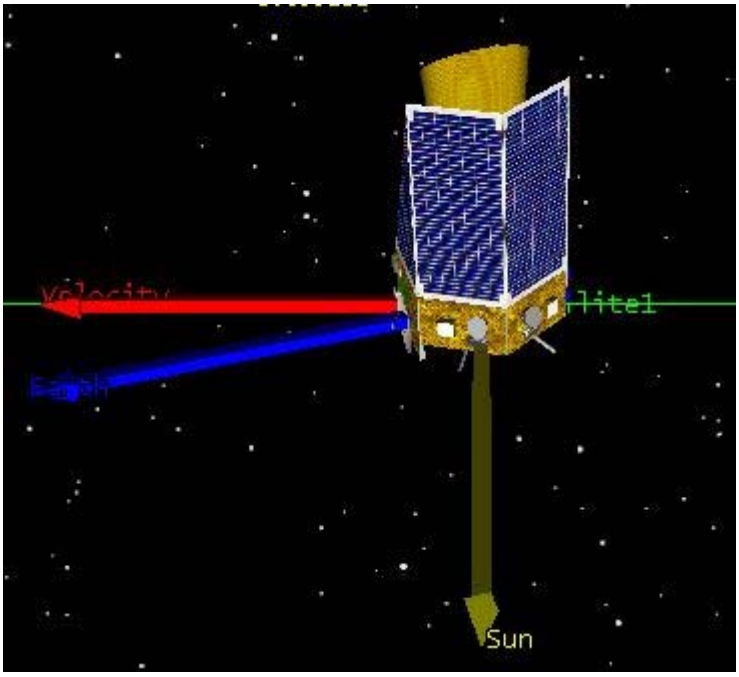

Figure 49 Spacecraft Approximate Final Orientation (Earth Point)

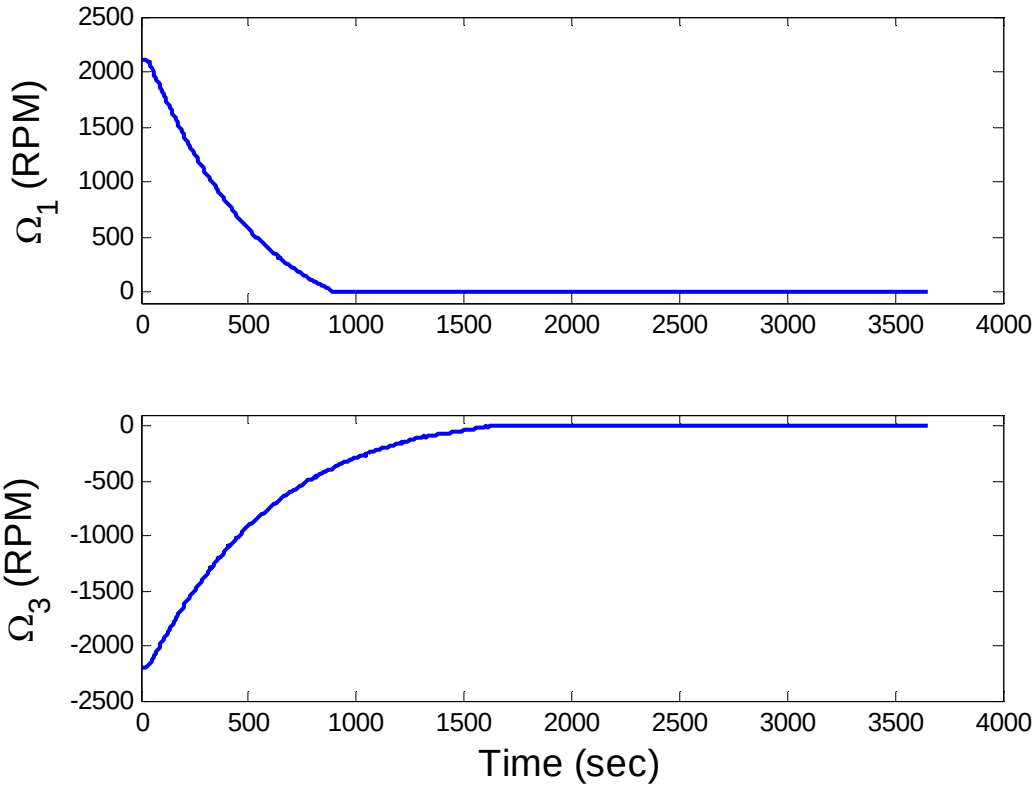

Figure 50 RWA Telemetry for K2 Large Angle Maneuver

	q1	q2	q3	q4	Ω_1 (RPM)	Ω_3 (RPM)
Initial	-0.054248	-0.979457	-0.194210	0.001571	2115.8	-2199.1
Final	0.158324	-0.689780	-0.125839	0.695199	0	0

Table 11 Initial and Final Conditions for a K2 Rest-to-Rest Slew from Science Point to Earth Point

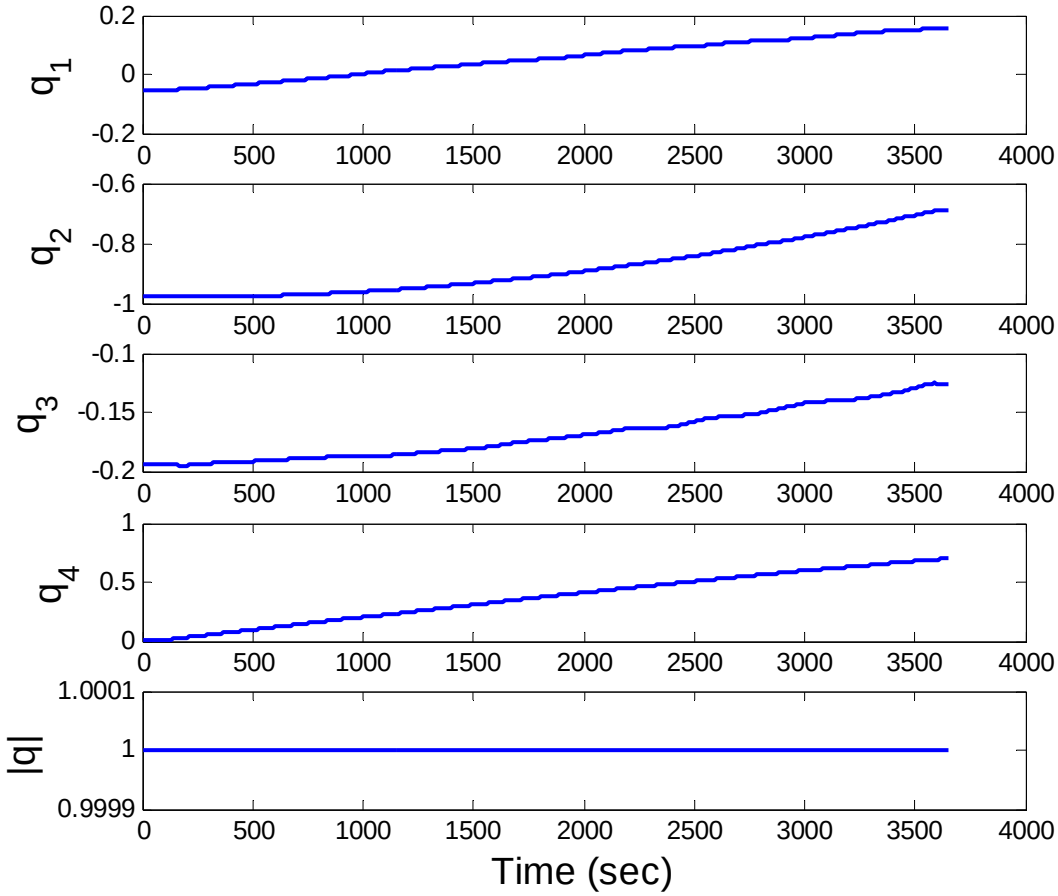

Figure 51 Attitude Telemetry for K2 Large Angle Maneuver

A. APPLICATION OF OPTIMAL CONTROL TO A LARGE ANGLE MANEUVER

In this section, optimal control is applied to the large angle Earth point slew. The maneuver was performed in two stages. The first step assumed an optimal reaction wheel desaturation to bring the reaction wheel momentum to zero. The second step was a reaction wheel only rest-to-rest slew of the spacecraft from science attitude to Earth point attitude. Performing the reorientation in this manner shows that it is also possible to save

fuel using the optimal control and that it is also possible to perform a rest-to-rest slew using two reaction wheels if all momentum is initially removed from the system.

Using the same optimal control method for momentum management as was described in Chapter IV, the reaction wheels were taken from the initial states to the final states given in Table 11. Spinning the wheels down from 2118 RPM and -2199 RPM to zero used 12.80 thruster seconds. The savings between an optimal control resaturation and a current K2 resaturation is 22.5% based on the results in Chapter IV. Using Equation (4.3), it is found that the equivalent reaction wheel desaturation, if done on K2, would likely use approximately 16.41 seconds. The difference is the fuel saved using the wheels only slew.

Once the reaction wheels are spun down to zero, a maneuver from the science attitude to the Earth point attitude was calculated by solving the minimum time optimal control problem shown in Equations (5.1). The boundary conditions for the rest-to-rest maneuver are shown in Table 12. For this maneuver, a constraint was placed on the angle between the solar vector and the y-axis to guarantee that the solar panels would never be more than 30 degrees off the Sun. This also has the effect of preventing the boresight, which is aligned with the x-axis, from ever pointing at the Sun.

$$x = [q_1, q_2, q_3, q_4, \omega_1, \omega_2, \omega_3, h_1, h_2, h_3, h_4]^T \in \mathbb{R}^{11}; u \in \mathbb{R}^4$$

Minimize:

$$J[x(\bullet), u(\bullet), \mathrm{t}] = t_f$$

Subject To:

$$\dot{q} = \frac{1}{2}\begin{bmatrix} 0 & \omega_3 & -\omega_2 & \omega_1 \\ -\omega_3 & 0 & \omega_1 & \omega_2 \\ \omega_2 & -\omega_1 & 0 & \omega_3 \\ -\omega_1 & -\omega_2 & -\omega_3 & 0 \end{bmatrix} * \begin{bmatrix} q_1 \\ q_2 \\ q_3 \\ q_4 \end{bmatrix}$$

$$\dot{\omega} = J^{-1}[-\mathrm{T}_{RW} - \omega \times (J\omega + h)]$$

where:

$$\dot{h}_1 = u_1$$

$$\dot{h}_2 = u_2 = 0$$

$$\dot{h}_3 = u_3$$

$$\dot{h}_4 = u_4 = 0$$

$$t_0 = 0$$

$$\cos^{-1}\left(\begin{bmatrix} 2(q_1 q_2 + q_3 q_4) \\ 1 - 2({q_1}^2 + {q_3}^2) \\ 2(q_3 q_2 - q_1 q_4) \end{bmatrix} \bullet \begin{bmatrix} 0 \\ 1 \\ 0 \end{bmatrix}\right) * \frac{180}{\pi} \leq 30$$

$$\left[q(t_0), \omega(t_0), h(t_0)\right] = \left[q_0, \omega_0, h_0\right] \tag{5.1}$$

$$\left[q(t_f), \omega(t_f), h(t_f)\right] = \left[q_f, \omega_f, h_f\right]$$

$$-0.2 \leq [u_1, u_2, u_3, u_4]^T \leq 0.2$$

$$-1 \leq [q_1, q_2, q_3, \mathrm{q}_4]^T \leq 1$$

$$[-16.6, 0, -16.6, 0]^T \leq [h_1, h_2, h_3, h_4]^T \leq [16.6, 0, 16.6, 0]^T$$

	q1	q2	q3	q4	Ω_1 (RPM)	Ω_3 (RPM)
Initial	-0.054248	-0.979457	-0.194210	0.001571	0	0
Final	0.158324	-0.689780	-0.125839	0.695199	0	0

Table 12 Large Angle Maneuver Boundary Conditions

B. WHEELS ONLY SLEW RESULTS

The optimal control problem given in (5.1) was solved. The solution showed that a wheels only slew for reorienting Kepler from science point to Earth point exists and can be completed in 616 seconds. The quaternions for the optimal large angle slew maneuver are shown in Figure 52. When compared to the current K2 maneuver, it can be seen that the rotation of the spacecraft must be carefully choreographed to reach the desired final attitude. Figure 53 shows the reaction wheel control trajectory for the maneuver.

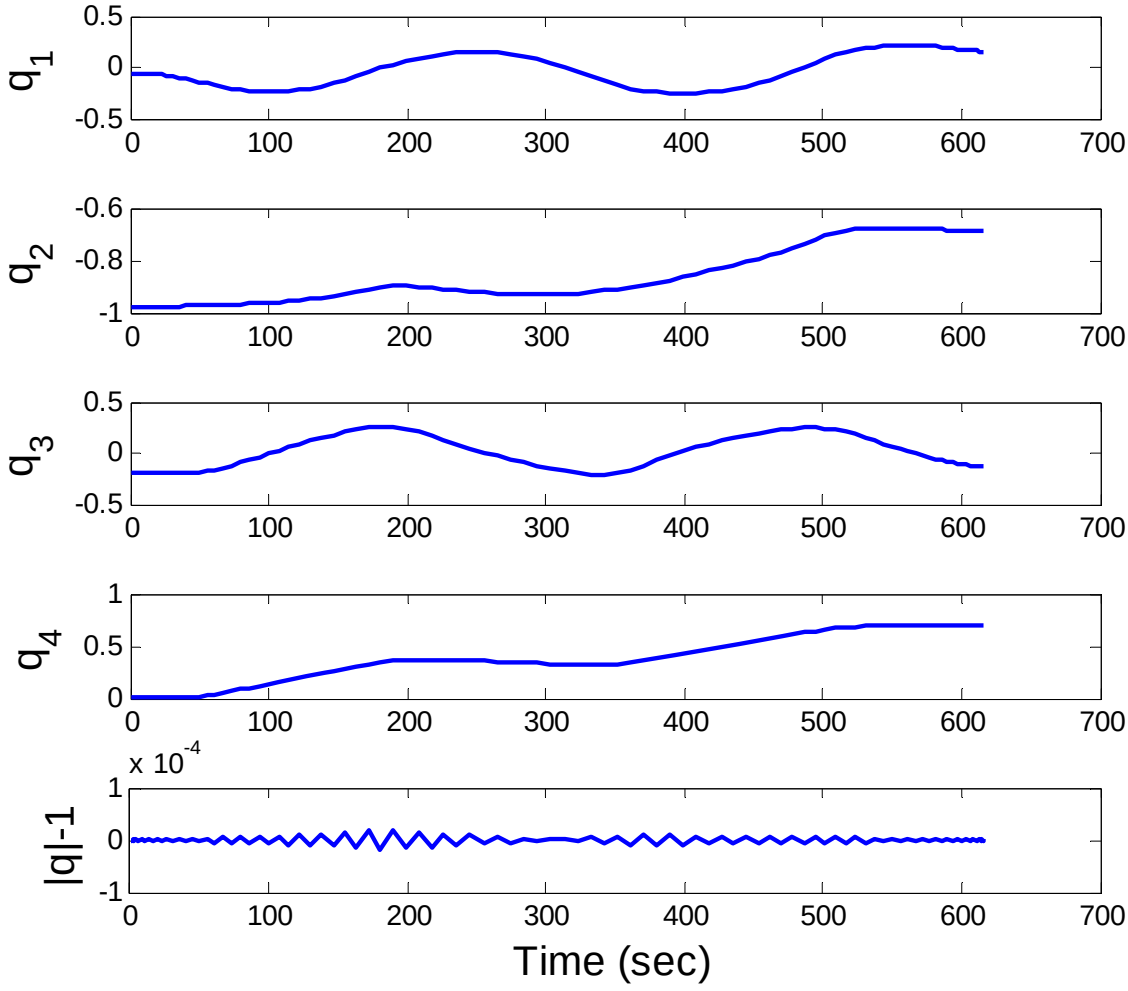

Figure 52 Optimal Control Maneuver in Quaternions

Figure 54 shows the angle between the solar vector and the spacecraft y-axis, which is approximately located at the seam between the two large solar panels. The angle stays between 16 and 30 degrees, never violating the 30 degree imposed angle constraint. Figure 55 shows the angle between the solar vector and the spacecraft boresight. Note that spacecraft never goes inside the 55 degree sun avoidance angle as described in Chapter I.

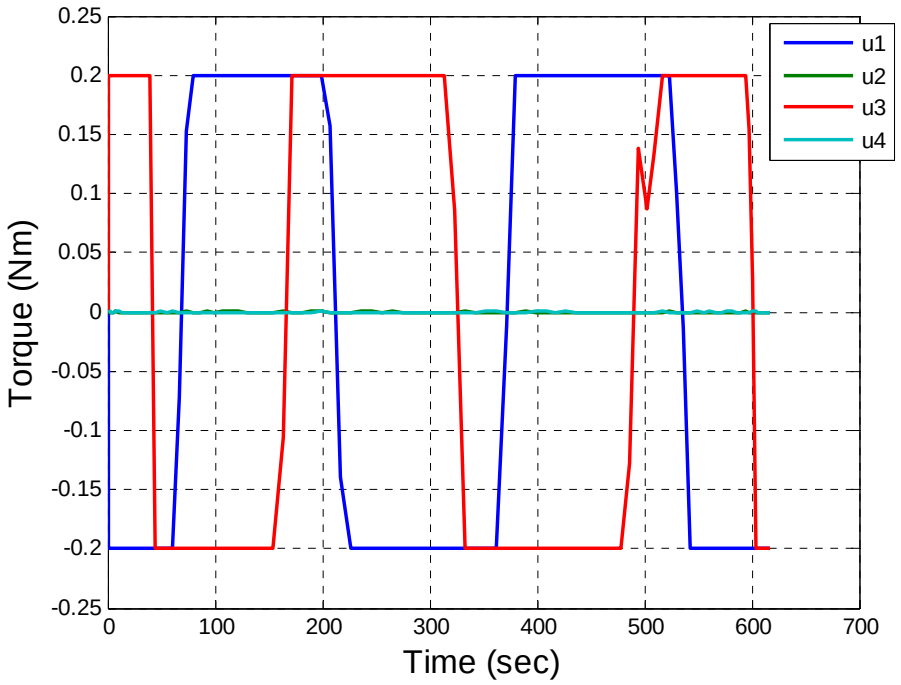

Figure 53 Reaction Wheel Control Trajectory

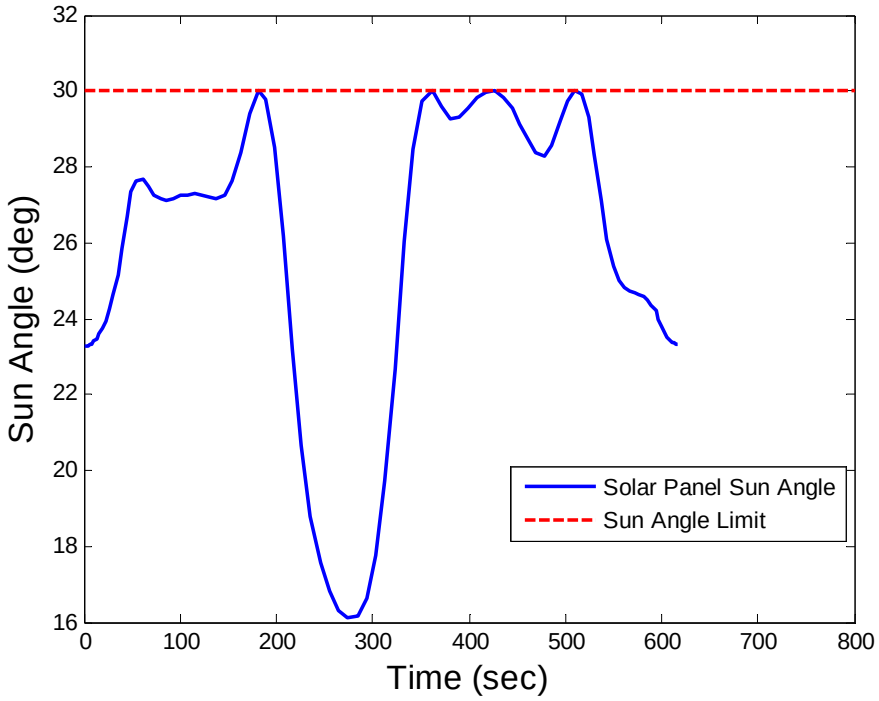

Figure 54 Angle between Solar Vector and the Y-Axis

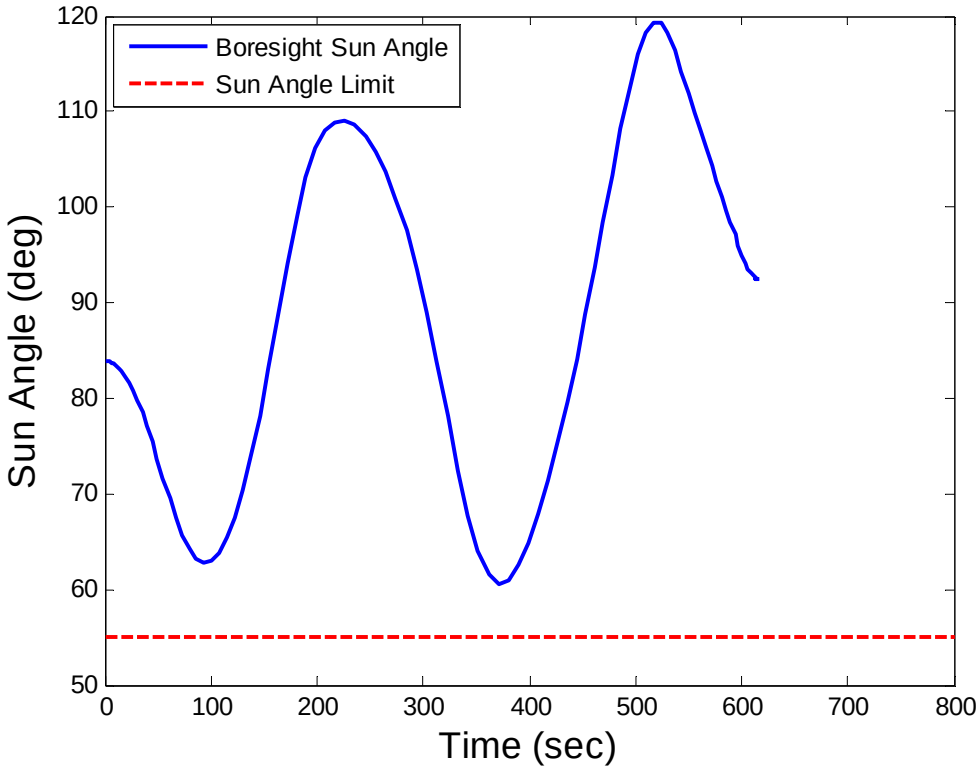

Figure 55 Angle between Solar Vector and the Boresight

C. VERIFICATION AND VALIDATION

As with the momentum management maneuvers, V&V was also performed on the large angle maneuver solution. Figure 56 shows the propagated quaternions from the control signal through the spacecraft plant equations. The results of the propagated case follow closely with the optimal control solution results. In addition, as required, the two norm for both the propagated results and optimal control solution results are equal to one. Figure 57 and Figure 58 show the spacecraft angular velocity and the reaction wheel momenta, respectively. In both figures the propagated results follow the optimal control solution closely, further validating the solution.

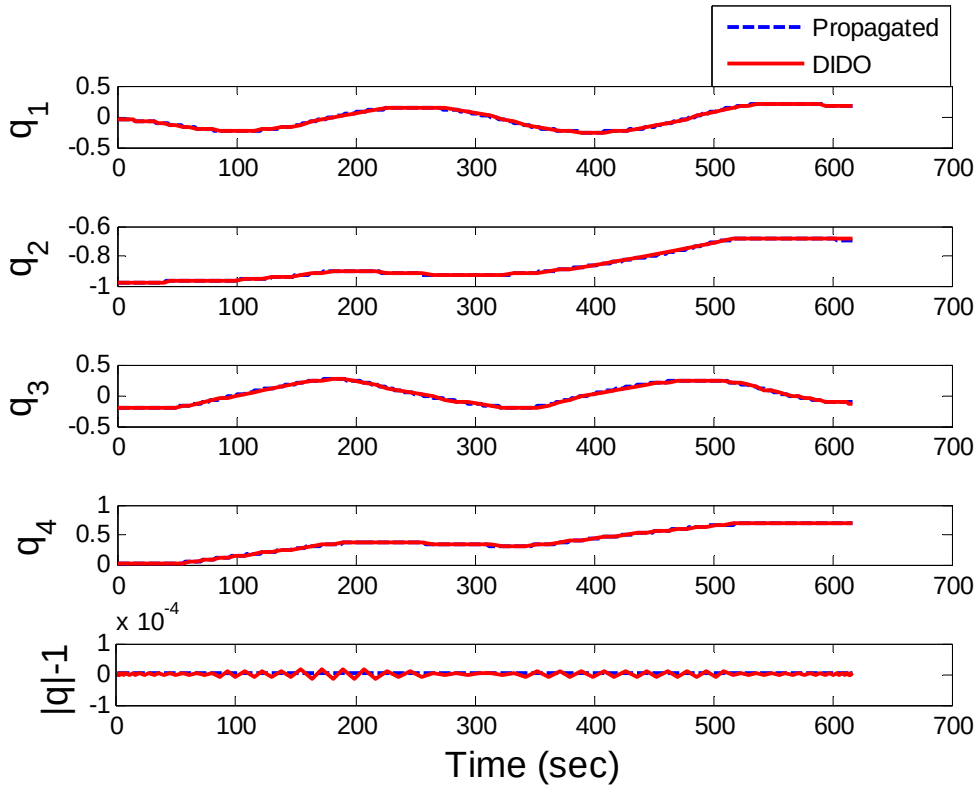

Figure 56 Propagated Quaternions for Large Angle Maneuver

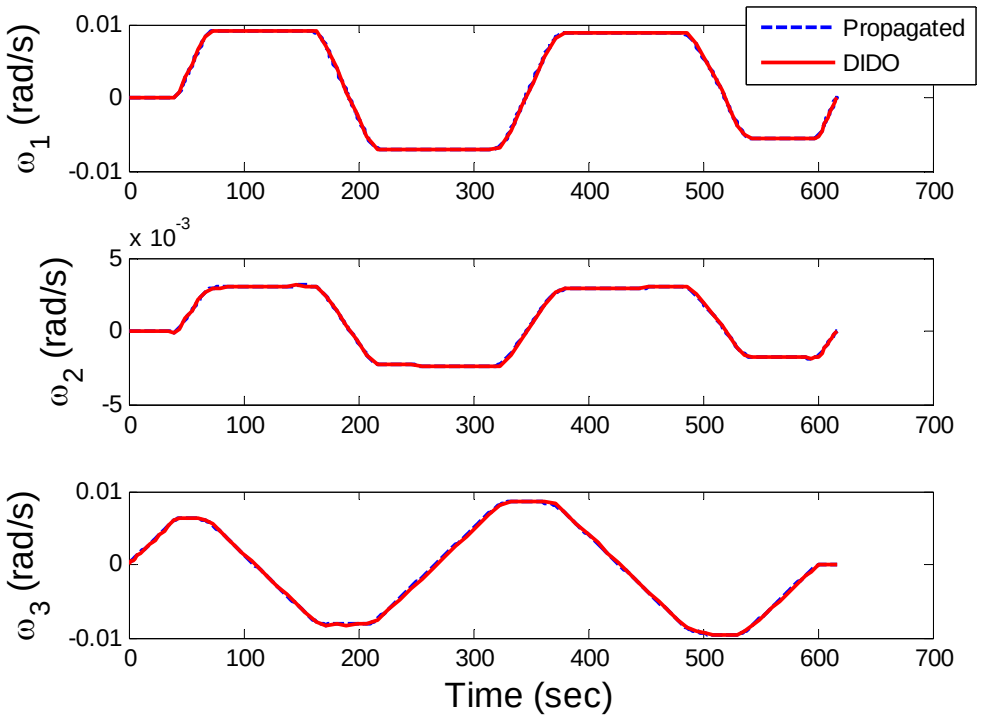

Figure 57 Propagated Angular Velocity for Large Angle Maneuver

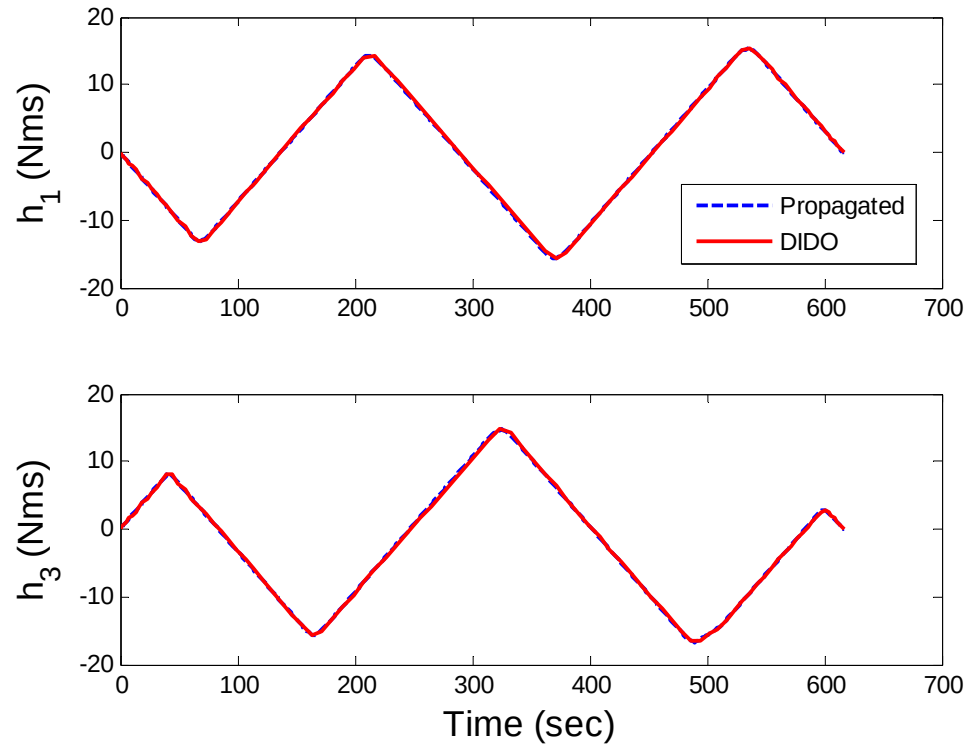

Figure 58 Propagated Reaction Wheel Momentum for Large Angle Maneuver

The final V&V activity performed was to confirm that the Hamiltonian was a constant value in accordance with the Hamiltonian Value Condition. For a minimum time problem, the Hamiltonian should be constant at a value of negative one [20]. Figure 59 shows the Hamiltonian as a relatively constant value of negative one, which verifies the solution to the problem.

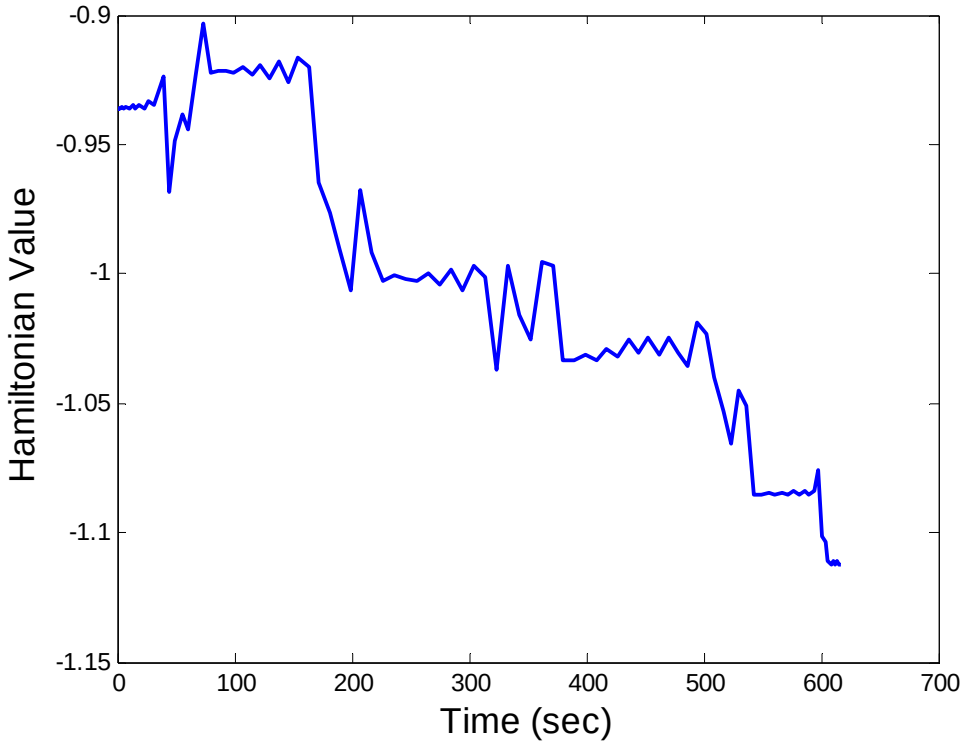

Figure 59 Time History of the Hamiltonian for Large Angle Maneuver

D. RESULTS SUMMARY

A summary of fuel consumption for the wheels only large angle slew is shown in Table 13. If a large angle maneuver is implemented using optimal control after a conventional momentum dump, a fuel savings of 10.8 percent can be realized. If an optimal control based momentum dump is applied in conjunction with a zero fuel large angle maneuver, it is possible to save up to 30.4 percent in fuel (or 5.6 thruster seconds) per maneuver. Thus, there is a potential to extend the spacecraft life by implementing wheels only large angle slews. This is particularly important in science campaigns where

many large slews are necessary, such as the Baade's window campaign planned for CY16 [11].

Method	Pulse Time	% Savings
K2 Telemetry	18.4	0
K2 Dump with Zero Fuel Slew	16.4	10.8
Optimal Static Dump with Zero Fuel Slew	12.8	30.4

Table 13 Summary of Fuel Consumption for a Large Angle Maneuver

VI. CONCLUSIONS AND FURTHER WORK

A. RESEARCH SUMMARY

This thesis has explored a variety of concepts based on optimal control that can extend the life of a spacecraft by reducing fuel consumption. The ideas range from the implementation of thruster firing methods to reduce cycling of thrusters during momentum management to the application of methods for controlling a satellite with fewer than three reaction wheels. This thesis also outlined an approach for controlling a satellite using hybrid controls with a traditional attitude control feedback loop, a method that seems to be consistent with the approach currently in use on Kepler for the K2 mission. Through the use of optimal control concepts, this work has shown that it is possible to more effectively use the remaining fuel on board Kepler to further its mission life. This is true for both momentum management and large angle maneuvers. Potential savings for the K2 mission range from 16 to 28 percent for momentum management maneuvers while savings for large angle maneuvers range from 10 to 30 percent, depending on the specific method utilized to perform the slew.

The results of this thesis do not only positively impact Kepler, but can benefit other spacecraft as well. Optimal control techniques can be applied to any satellite to minimize fuel consumption or perform maneuvers that are not possible using conventional approaches. The application of optimal control makes it possible to exploit the nonlinearities of the dynamics equations that govern the motion of a spacecraft and this, in turn, allows the spacecraft operator to get the most from the system.

B. FURTHER WORK

The use of optimal control will benefit Kepler as well as future systems, if implemented. However, further work is required before implementation can take place. The optimal control solution is fundamentally an open control loop solution, with no feedback to correct for uncertainties between the model and the actual satellite. A method for integrating the control signal with the attitude control system in a way that allows for feedback needs to be devised. One approach could be to feed the optimal control signal to

the reaction wheels and use the feedback loop to regulate the actual path of the satellite to the optimal path. This approach has been used to implement optimal control maneuvers on other NASA spacecraft like the International Space Station and TRACE [19].Further work also needs to be done to incorporate solar torque into the model that updates with orientation of the spacecraft. It would then be possible to determine if solar pressure effects can be harnessed to further reduce fuel consumption during maneuvers and momentum management operations.

In order to effectively implement optimal control on Kepler, the Naval Postgraduate School will have to work closely with the Kepler program office and Ball Aerospace to verify the current spacecraft properties, such as the moments of inertia, as well as the operational constraints of the system. Verification and validation maneuvers should then be implemented on Kepler ground simulators to ensure maneuvers can be executed correctly and do not violate any of the constraints of the spacecraft. Through this teamwork, it may be possible to extend the K2 mission and provide this benefit to the science community for years to come.

APPENDIX. APPLICATION OF PONTRYAGIN'S PRINCIPLE

In order to explore the optimality of solutions to the optimal control problem for momentum dumping or maneuvering, Pontryagin's Principle can be applied [20]. The necessary conditions for optimality are obtained by constructing the Hamiltonian, minimizing the Hamiltonian, finding the adjoint equations, and evaluating for transversality conditions. In order to illustrate this process, it is assumed that the inertia matrix is diagonal and the thrusters produce forces in the positive or negative x, y, or z directions. The diagonal inertia matrix is shown in Equation (A.1) and the thruster matrix is shown in Equation (A.2). The reaction wheel matrix is shown in Equation (A.3).

$$J = \begin{bmatrix} J_{11} & 0 & 0 \\ 0 & J_{22} & 0 \\ 0 & 0 & J_{33} \end{bmatrix} \tag{A.1}$$

$$Z_{thruster} = \begin{bmatrix} 1 & -1 & 0 & 0 & 0 & 0 \\ 0 & 0 & 1 & -1 & 0 & 0 \\ 0 & 0 & 0 & 0 & 1 & -1 \end{bmatrix} \tag{A.2}$$

$$Z_{RW} = \begin{bmatrix} a & -a & a & -a \\ b & b & b & b \\ c & c & -c & -c \end{bmatrix} \tag{A.3}$$

The statement of the optimal control problem shown in Equation (A.4) is for a satellite momentum management maneuver where it is desired to minimize the use of the thrusters (u_5-u_{10}), subject to the rotational equations of motion of the satellite. The outputs of the thrusters are limited to values between 0 and F_{max} and the reaction wheel torques (u_1-u_4) are limited between τ_{min} and τ_{max}. Boundary conditions on the quaternions, angular velocity, and/or reaction wheel momentum can be used as constraints to influence the outcome of the problem.

$$x = [q_1, q_2, q_3, q_4, \omega_1, \omega_2, \omega_3, h_1, h_2, h_3, h_4]^T \in \mathbb{R}^{11}; u \in \mathbb{R}^{10}$$

Minimize:

$$J[x(\bullet), u(\bullet)] = \int_{t_0}^{t_f} \sum_{i=5}^{10} u_i dt$$

Subject To:

$$\dot{q}_1 = 0.5(\omega_1 q_4 - \omega_2 q_3 + \omega_3 q_2)$$

$$\dot{q}_2 = 0.5(\omega_1 q_3 + \omega_2 q_4 - \omega_3 q_1)$$

$$\dot{q}_3 = 0.5(-\omega_1 q_2 + \omega_2 q_1 + \omega_3 q_4)$$

$$\dot{q}_4 = 0.5(-\omega_1 q_1 - \omega_2 q_1 - \omega_3 q_3)$$

$$\dot{\omega}_1 = \frac{A + B + C}{J_{11}}$$

$$\dot{\omega}_2 = \frac{D + E + F}{J_{22}}$$

$$\dot{\omega}_3 = \frac{G + H}{J_{33}}$$

where:

$$A = u_5 - u_6 - au_1 + au_2 - au_3 + au_4 + J_{22}\omega_2\omega_3 - J_{33}\omega_2\omega_3$$

$$B = bh_1\omega_3 + bh_2\omega_3 + bh_3\omega_3 + bh_4\omega_3$$

$$C = -ch_1\omega_2 - ch_2\omega_2 + ch_3\omega_2 + ch_4\omega_2$$

$$D = u_7 - u_8 - bu_1 - bu_2 - bu_3 - bu_4 - J_{11}\omega_1\omega_3 + J_{33}\omega_1\omega_3$$

$$E = -ah_1\omega_3 + ah_2\omega_3 - ah_3\omega_3 + ah_4\omega_3$$

$$F = ch_1\omega_1 + ch_2\omega_1 - ch_3\omega_1 - ch_4\omega_1$$

$$G = u_9 - u_{10} - cu_1 - cu_2 + cu_3 + cu_4 + J_{11}\omega_1\omega_2 - J_{22}\omega_1\omega_2$$

$$H = ah_1\omega_2 - ah_2\omega_2 + ah_3\omega_2 - ah_4\omega_2 - bh_1\omega_1 - bh_2\omega_1 - bh_3\omega_1 - bh_4\omega_1$$

$$\dot{h}_1 = u_1$$

$$\dot{h}_2 = u_2$$

$$\dot{h}_3 = u_3$$

$$\dot{h}_4 = u_4$$

$$t_0 = 0$$

$$[q(t_0), \omega(t_0), h(t_0)] = [q_0, \omega_0, h_0]$$

$$[q(t_f), \omega(t_f), h(t_f)] = [q_f, \omega_f, h_f]$$

$$\tau_{\min} \le [u_1, u_2, u_3, u_4]^T \le \tau_{\max} \qquad \text{(A.4)}$$

$$0 \le [u_5, u_6, u_7, u_8, u_9, u_{10}]^T \le F_{\max}$$

A. DERIVATION OF THE NECESSARY CONDITIONS

The first step is to construct the Hamiltonian as shown in Equation (A.5).

$$
\begin{aligned}
&H = F + \lambda^T f \\
&Where: \\
&F = u_5 + u_6 + u_7 + u_8 + u_9 + u_{10} \\
&f = \begin{bmatrix} \dot{q}_1 & \dot{q}_2 & \dot{q}_3 & \dot{q}_4 & \dot{\omega}_1 & \dot{\omega}_2 & \dot{\omega}_3 & \dot{h}_1 & \dot{h}_2 & \dot{h}_3 & \dot{h}_4 \end{bmatrix}^T \\
&\lambda = \begin{bmatrix} \lambda_{q1} & \lambda_{q2} & \lambda_{q3} & \lambda_{q4} & \lambda_{\omega 1} & \lambda_{\omega 2} & \lambda_{\omega 3} & \lambda_{h1} & \lambda_{h2} & \lambda_{h3} & \lambda_{h4} \end{bmatrix}^T
\end{aligned}
\tag{A.5}
$$

Substituting the equations of motion for "f," the Hamiltonian becomes:

$$
\begin{aligned}
&H = u_5 + u_6 + u_7 + u_8 + u_9 + u_{10} + u_{11} + u_{12} + \\
&\lambda_{q1}\left(\frac{q_2\omega_3}{2} - \frac{q_3\omega_2}{2} + \frac{q_4\omega_1}{2}\right) + \\
&\lambda_{q2}\left(\frac{q_3\omega_1}{2} - \frac{q_1\omega_3}{2} + \frac{q_4\omega_2}{2}\right) + \lambda_{q3}\left(\frac{q_1\omega_2}{2} - \frac{q_2\omega_1}{2} + \frac{q_4\omega_3}{2}\right) \\
&- \lambda_{q4}\left(\frac{q_1\omega_1}{2} + \frac{q_2\omega_2}{2} + \frac{q_3\omega_3}{2}\right) \\
&+ \lambda_{h1}u_1 + \lambda_{h2}u_2 + \lambda_{h3}u_3 + \lambda_{h4}u_4 \\
&+ \lambda_{\omega 1}\left(\frac{A + B}{J_{11}}\right) \\
&- \lambda_{\omega 3}\left(\frac{C + D}{J_{33}}\right) \\
&- \lambda_{\omega 2}\left(\frac{E + F}{J_{22}}\right)
\end{aligned}
$$

where:

$$
\begin{aligned}
A &= u_5 - u_6 - au_1 + au_2 - au_3 + au_4 + J_{22}\omega_2\omega_3 - J_{33}\omega_2\omega_3 \\
B &= bh_1\omega_3 + bh_2\omega_3 + bh_3\omega_3 + bh_4\omega_3 - ch_1\omega_2 - ch_2\omega_2 + ch_3\omega_2 + ch_4\omega_2 \\
C &= u_{10} - u_9 + cu_1 + cu_2 - cu_3 - cu_4 - J_{11}\omega_1\omega_2 + J_{22}\omega_1\omega_2 \\
D &= -ah_1\omega_2 + ah_2\omega_2 - ah_3\omega_2 + ah_4\omega_2 + bh_1\omega_1 + bh_2\omega_1 + bh_3\omega_1 + bh_4\omega_1 \\
E &= u_8 - u_7 + bu_1 + bu_2 + bu_3 + bu_4 + J_{11}\omega_1\omega_3 - J_{33}\omega_1\omega_3 \\
F &= ah_1\omega_3 - a\,h_2\omega_3 + ah_3\omega_3 - ah_4\omega_3 - ch_1\omega_1 - ch_2\omega_1 + ch_3\omega_1 + ch_4\omega_1
\end{aligned}
\tag{A.6}
$$

The next step is to minimize the Hamiltonian with respect to the control inputs. This is done by taking the partial derivative of the Hamiltonian with respect to each

control and setting the derivative equal to zero. The resulting equation is then solved for the control variable. Equation (A.7) shows the partial derivative of the Hamiltonian with respect to each of the control variables. Since the control variables do not explicitly appear in any of the terms in Equation (A.7), all of the partial derivatives must be interpreted as switching functions. This means that each control signal will either be at its minimum or maximum value during a maneuver. For the reaction wheels, this means the values of the controls will either be τ_{min} or τ_{max} and the thrusters will either be at zero or F_{max}. This result is useful for validating a candidate optimal solution, such as the results from a successful run of the DIDO software. Furthermore, if the optimal controls minimize the Hamiltonian, the time variation of the Hamiltonian should be zero [20]. This provides another check on the optimality of the solution.

$$
\begin{aligned}
\frac{\partial H}{\partial u_1} &= \lambda_{h1} - \frac{a\lambda_{\omega 1}}{J_{11}} - \frac{b\lambda_{\omega 2}}{J_{22}} - \frac{c\lambda_{\omega 3}}{J_{33}} = 0 \\
\frac{\partial H}{\partial u_2} &= \lambda_{h2} + \frac{a\lambda_{\omega 1}}{J_{11}} - \frac{b\lambda_{\omega 2}}{J_{22}} - \frac{c\lambda_{\omega 3}}{J_{33}} = 0 \\
\frac{\partial H}{\partial u_3} &= \lambda_{h3} - \frac{a\lambda_{\omega 1}}{J_{11}} - \frac{b\lambda_{\omega 2}}{J_{22}} + \frac{c\lambda_{\omega 3}}{J_{33}} = 0 \\
\frac{\partial H}{\partial u_4} &= \lambda_{h4} + \frac{a\lambda_{\omega 1}}{J_{11}} - \frac{b\lambda_{\omega 2}}{J_{22}} + \frac{c\lambda_{\omega 3}}{J_{33}} = 0 \\
\frac{\partial H}{\partial u_5} &= 1 + \frac{\lambda_{\omega 1}}{J_{11}} = 0 \\
\frac{\partial H}{\partial u_6} &= 1 - \frac{\lambda_{\omega 1}}{J_{11}} = 0 \\
\frac{\partial H}{\partial u_7} &= 1 + \frac{\lambda_{\omega 2}}{J_{22}} = 0 \\
\frac{\partial H}{\partial u_8} &= 1 - \frac{\lambda_{\omega 2}}{J_{22}} = 0 \\
\frac{\partial H}{\partial u_9} &= 1 + \frac{\lambda_{\omega 3}}{J_{33}} = 0 \\
\frac{\partial H}{\partial u_{10}} &= 1 - \frac{\lambda_{\omega 3}}{J_{33}} = 0
\end{aligned}
\tag{A.7}
$$

The next step is to calculate the adjoint equations, which give the dynamics of the costates. The adjoint equations are set up by finding the partial derivative of the Hamiltonian with respect to each of the states, as shown in Equation (A.8).

$$-\dot{\lambda}_x(t) = \frac{\partial H}{\partial x} \tag{A.8}$$

Taking the partial derivatives, the following equations are obtained:

$$\dot{\lambda}_{q1} = \frac{\lambda_{q2}\omega_3}{2} - \frac{\lambda_{q3}\omega_2}{2} + \frac{\lambda_{q4}\omega_1}{2}$$

$$\dot{\lambda}_{q2} = \frac{\lambda_{q3}\omega_1}{2} - \frac{\lambda_{q1}\omega_3}{2} + \frac{\lambda_{q4}\omega_2}{2}$$

$$\dot{\lambda}_{q3} = \frac{\lambda_{q1}\omega_2}{2} - \frac{\lambda_{q2}\omega_1}{2} + \frac{\lambda_{q4}\omega_3}{2}$$

$$\dot{\lambda}_{q4} = -\frac{\lambda_{q1}\omega_1}{2} - \frac{\lambda_{q2}\omega_2}{2} - \frac{\lambda_{q3}\omega_3}{2}$$

$$\dot{\lambda}_{\omega1} = \frac{\lambda_{q3}q_2}{2} - \frac{\lambda_{q2}q_3}{2} - \frac{\lambda_{q1}q_4}{2} + \frac{\lambda_{q4}q_1}{2}$$
$$+ \frac{\lambda_{\omega3}\ (J_{11}\omega_1 - J_{22}\omega_1 + ah_1 - ah_2 + ah_3 - ah_4)}{J_{33}}$$
$$+ \frac{\lambda_{\omega2}\ (J_{11}\omega_3 - J_{33}\omega_3 - ch_1 - ch_2 + ch_3 + ch_4)}{J_{22}}$$

$$\dot{\lambda}_{\omega2} = \frac{\lambda_{q1}q_3}{2} - \frac{\lambda_{q3}q_1}{2} - \frac{\lambda_{q2}q_4}{2} + \frac{\lambda_{q4}q_2}{2}$$
$$+ \frac{\lambda_{\omega3}\ (J_{11}\omega_1 - J_{22}\omega_1 + ah_1 - ah_2 + ah_3 - ah_4)}{J_{33}}$$
$$+ \frac{\lambda_{\omega1}\ (J_{22}\omega_3 - J_{33}\omega_3 - ch_1 - ch_2 + ch_3 + ch_4)}{J_{11}}$$

$$\dot{\lambda}_{\omega3} = \frac{\lambda_{q2}q1}{2} - \frac{\lambda_{q1}q_2}{2} - \frac{\lambda_{q3}q_4}{2} + \frac{\lambda_{q4}q_3}{2}$$
$$+ \frac{\lambda_{\omega3}\ (J_{11}\omega_1 - J_{33}\omega_1 + ah_1 - ah_2 + ah_3 - ah_4)}{J_{22}}$$
$$- \frac{\lambda_{\omega1}\ (J_{22}\omega_2 - J_{33}\omega_2 + bh_1 + bh_2 + bh_3 + bh_4)}{J_{11}}$$

$$\dot{\lambda}_{h1} = \frac{\lambda_{\omega2}(a\omega_3 - c\omega_1)}{J_{22}} - \frac{\lambda_{\omega3}(a\omega_2 - b\omega_1)}{J_{33}} - \frac{\lambda_{\omega1}(b\omega_3 - c\omega_2)}{J_{11}}$$

$$\dot{\lambda}_{h2} = \frac{\lambda_{\omega3}(a\omega_2 + b\omega_1)}{J_{33}} - \frac{\lambda_{\omega2}(a\omega_3 - c\omega_1)}{J_{22}} - \frac{\lambda_{\omega1}(b\omega_3 - c\omega_2)}{J_{11}}$$

$$\dot{\lambda}_{h3} = \frac{\lambda_{\omega2}(a\omega_3 + c\omega_1)}{J_{22}} - \frac{\lambda_{\omega3}(a\omega_2 - b\omega_1)}{J_{33}} - \frac{\lambda_{\omega1}(b\omega_3 + c\omega_2)}{J_{11}} \qquad \text{(A.9)}$$

$$\dot{\lambda}_{h4} = \frac{\lambda_{\omega3}(a\omega_2 + b\omega_1)}{J_{33}} - \frac{\lambda_{\omega2}(a\omega_3 - c\omega_1)}{J_{22}} - \frac{\lambda_{\omega1}(b\omega_3 + c\omega_2)}{J_{11}}$$

The transversality conditions give information on the values of the costates at the final time. Equation (A.11) shows the endpoint Lagrangian $\bar{E} = E + \nu e$, where E=0 is the endpoint cost and ν are the Lagrange multipliers:

$$\nu = \begin{bmatrix} \nu_{q1} & \nu_{q2} & \nu_{q3} & \nu_{q4} & \nu_{\omega 1} & \nu_{\omega 2} & \nu_{\omega 3} & \nu_{h1} & \nu_{h2} & \nu_{h3} & \nu_{h4} \end{bmatrix}^T \tag{A.10}$$

Functions e are the endpoint conditions:

$$e = \begin{bmatrix} q_{1f} - q_1^f \\ q_{2f} - q_2^f \\ q_{3f} - q_3^f \\ q_{4f} - q_4^f \\ \omega_{1f} - \omega_1^f \\ \omega_{2f} - \omega_2^f \\ \omega_{f3} - \omega_3^f \\ h_{1f} - h_1^f \\ h_{2f} - h_2^f \\ h_{3f} - h_3^f \\ h_{4f} - h_4^f \end{bmatrix} \tag{A.11}$$

It is possible to then find the fixed values of the costates from the transversality conditions by taking the partial derivative of the endpoint lagrangian with respect to each state, as shown in Equation (A.12).

$$\lambda(\mathrm{t}_f) = \frac{\partial \bar{E}}{\partial x_f} \tag{A.12}$$

Equation (A.13) shows the partials. It is observed from Equation (A.13) that the only output to the equation is the value of each costate at the final time is a function of an unknown constant, ν. This indicates that in this case transversality yields no useful information for V&V.

$$
\begin{aligned}
\lambda_{q1}(t_f) &= \frac{\partial \bar{E}}{\partial q_{1f}} = \nu_{q1} {q_1}^f \\
\lambda_{q2}(t_f) &= \frac{\partial \bar{E}}{\partial q_{2f}} = \nu_{q2} {q_2}^f \\
\lambda_{q3}(t_f) &= \frac{\partial \bar{E}}{\partial q_{3f}} = \nu_{q2} {q_3}^f \\
\lambda_{q4}(t_f) &= \frac{\partial \bar{E}}{\partial q_{4f}} = \nu_{q4} {q_4}^f \\
\lambda_{w1}(t_f) &= \frac{\partial \bar{E}}{\partial w_{1f}} = \nu_{w1} {\omega_1}^f \\
\lambda_{w2}(t_f) &= \frac{\partial \bar{E}}{\partial w_{2f}} = \nu_{w2} {\omega_2}^f \\
\lambda_{w3}(t_f) &= \frac{\partial \bar{E}}{\partial w_{3f}} = \nu_{w3} {\omega_3}^f \\
\lambda_{h1}(t_f) &= \frac{\partial \bar{E}}{\partial h_{1f}} = \nu_{h1} {h_1}^f \\
\lambda_{h2}(t_f) &= \frac{\partial \bar{E}}{\partial h_{2f}} = \nu_{h2} {h_2}^f \\
\lambda_{h3}(t_f) &= \frac{\partial \bar{E}}{\partial h_{3f}} = \nu_{h3} {h_3}^f \\
\lambda_{h4}(t_f) &= \frac{\partial \bar{E}}{\partial h_{4f}} = \nu_{h4} {h_4}^f
\end{aligned}
\qquad \text{(A.13)}
$$

LIST OF REFERENCES

[1] D. G. Koch et al. “Kepler mission design, realized photometric performance, and early science,” *The Astrophysical Journal Letters,* vol. 713, pp. L79-L86, Apr 20, 2010.

[2] D. A. Caldwell, “The Kepler mission: zeroing in on habitable earths,” in *Vacuum Electronics Conf (IVEC), 2012 IEEE Thirteenth International,* Monterey, CA, 2012, pp. 3–6.

[3] NASA Exoplanet Archive. (2014, Oct 23). California Technical University. [Online]. Available: http://exoplanetarchive.ipac.caltech.edu/

[4] E. V. Quintana et al., “An Earth-sized planet in the habitable zone of a cool star,” *Science,* vol. 344, pp. 277–280, Apr 18, 2014.

[5] NASA Kepler results usher in a new era of astronomy (4 Nov, 2013). [Online]. Available:http://www.nasa.gov/content/nasa-kepler-results-usher-in-a-new-era-of-astronomy/#.VFAYTPnF9qI

[6] C. N. Schira and D. S. Putnam, “Kepler ADCS overview and early mission experiences,” in *33rd Annual AAS Guidance and Control Conf.,* Breckenridge, Colorado, 2010, vol. 137, pp. 761–774.

[7] B. Cooke et al., “The Kepler end-to-end data pipeline: From photons to far away worlds,” in *Aerospace Conf., 2012 IEEE,* Big Sky, MT, 2012, pp. 1–9.

[8] J. Van Leve et al., “Kepler data release 4 notes,” NASA Ames Research Center, Moffett Field, CA, Tech. Rep. KSCI-19044–001, Apr. 2010.

[9] D. Putnam and D. Weimer, “Hybrid control architecture for the Kepler spacecraft,” in *37th Annual American Astronautical Society Guidance and Control Conf.,* Breckenridge, Colorado, 2014, vol. 151, pp. 605–616.

[10] S. B. Howell et al., “The K2 mission: characterization and early results,” *Publications of the Astronomical Society of the Pacific,* vol. 126, pp. 398–408, Apr. 2014.

[11] S. B. Howell and C. Sobeck, “The NASA K2 mission, extending Kepler’s power to the ecliptic, NASA astrophysics division senior review,” unpublished.

[12] S. B. Howell et al., “K2 mission: Extending Kepler’s power to the ecliptic, NASA Astrophysics Senior Review (Slideshow),” unpublished.

[13] M. Karpenko et al., "Precision pointing for a skewed 2-reaction wheel control system," in *37ith Annual American Astronautical Society Guidance and Control Conference,* Breckenridge, Colorado, 2014, vol. 151, pp. 627–639.

[14] S. R. Crews, "Increasing slew performance of reaction wheel attitude control systems," M.S. thesis, Dept. of Mech. and Aerospace Eng., Naval Postgraduate School, Monterey, CA, 2013.

[15] C. D. Brown, *Elements of Spacecraft Design,* Reston, VA, American Institute of Aeronautics and Astronautics, Inc., 2002, ch. 5, sec. 2, pp 267.

[16] B. Wie, *Space Vehicle Dynamics and Control*, Reston, VA, American Institute of Aeronautics and Astronautics, Inc., 1998 ch. 7, pp 448–456.

[17] "Thrust Modulation Methods," class notes for Spacecraft Attitude Dynamics & Control, Dept. of Mechanical and Aerospace Engineering, Naval Postgraduate School, Monterey, CA, Fall 2013.

[18] M. Karpenko, private communication, Jul. 2014.

[19] I. M. Ross and M. Karpenko, "A review of pseudospectral optimal control: From theory to flight," *Annual Reviews in Control,* vol. 36, no. 2, pp. 182–197, Dec. 2012.

[20] I. M. Ross, *A Primer on Pontryagin's Principle in Optimal Control.* Carmel, CA: Collegiate Publishers, 2009, ch. 2, sec. 2, pp 28–30.

INITIAL DISTRIBUTION LIST

1. Defense Technical Information Center
   Ft. Belvoir, Virginia

2. Dudley Knox Library
   Naval Postgraduate School
   Monterey, California